RMP
REGIONAL MONITORING
PROGRAM FOR WATER QUALITY
IN SAN FRANCISCO BAY

sfei.org/rmp

Simulating Sediment Flux Through the Golden Gate.

Prepared by:

Anchor QEA, LLC
130 Battery Street, Suite 400
San Francisco, California 94111

CONTRIBUTION NO. 1033 / March 2021

San Francisco Estuary Institute • 4911 Central Ave., Richmond, CA • www.sfei.org

March 2021
RMP Sediment Modeling Studies

ANCHOR QEA

Simulating Sediment Flux Through the Golden Gate

Prepared for the San Francisco Bay Regional Monitoring Program

March 2021
RMP Sediment Modeling Studies

Simulating Sediment Flux Through the Golden Gate

Prepared for
San Francisco Bay Regional
Monitoring Program
San Francisco Estuary Institute
4911 Central Avenue
Richmond, California 94804

Prepared by
Anchor QEA, LLC
130 Battery Street, Suite 400
San Francisco, California 94111

Suggested Citation: Anchor QEA, LLC. 2021. Simulating Sediment Flux Through the Golden Gate. Prepared for Regional Monitoring Program for Trace Substances in San Francisco Bay (RMP). March 2021, 115pp.

TABLE OF CONTENTS

TABLES

FIGURES

ABBREVIATIONS

µm	micrometer
ADCP	acoustic Doppler current profiler
BAAQMD	Bay Area Air Quality Management District
Bay	San Francisco Bay
CCWD	Contra Costa Water District
CIMIS	California Irrigation Management Information System
Delta	Sacramento-San Joaquin Delta
DICU	Delta Island Consumptive Use
kg	kilogram
LiDAR	Light Detection and Ranging
m	meter
m^2s	meters squared seconds
m^3	cubic meter
mg/L	milligrams per liter
mm	millimeter
NA	not applicable
NOAA	National Oceanic and Atmospheric Administration
Pa	pascal
RMP	Regional Monitoring Program
$RMSD_N$	normalized root-mean-square difference
s	second
SFEI	San Francisco Estuary Institute
SSC	suspended sediment concentration
SWAN	Simulating WAves Nearshore
ubRMSD	unbiased root-mean-square difference
$ubRMSD_N$	unbiased normalized root-mean-square difference
UnTRIM	Unstructured nonlinear Tidal Residual Intertidal Mudflat
USACE	U.S. Army Corps of Engineers
USGS	U.S. Geological Survey

Executive Summary

There is significant uncertainty in the quantity and timing of the sediment flux between San Francisco Bay (Bay) and the Pacific Ocean through the constriction at the Golden Gate. An improved understanding of the sediment flux through the Golden Gate is needed to better quantify sediment budgets for the Bay. The U.S. Geological Survey (USGS) conducted a boat-based data collection to estimate the suspended sediment flux through the Golden Gate during 2016 and again during the period of high Sacramento-San Joaquin Delta (Delta) outflow in 2017 (Downing-Kunz et al. 2018). The results of the 2017 sampling suggested net sediment flux into the Bay over a 16.5-hour period spanning half of the mixed semidiurnal tidal cycle, during the receding limb of a high Delta outflow flow period.

The high-resolution Unstructured nonlinear Tidal Residual Intertidal Mudflat (UnTRIM) Bay-Delta model was used to simulate hydrodynamics, waves, and suspended sediment transport throughout the Bay and the Delta. One of the goals of this Bay Regional Monitoring Program (RMP) sediment modeling study was to predict suspended sediment flux through the Golden Gate over the entire 2017 period of high Delta outflow and relate findings from the model simulation to the data-based estimates of sediment flux from USGS.

During any individual half of the mixed semidiurnal tidal cycle (one flood and the following ebb), the model simulations demonstrate that the net water flow can be into or out of the Bay depending on tidal asymmetry and the freshwater inflow to the Bay (Figure 5.2-3). The model simulations also confirm that the net water flow over a complete tidal cycle (two floods and two ebbs) can be either into the Bay or out of the Bay during periods of low freshwater inflow to the Bay and likely alternates between into and out of the Bay based on spring-neap cycles. During periods of elevated freshwater inflow to the Bay, such as during the 2017 high Delta outflow period, the net water flow over complete tidal cycles is out of the Bay. The net water flow decreased following the high Delta outflows in 2017 but remained out of the Bay because of the higher Delta outflow following the 2017 high Delta outflow period than prior to the high outflow period.

Analysis of the model results suggests that the sediment flux through the Golden Gate can be in either the flood or ebb direction, dependent on tidal asymmetry and the duration of the analysis period. When evaluating sediment flux over a half of the mixed semidiurnal tidal cycle (one flood and the following ebb), the predicted sediment flux was often in the flood direction. However, the predicted sediment flux was always in the ebb direction when evaluated over a complete tidal cycle (two floods and two ebbs). The predicted sediment flux also had two periods during the 2017 high Delta outflow period when the net flood-directed flux was increasing while the net ebb-directed flux was decreasing, resulting in the flood- and ebb-directed sediment fluxes becoming closer in magnitude. Since the USGS data collection spanned half a tidal cycle and occurred during a period

when the predicted flood- and ebb-directed fluxes were becoming closer in magnitude, either or a combination of the short data collection period and the decrease in the difference in the net flood- and ebb-directed fluxes could be resulting in the USGS-observed sediment flux in the flood (into the Bay) direction. However, there could also be other factors or physical processes influencing the sediment fluxes calculated from the acoustic Doppler current profiler (ADCP) data. Another data collection study that spanned a complete tidal cycle consisting of two flood and two ebb tides during both periods with large asymmetry in the tides and with minimal asymmetry in the tides would provide valuable information for further evaluating the periodic nature of the predicted sediment flux into the Bay.

Surrogate measurements of water flow through the Golden Gate and suspended sediment concentration (SSC) were used to calculate surrogate estimates of sediment flux through the Golden Gate. These surrogate estimates of sediment flux were compared to the predicted UnTRIM cross-sectional sediment flux through the Golden Gate to evaluate the accuracy of the surrogate sediment fluxes. This comparison evaluated how well each surrogate sediment flux estimates represented the modeled sediment flux. This analysis showed that the predicted UnTRIM cross-sectional sediment flux could be moderately well represented using water flow at the Golden Gate derived from the publicly available National Oceanic and Atmospheric Administration (NOAA)-predicted velocity and SSC near the Golden Gate. The accuracy of the surrogate sediment flux decreased as the distance from the Golden Gate to the location of the SSC increased. For example, using predicted SSC at Alcatraz resulted in a surrogate sediment flux that did not match the predicted flux as well as surrogate sediment fluxes calculated using point measures of SSC located closer to the Golden Gate. This analysis suggests that the closer to the channel at the Golden Gate the SSC can be observed, the better the surrogate estimates of sediment flux will be. Further work incorporating a metric for net flow, such as Delta Outflow, would likely improve the estimated water flow from the surrogate measurements and improve the estimated surrogate sediment flux.

1 Introduction

There is significant uncertainty in the quantity and timing of the sediment flux between San Francisco Bay (Bay) and the Pacific Ocean through the constriction at the Golden Gate. An improved understanding of the sediment flux through the Golden Gate is needed to better quantify sediment budgets for the Bay. The U.S. Geological Survey (USGS) conducted a boat-based data collection to estimate the suspended sediment flux through the Golden Gate during 2016 and again during the period of high Sacramento-San Joaquin Delta (Delta) outflow in 2017 (Downing-Kunz et al. 2018). The results of the 2017 sampling suggested net sediment flux into the Bay over a 16.5-hour period spanning half of the mixed semidiurnal tidal cycle, during the receding limb of a high flow period. Based on the measurements collected during this single ebb and flood tide, USGS estimated a net sediment flux into the Bay (Downing-Kunz et al. 2017), which is inconsistent with the expected flux of sediment from the Bay to the Pacific Ocean during periods of high Delta outflow. One of the goals of this analysis was to simulate the period spanning the 16.5-hour USGS data collection period to better understand how this single observed ebb tide and flood tide sediment flux fit into the larger context of sediment flux across the longer high flow period.

The high-resolution Unstructured nonlinear Tidal Residual Intertidal Mudflat (UnTRIM) Bay-Delta model was used to simulate hydrodynamics, waves, and suspended sediment transport throughout the Bay and the Delta as part of a set of modeling studies overseen by the San Francisco Estuary Institute (SFEI) and funded through the Bay Regional Monitoring Program (RMP) and the Nutrient Management Strategy. One of the goals of this Bay RMP sediment modeling study was to predict suspended sediment flux through the Golden Gate over the entire 2017 period of high Delta outflow and relate findings from the model simulation to the data-based estimates of sediment flux from USGS. The benefits of modeling the sediment transport are that the predicted sediment flux through the Golden Gate can be computed over longer periods and the sediment flux can be examined on various timescales. For example, this report describes the predicted sediment flux over the tidal cycle corresponding to the USGS data collection and relates the sediment flux during that relatively short period of time to the predicted sediment flux over the entire period of high Delta outflow.

Additional calibration of the sediment transport model was outside the scope of this study. However, predicted suspended sediment concentration (SSC) throughout the Bay was validated to observed data. This validation included time series SSC at discrete locations and vertical profiles of SSC along a transect spanning from the far South Bay to Rio Vista. Predicted SSC was also compared to the 2017 USGS estimated SSC along the Golden Gate transects. This validation provides a description of the accuracy of the predicted SSC over various spatial and temporal scales. Predicted water flux through the Golden Gate was also compared to water flux estimated by the USGS for the 2017 Golden Gate transects.

This report documents the 3D hydrodynamic, wave, and sediment transport model simulation used to examine the sediment flux through the Golden Gate. It is divided into the following seven primary sections and two appendices:

- **Section 1: Introduction.** This section provides a description of the motivation for the project and a summary of the scope and organization of the report.
- **Section 2: UnTRIM Bay-Delta Model Overview**. This section provides a brief description of the Golden Gate high-resolution UnTRIM Bay-Delta model.
- **Section 3: Model Simulation Period and Analysis.** This section presents the model simulation period and the various methods used in this report for calculating water flow and sediment flux
- **Section 4: Comparison of Predicted and Observed Acoustic Doppler Current Profiler Transects.** This section provides a validation of the predicted velocity, SSC, water flow, and sediment flux along the USGS transects.
- **Section 5: Predicted Sediment Flux.** This section provides a description of the predicted water flow and sediment flux through the Golden Gate spanning the complete 4.5-month analysis period.
- **Section 6: Surrogate Measurements for Estimating Sediment Flux through the Golden Gate.** This section describes a possible surrogate method for estimating the sediment flux through the Golden Gate based on continuous point estimates of water flow and SSC.
- **Section 7: Summary and Conclusions.** This section provides a summary of the results of this study and the conclusions.
- **Appendix A: Model Validation.** This section presents validation of predicted SSC in the Bay.
- **Appendix B: Assumptions and Limitations of the Coupled Modeling System.** This section details the assumptions and limitations inherent in the UnTRIM Bay-Delta hydrodynamic, wave, and sediment transport modeling system.

2 UnTRIM Bay-Delta Model Overview

The high-resolution UnTRIM Bay-Delta model is a 3D hydrodynamic model of the Bay and the Delta, which has been developed using the UnTRIM hydrodynamic model (MacWilliams et al. 2007, 2008, 2009, 2015). The UnTRIM Bay-Delta model extends from the Pacific Ocean through the entire Delta and takes advantage of the grid flexibility allowed in an unstructured mesh by gradually varying grid cell sizes, beginning with large grid cells in the Pacific Ocean and gradually transitioning to finer grid resolution in the smaller channels of the Delta. This approach offers significant advantages in terms of numerical efficiency and accuracy and allows for local grid refinement for detailed analysis of local hydrodynamics, while still incorporating the overall hydrodynamics of the larger estuary in a single model. The resulting model contains more than 130,000 horizontal grid cells and more than 1 million 3D grid cells (Figure 2-1). Extensive details of the hydrodynamic model and model inputs are available in MacWilliams et al. (2015).

The UnTRIM Bay-Delta model has been applied to the Bay-Delta as part of the Delta Risk Management Strategy (MacWilliams and Gross 2007), several studies to evaluate the mechanisms behind the Pelagic Organism Decline (e.g., MacWilliams et al. 2008), the Bay Delta Conservation Plan (MacWilliams and Gross 2010), and for examining X2 and the Low Salinity Zone (MacWilliams et al. 2015). The UnTRIM Bay-Delta model has also been applied for a range of studies by the U.S. Army Corps of Engineers (USACE), including the Hamilton Wetlands Restoration Project (MacWilliams and Cheng 2007), the Sacramento River Deep Water Ship Channel Deepening Study (MacWilliams et al. 2009), the San Francisco Bay to Stockton Navigation Project Deepening Study (MacWilliams et al. 2014), and the South San Francisco Bay Shoreline Study (MacWilliams et al. 2012a). The UnTRIM Bay-Delta model has also been applied to several studies of sediment transport in support of the San Francisco Bay Regional Dredged Material Management Program (MacWilliams et al. 2012b; Bever and MacWilliams 2013, 2014; Bever et al. 2014; Delta Modeling Associates 2015) and for turbidity modeling in the Bay-Delta (Anchor QEA 2017; Bever et al. 2018).

The UnTRIM Bay-Delta model has been calibrated using water level, flow, salinity, SSC, and turbidity data collected in the Bay-Delta in numerous previous studies (e.g., MacWilliams et al. 2008, 2009; MacWilliams and Gross 2010; Bever and MacWilliams 2013; MacWilliams et al. 2015; MacWilliams et al. 2016; Bever et al. 2018). The model has been shown to accurately predict salinity, tidal flows, water levels, and sediment transport throughout the Bay-Delta under a wide range of conditions. This report documents the model validation for SSC in the Bay during the study period in Appendix A. Appendix B details the assumptions and limitations of the coupled modeling system that may influence model predictions and the comparison of predicted to observed values.

Figure 2-1
Golden Gate High-Resolution UnTRIM San Francisco Bay-Delta Model Domain, Bathymetry, and Locations of Model Boundary Conditions that Include Inflows, Export Facilities, Contra Costa Water District (CCWD) Intakes, Wind Stations from the Bay Area Air Quality Management District (BAAQMD), Evaporation and Precipitation from California Irrigation Management Information System (CIMIS) Weather Stations, Delta Island Consumptive Use (DICU), and Flow Control Structures

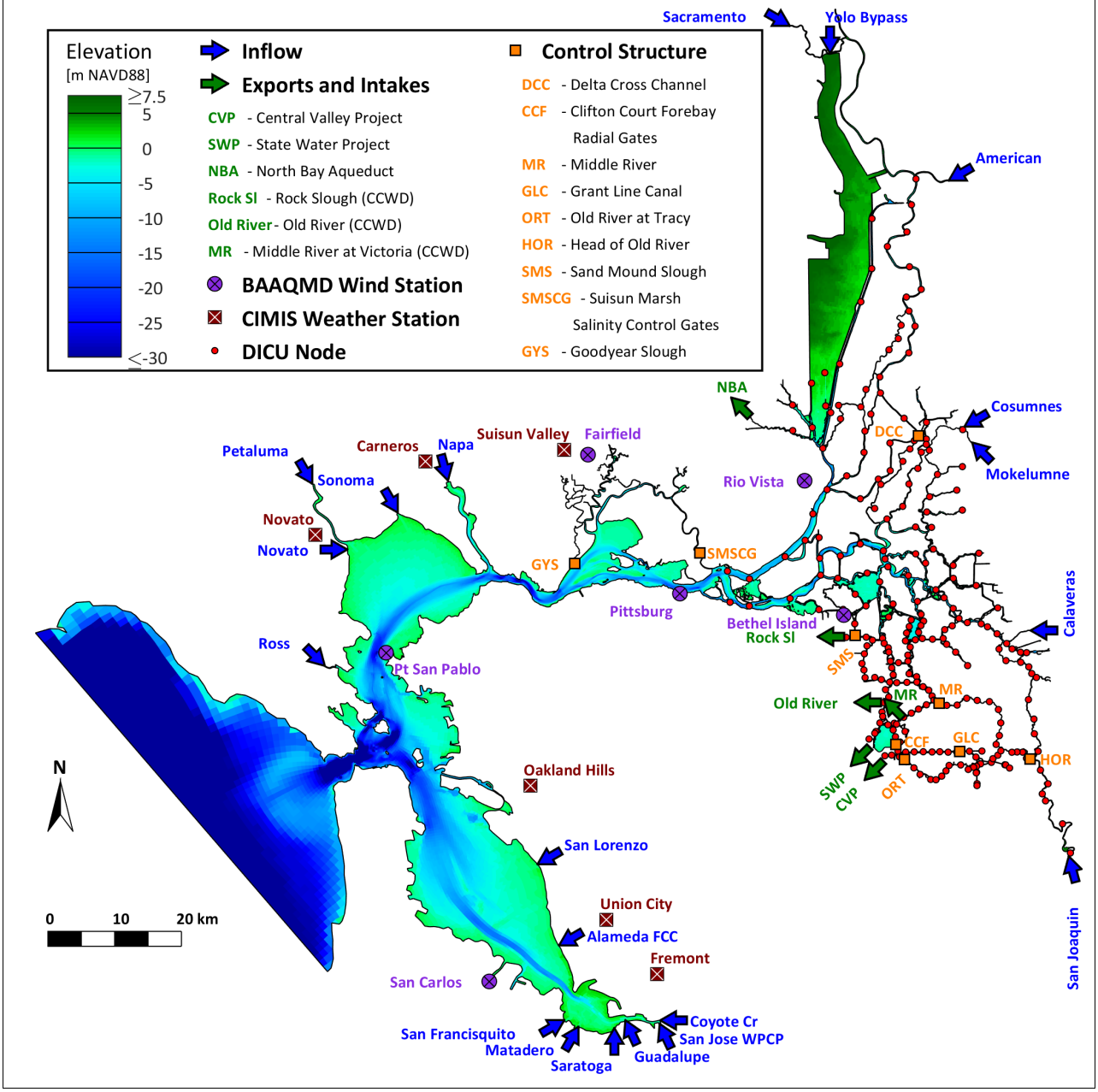

2.1 Golden Gate High-resolution Model Grid

The sediment transport modeling for predicting sediment flux through the Golden Gate used a version of the UnTRIM Bay-Delta model grid that has very high resolution around the Golden Gate (Figure 2-2). This Golden Gate high-resolution model grid has a horizontal resolution down to 20 m in the vicinity of the Golden Gate. The model grid resolves the complex bathymetry around the Golden Gate and even the southern bridge piling (Figure 2-2). The Golden Gate high-resolution model grid is identical to the normal UnTRIM Bay-Delta model grid away from the Golden Gate. This study used the same 90 s model time step as used in the normal UnTRIM Bay-Delta model grid for most of the simulation. A shorter 15 s time step was used during the USGS data collection period to best represent the period of the data collection. Increased computation time with a 15 s time step precluded the use of a 15 s time step for the complete simulation period.

Figure 2-2
Golden Gate High-Resolution Model Grid (left) and Normal UnTRIM Bay-Delta Model Grid (right)

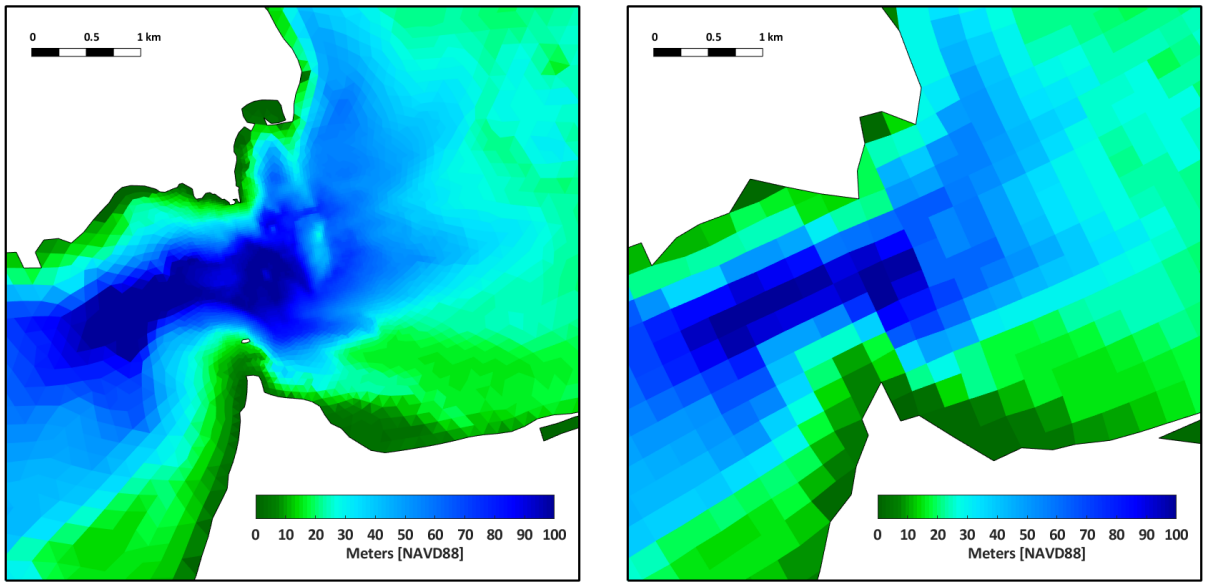

2.2 Sediment Modeling Background

The UnTRIM Bay-Delta model (MacWilliams et al. 2007, 2008, 2009, 2015) has been applied together with the Simulating WAves Nearshore (SWAN) wave model (SWAN Team 2009a) and the SediMorph sediment transport and seabed morphology model (BAW 2005) as a fully coupled hydrodynamic wave-sediment transport model. This coupled modeling system has been used previously to predict sediment transport throughout the Bay-Delta system. Most recently, the model was used to estimate reductions in turbidity throughout Suisun Bay and the confluence region from observed decreases in

the wind speed (Bever et al. 2018). The model has also been applied as part of two projects for USACE to investigate how sea level rise and reduced sediment supply to the Delta impacted sediment routing through the Bay-Delta system and sediment deposition within Suisun and San Pablo bays (MacWilliams et al. 2012b; Bever and MacWilliams 2014). The coupled models were also used to investigate the effects of breaching Prospect Island on regional turbidity and sediment dynamics in the north Delta and Cache Slough region (Delta Modeling Associates 2014). Other applications of the sediment transport model include simulations of dredged material dispersal in the Northern Bay (MacWilliams et al. 2012b) and the South Bay (Bever and MacWilliams 2014; Bever et al. 2014) to determine the fate of dredged material and investigate whether open-water placements can be used to augment mudflat and marsh sedimentation. Bever and MacWilliams (2013) have also applied the coupled modeling system to investigate wave shoaling and sediment fluxes between the channel and shoals in San Pablo Bay. The UnTRIM Bay-Delta model can be used to predict turbidity as well as sediment transport.

The SWAN model (SWAN Team 2009a) is a widely used model for predicting wind wave properties in coastal areas (e.g., Funakoshi et al. 2008). SWAN "represents the effects of spatial propagation, refraction, shoaling, generation, dissipation and nonlinear wave-wave interactions" (SWAN Team 2009b) on wind waves. Therefore, SWAN can estimate the wind waves in coastal regions with variable bathymetry and ambient currents. SWAN can also accommodate spatial variability in bottom friction parameters and wind velocity. In the coupled modeling system, the SWAN model runs on the same unstructured grid as UnTRIM, providing high resolution in areas where it is needed.

The primary purpose of the SediMorph module is to compute the sedimentological processes at the alluvial bed of a free-surface flow, including the following (Weilbeer 2005):

- The roughness of the bed resulting from grain and form roughness (ripples and/or dunes)
- The bottom shear stress as a result of roughness, flow, and waves
- Bed load transport rates (fractioned)
- Erosion and deposition rates (fractioned)
- Bed evolution
- Sediment distribution within the bed exchange layer

SediMorph is designed to use the same horizontal computational mesh as the UnTRIM hydrodynamic model. In the vertical, the SediMorph module allows for evolution of the bed elevation above a pre-defined rigid layer in each cell. Above the rigid layer, SediMorph includes at least one exchange layer, in which sediments are mixed and exchange processes such as erosion and deposition occur. Figure 2-3 shows the horizontal and vertical grid structure of the UnTRIM and SediMorph models and provides a schematic representation of the location of the sediment transport processes within the model grid structures.

Figure 2-3
Horizontal and Vertical Grid Structure of the UnTRIM and SediMorph Models (right); Schematic (left) and Process List (middle) Show the Location of the Sediment Transport Processes Within the Model Grid Structures

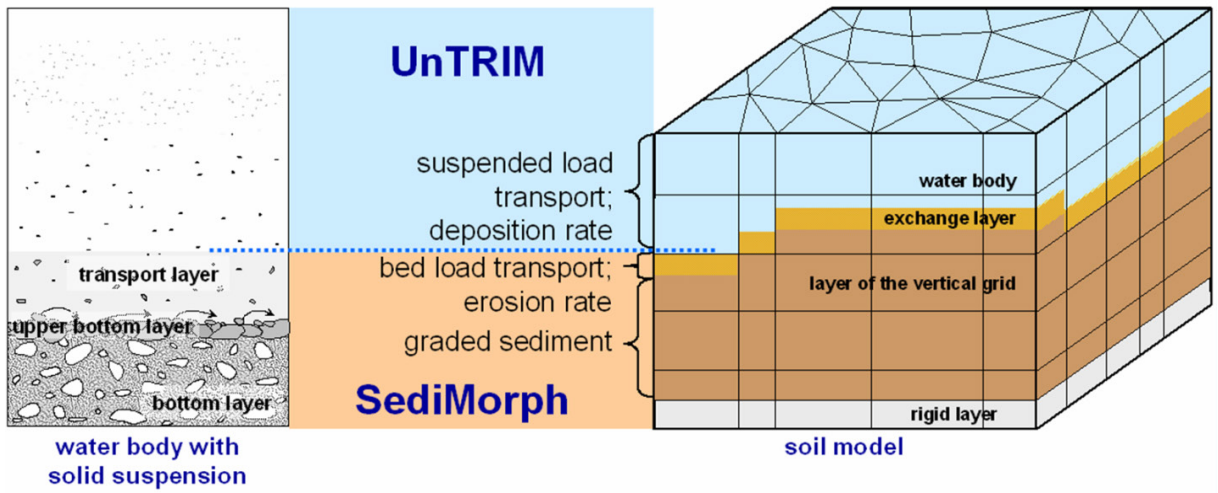

Source: BAW

Sediment transport simulations using the UnTRIM Bay-Delta Model include multiple sediment classes, an initial sediment bed based on over 1,300 observed seabed grain size distributions within the Bay and Delta, sediment input from 11 Bay-Delta tributaries, and wave- and current-driven sediment resuspension and transport. In this coupled modeling system, UnTRIM calculates the flow, water level, and salinity, along with suspended sediment advection, settling, and mixing. SWAN calculates the temporally and spatially varying waves needed for accurate predictions of sediment resuspension in the presence of wind waves. SediMorph calculates the erosion and deposition of sediment and the seabed morphologic change and keeps track of the sedimentological properties within the seabed. The model bathymetry in each grid cell is adjusted each time step to account for erosion and deposition. The configuration of the coupled modeling system, the sediment transport model, and model inputs used in this study is nearly identical to that described in Bever et al. (2018). The one exception is that an additional sediment class was added to the tributary inflows before this study to improve the predicted SSC and turbidity in the Delta (Table 2-1). This sediment class represents very fine sediments that settle very slowly.

Table 2-1
Sediment Class Characteristics

Sediment Class	Settling Velocity (mm/s)	Critical Shear Stress (Pa)	Diameter	Density (kg/m^3)	Erosion Rate Parameter (kg/m^2s)
Fine Silt	0.001	0.0379	11 µm	2,650	$2.5x10^{-5}$ to $10x10^{-5}$
Silt	0.038	0.0379	11 µm	2,650	$2.5x10^{-5}$ to $10x10^{-5}$
Flocculated Silt and Clay	2.25	0.15	200 µm	1,300	$3x10^{-5}$ to $12x10^{-5}$
Sand	23	0.19	250 µm	2,650	$5x10^{-5}$ to $20x10^{-5}$
Gravel	NA	NA	8 mm	2,650	NA

2.3 Sediment Model-Data Comparisons

The SWAN wave results have been calibrated and validated to observed wave properties in San Pablo Bay and Suisun Bay and at four locations south of Dumbarton Bridge. The sediment transport within the coupled modeling system has been calibrated using a variety of observed data, including SSC time series at multiple locations within the Bay, continuous monitoring stations within Suisun Bay and the Delta, and vertical profiles of SSC along a transect along the axis of the Bay from the far South Bay to Rio Vista. The model has also been validated through comparison of observed and predicted deposition within a breached salt pond during the period following the initial breach (Bever and MacWilliams 2014). Turbidity has been validated using continuous monitoring time series in the Bay and Delta and surface remotely sensed data (Anchor QEA 2017; Bever et al. 2018). The sediment validation demonstrates that the coupled hydrodynamic-wind wave-sediment model is accurately capturing the dominant processes that resuspend, deposit, and transport sediment throughout the Bay-Delta system and would therefore be suitable for predicting SSC throughout the Bay-Delta. A detailed validation of predicted SSC using time series at discrete locations and vertical profiles spanning from the far South Bay to Rio Vista is presented in Appendix A. Validation of predicted velocity, SSC, water flux, and sediment flux to the USGS estimates along the transects near the Golden Gate is presented in Section 4.

3 Model Simulation Period and Analysis

This section describes the model simulation and analysis period and the analyses for calculating water flow and sediment flux through the Golden Gate.

3.1 Model Simulation Period

This study evaluated sediment flux through the Golden Gate from December 1, 2016, through April 15, 2017. The model was initialized on July 27, 2016, allowing 4 months for spin-up prior to the beginning of the analysis period. The December 2016 to mid-April 2017 period completely spans the period of high Delta outflow that occurred from about January 4 through March 12, 2017. This period of high outflow is collectively referred to as the "2017 high outflow period" in this report since it spans the sediment pulse associated with the periods of high Delta outflow in water year 2017. The analysis time period provides about 1 month before and after the 2017 high outflow period for evaluating predicted sediment flux before, during, and after the high Delta outflows (Figure 3.1-1).

The 4.5-month time period of this study is a difficult period both to collect observational data for and to model. The large freshet and associated meteorology in 2017 create a complex set of conditions that influence net (tidal-averaged) flows through the Golden Gate, sediment supply from Delta and Bay tributaries, wind-wave resuspension, and salinity stratification throughout the Bay. These various factors all interact with the regular tidal movement of water and sediment to result in the net sediment flux through the Golden Gate over the study period. Due to the complexity of the system, especially on the trailing limb of a period of high Delta outflow, it is not expected that the model predictions and USGS data collected on February 27 and 28, 2017 (summarized in Section 3.2), will match exactly. The similarities and differences between the observed data and model predictions are explored in this document to better understand the observed data and the model predictions.

Figure 3.1-1
Time Series of Dayflow Delta Outflow During the Analysis Period in Water Year 2017

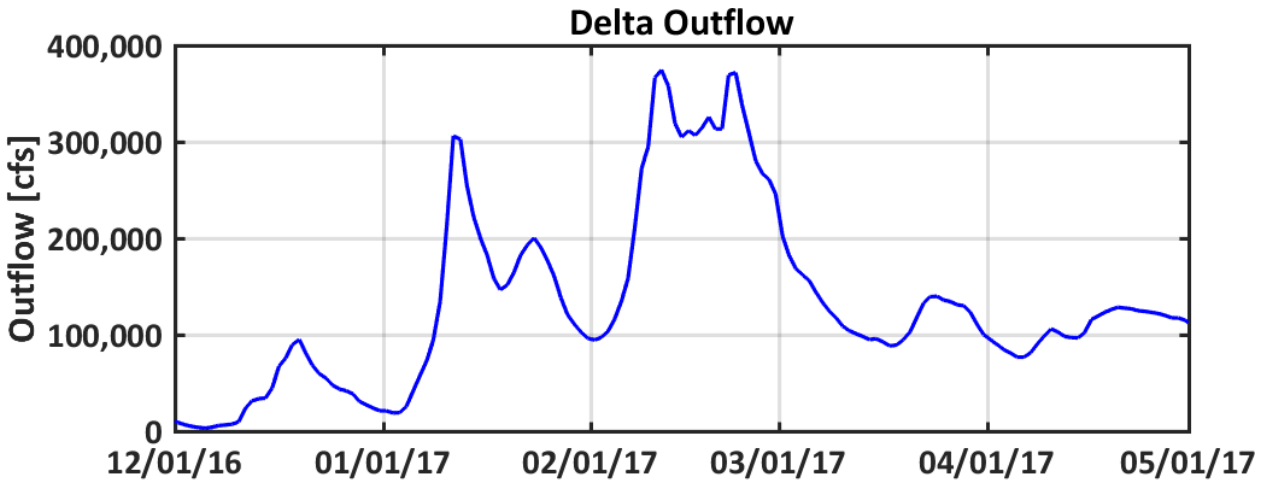

3.2 Summary of USGS Data Collection and Analysis

On February 27 and 28, 2017, USGS conducted boat-based sampling to estimate the sediment flux through the Golden Gate over a complete tidal cycle on the trailing end of the 2017 high Delta outflow period (Downing-Kunz et al. 2017). A total of 32 transects across the Golden Gate were conducted over a period of 16.5 hours, with each transect spanning about 20 minutes. The transects were located to the east of the Golden Gate where the water is shallower than directly under the Golden Gate (Figure 3.2-1). A boat-mounted acoustic Doppler current profiler (ADCP) was used to collect vertical profiles of current velocity and acoustic backscatter during each of the transects. Water samples were collected to develop a calibration curve that relates acoustic backscatter to SSC, and the acoustic backscatter from the ADCP was then converted to SSC.

Figure 3.2-1
General Path of USGS Data Collection Transects

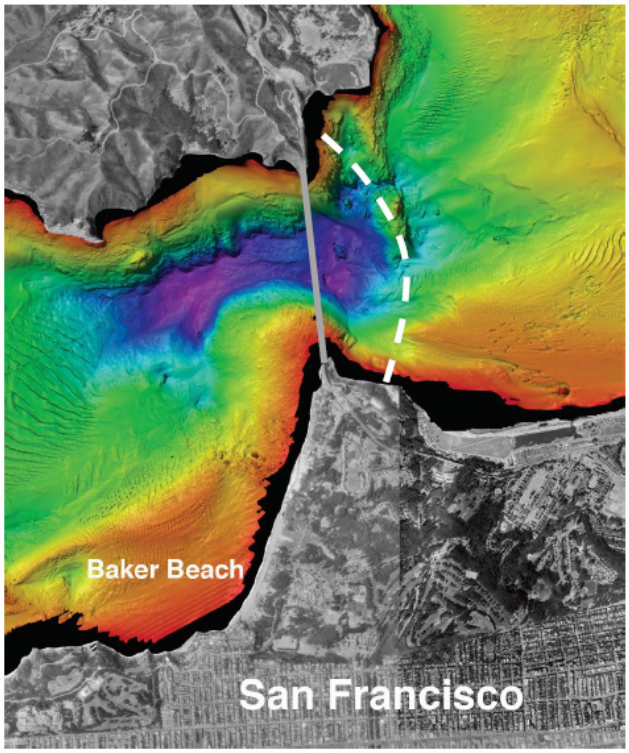

Note: The dashed line represents the general path of the USGS data collection transects. Figure from Downing-Kunz et al. (2017).

Velocity data from the ADCP were processed to determine the velocity perpendicular to the boat track. The vertical profiles of the velocity perpendicular to the boat track were used to estimate the total water flux through the transect and were assumed to equal the water flux between the Bay and the Pacific Ocean. The velocity perpendicular to the boat track was multiplied by the SSC to estimate the sediment flux in each vertical ADCP bin. The sediment flux was summed vertically and along the transect to estimate the total sediment flux through the transect and assumed to equal the sediment flux between the Bay and the Pacific Ocean. Summing the water and sediment fluxes over the ebb and flood portions of the tide resulted in a net water flux out of the Bay but a net sediment flux into the Bay. That is, more sediment was estimated to be imported to the Bay on flood tide than was exported on ebb tide. These USGS estimated values are referred to in this report as the data-based ADCP water and sediment fluxes. Anchor QEA, LLC, discussed the details of the processing methods with USGS. USGS provided the MATLAB script that was used to process the ADCP data and the resulting water and sediment fluxes through the transects to aid Anchor QEA's analysis of sediment transport model output.

3.3 Analysis of Predicted Water and Sediment Fluxes

Model-based ADCP water and sediment fluxes were calculated from the model output in the same manner as the data-based water and sediment fluxes. Current velocities and SSC were extracted from the 3D model at the same times and locations as they were observed by USGS along the ADCP transects. That is, at the time of each ADCP ensemble the predicted current velocity at the horizontal location of the ADCP measurement was saved at the vertical resolution of the model, creating predicted velocity and SSC transects at the same times and locations as the observed velocity. Because the ADCP observations were at a finer resolution than the numerical model grid, the horizontal velocities at each ADCP profile location were interpolated from the velocities on the surrounding grid cell faces. The predicted SSC was set as the SSC in the corresponding 3D model grid cell.

The model-based ADCP transects were processed using the same methods as USGS used to process the ADCP data. The resulting model-based ADCP water and sediment fluxes were compared to the data-based ADCP water and sediment fluxes.

A cross section spanning the narrowest portion of the Golden Gate was added to the model output and used to track the predicted cross-sectional water and sediment fluxes through the Golden Gate over the duration of the analysis period (December 1, 2016, through April 15, 2017). The predicted cross-sectional water and sediment fluxes are the total predicted fluxes between the Bay and the Pacific Ocean. They are a summation across each model grid face at each time step of the water flow and sediment flux crossing through the Golden Gate in the model. The use of the term "predicted cross-sectional flux" is meant to distinguish the fluxes actually calculated by the model from the fluxes calculated using the model-based ADCP approach. These predicted cross-sectional fluxes were compared to the model-based ADCP water and sediment fluxes. This comparison examines how the fluxes calculated using the ADCP method compared to the total predicted cross-sectional water and sediment fluxes. Any differences between the predicted cross-sectional fluxes and the model-based ADCP fluxes can be used to provide insight into any biases that may arise from the ADCP calculation method or from sampling along the arc to the east of the Golden Gate rather than across the shortest straight-line cross section (Figure 3.2-1).

The predicted cross-sectional sediment flux was also extracted from the model at Benicia Bridge, Point San Pablo, and the Bay Bridge. These predicted sediment fluxes, along with the Golden Gate cross section, were used to determine the predicted sediment flux between the various subembayments of San Francisco Bay. The predicted net sediment flux between the embayments was calculated at these cross section locations for periods before (December 1, 2016, to January 3, 2017), during (January 4 through March 12, 2017), and after (March 13 to April 15, 2017) the 2017 high Delta outflow period.

4 Comparison of Predicted and Observed Acoustic Doppler Current Profiler Transects

Predicted velocity perpendicular to the boat track and predicted SSC were compared to the corresponding values from the USGS data. The presented cross sections span the entire tidal cycle, from maximum ebb-directed flow to maximum flood-directed flow. Model-based ADCP water and sediment fluxes were also compared to the data-based ADCP fluxes. These comparisons provide a general understanding of the predicted versus observed velocity, SSC, water flux, and sediment flux along the USGS ADCP transects.

4.1 Velocity Cross Sections

Figures 4.1-1 through 4.1-8 compare the predicted velocity perpendicular to the boat track from the model to the corresponding velocity from the ADCP data. The top panel is the observed velocity and the middle panel is the predicted velocity. The lower left panel is a map of the transect location and the lower right panel is the predicted water flow through the Golden Gate. Figures 4.1-1 through 4.1-8 span a complete tidal cycle and are representative of the 32 transects observed over the full sampling period.

Near slack water at the start of ebb-directed flow, the observed and predicted velocities were relatively low and there was not a consistent flow direction (Figure 4.1-1). That is, velocities over some of the transect were in the ebb direction and some were in the flood direction. During increasing ebb-directed flow, both the observed and predicted velocities were consistently in the ebb direction over the majority of the transect (Figure 4.1-2). Both the observed and predicted velocities were quite low near the northern end of the transect (right side of figure) but had the greatest magnitude right near the edge of this low velocity zone. Near maximum ebb-directed flow, observed and predicted velocities were relatively high over the majority of the transect and generally in the ebb direction (Figure 4.1-3). Similar to during increasing ebb-directed flow, velocities were quite low or even in the flood direction near the northern end of the transect (right side of figure) but had the greatest magnitude right near the edge of this low velocity zone. During decreasing ebb-directed flow, the majority of the observed and predicted velocities were in the ebb direction (Figure 4.1-4). Similar to other transects during ebb-directed flow, velocities were quite low near the northern end of the transect (right side of figure). During ebb tide, a region of strong flood-directed velocities was evident in the observed and predicted velocity at the southern end of the transect (left side of Figure 4.1-4), which we interpreted to be from a recirculating horizontal eddy at the southern end of the transect near the San Francisco shoreline. This region of flood-directed flow at the southern end of the transect occurred in five of the ebb tide transects. The effect of this eddy is explored in more detail in Section 5.3.2.

Near slack water at the start of flood-directed flow, the observed and predicted velocities were relatively low and there was not a consistent flow direction (Figure 4.1-5). That is, velocities over some of the transect were in the flood direction and some of the velocities were in the ebb direction. During increasing flood-directed flow, both the observed and predicted velocities were consistently in the flood direction over the majority of the transect (Figure 4.1-6). Observed and predicted velocities were relatively low at the northern end of the transect. Both the observed and predicted velocities were also relatively low in the center of the transect, around 1,600 to 2,000 m along the transect. Near maximum flood-directed flow, observed and predicted velocities were relatively high over the majority of the transect and generally in the flood direction (Figure 4.1-7). Observed and predicted velocities were relatively low at the northern end of the transect. The predicted velocity was higher than observed at the southern end of the transect. During decreasing flood-directed flow, both the observed and predicted velocities showed flood-directed flow in the center of the cross section and the transition to slower velocity and ebb-directed velocity near the ends of the transect (Figure 4.1-8)

Overall, the temporal and spatial patterns in the observed velocity were captured in the predicted velocity. Both the observed and predicted velocities showed a region of relatively low velocity at the northern end of the transects. Both the observed and predicted velocities showed a region of flood-directed flow at the southern end of the transect during decreasing ebb-directed flows, which is believed to result from a large recirculating eddy. Overall, the magnitudes of the observed velocity were captured in the predicted velocity, even though predicted velocity slightly underpredicted the observed velocity, most notably during periods of high flow and in the flood direction.

Figure 4.1-1
Observed (top) and Predicted (middle) Velocity on February 27, 2017, Around 12:59 near Slack Water at the Start of Ebb-Directed Flow

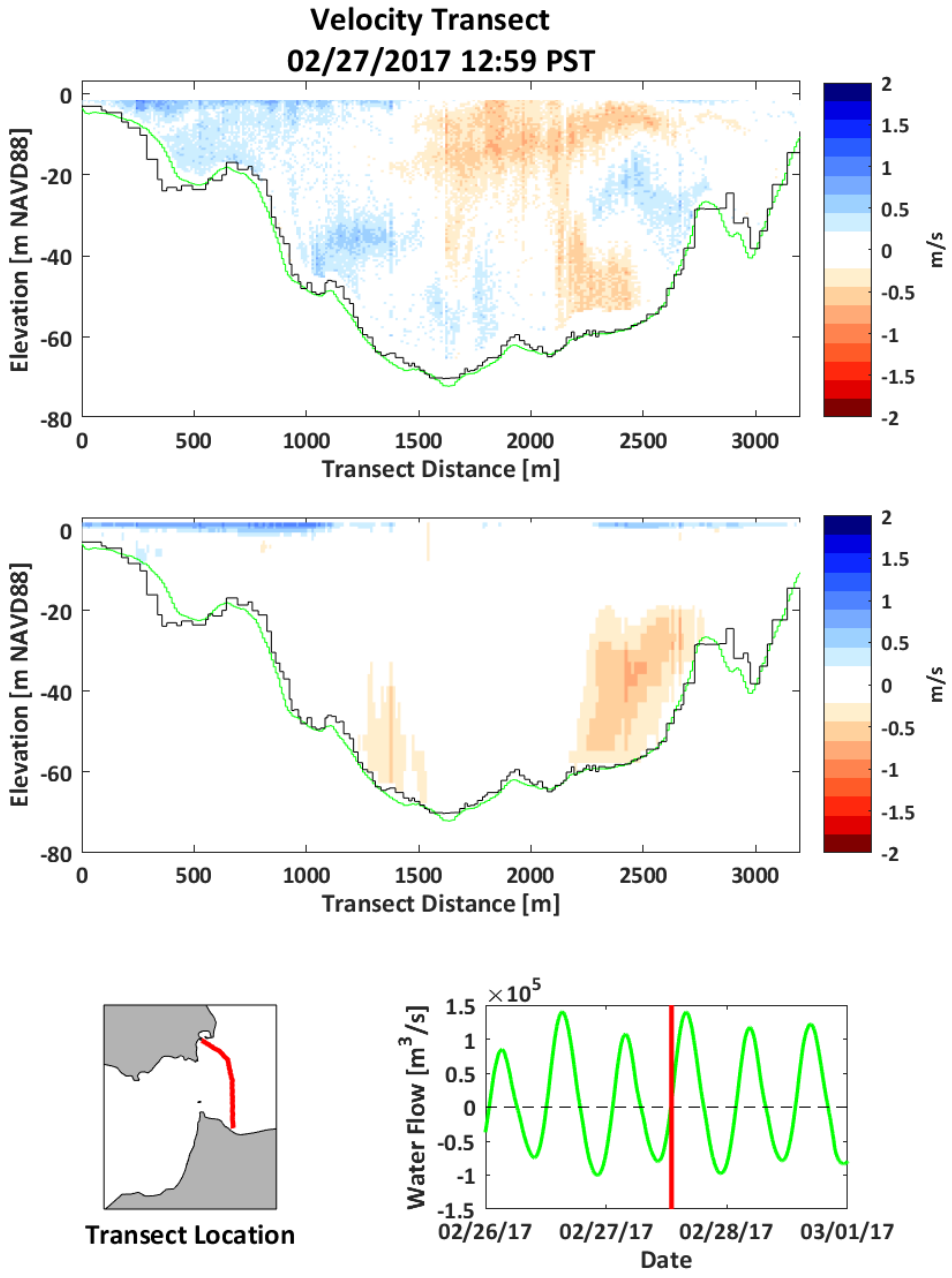

Notes: Figure shows velocities perpendicular to the boat track. Positive velocity is toward the west out of the Bay, and the left side of the upper panels corresponds to the southern end of the transect shown in the lower left panel. The lower right panel shows the water flow (positive out of the Bay). The seabed from the ADCP data is shown by the green line and from the model bathymetry by the black line.

Figure 4.1-2
Observed (top) and Predicted (middle) Velocity on February 27, 2017, Around 14:16 During Increasing Ebb-Directed Flow

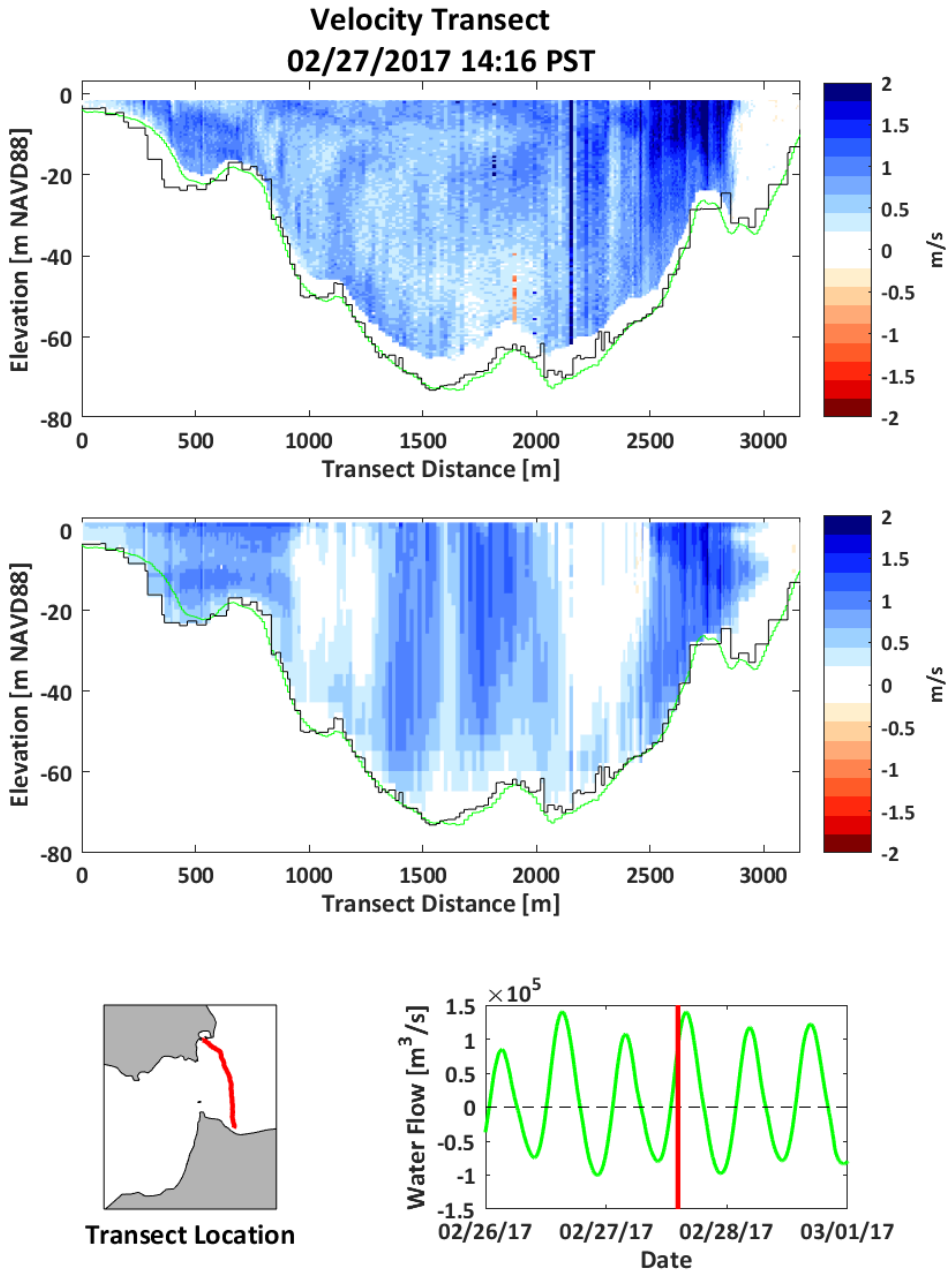

Notes: Figure shows velocities perpendicular to the boat track. Positive velocity is toward the west out of the Bay, and the left side of the upper panels corresponds to the southern end of the transect shown in the lower left panel. The lower right panel shows the water flow (positive out of the Bay). The seabed from the ADCP data is shown by the green line and from the model bathymetry by the black line.

Figure 4.1-3
Observed (top) and Predicted (middle) Velocity on February 27, 2017, Around 15:28 near Maximum Ebb-Directed Flow

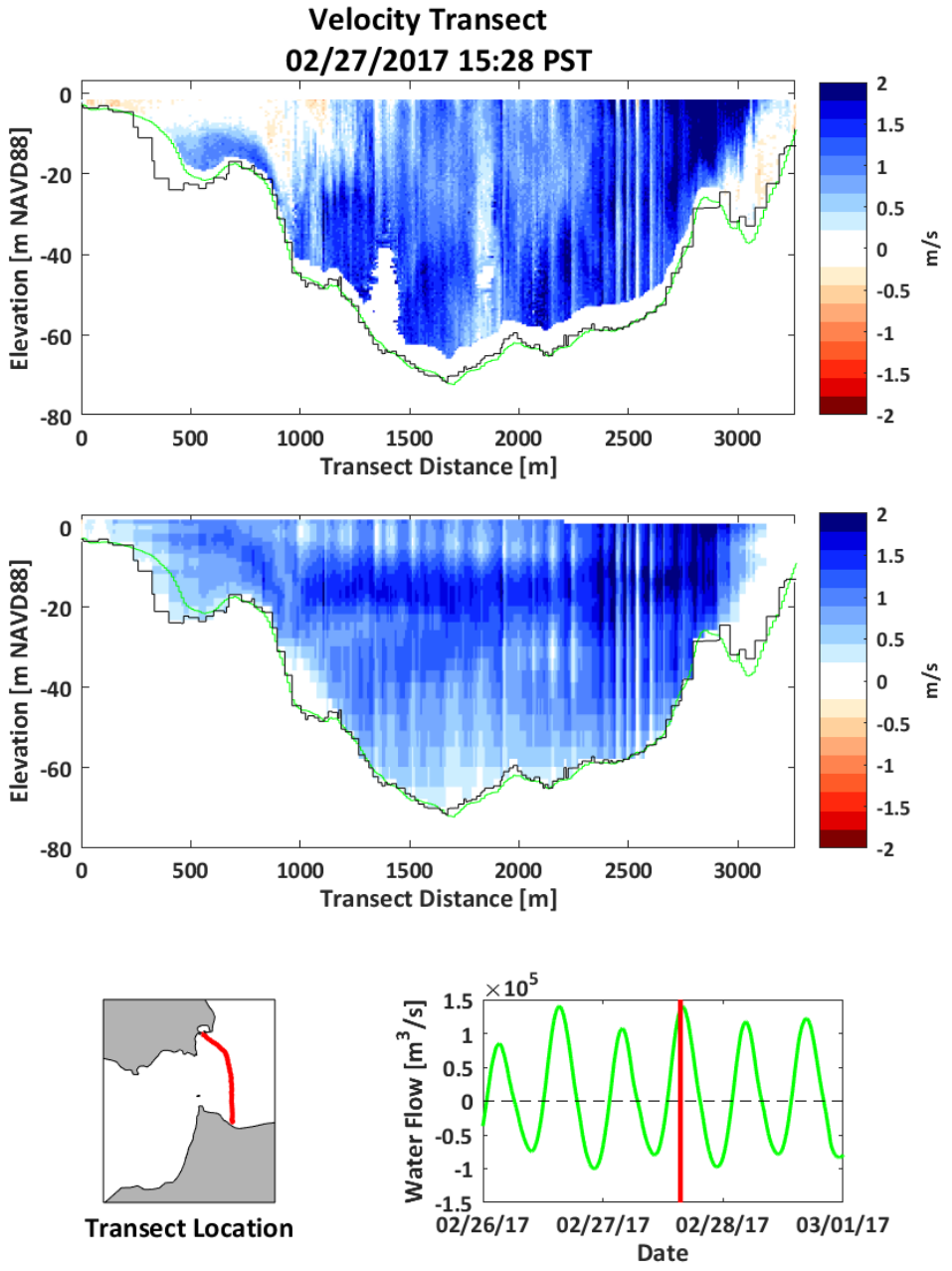

Notes: Figure shows velocities perpendicular to the boat track. Positive velocity is toward the west out of the Bay, and the left side of the upper panels corresponds to the southern end of the transect shown in the lower left panel. The lower right panel shows the water flow (positive out of the Bay). The seabed from the ADCP data is shown by the green line and from the model bathymetry by the black line.

Figure 4.1-4
Observed (top) and Predicted (middle) Velocity on February 27, 2017, Around 18:01 During Decreasing Ebb-Directed Flow

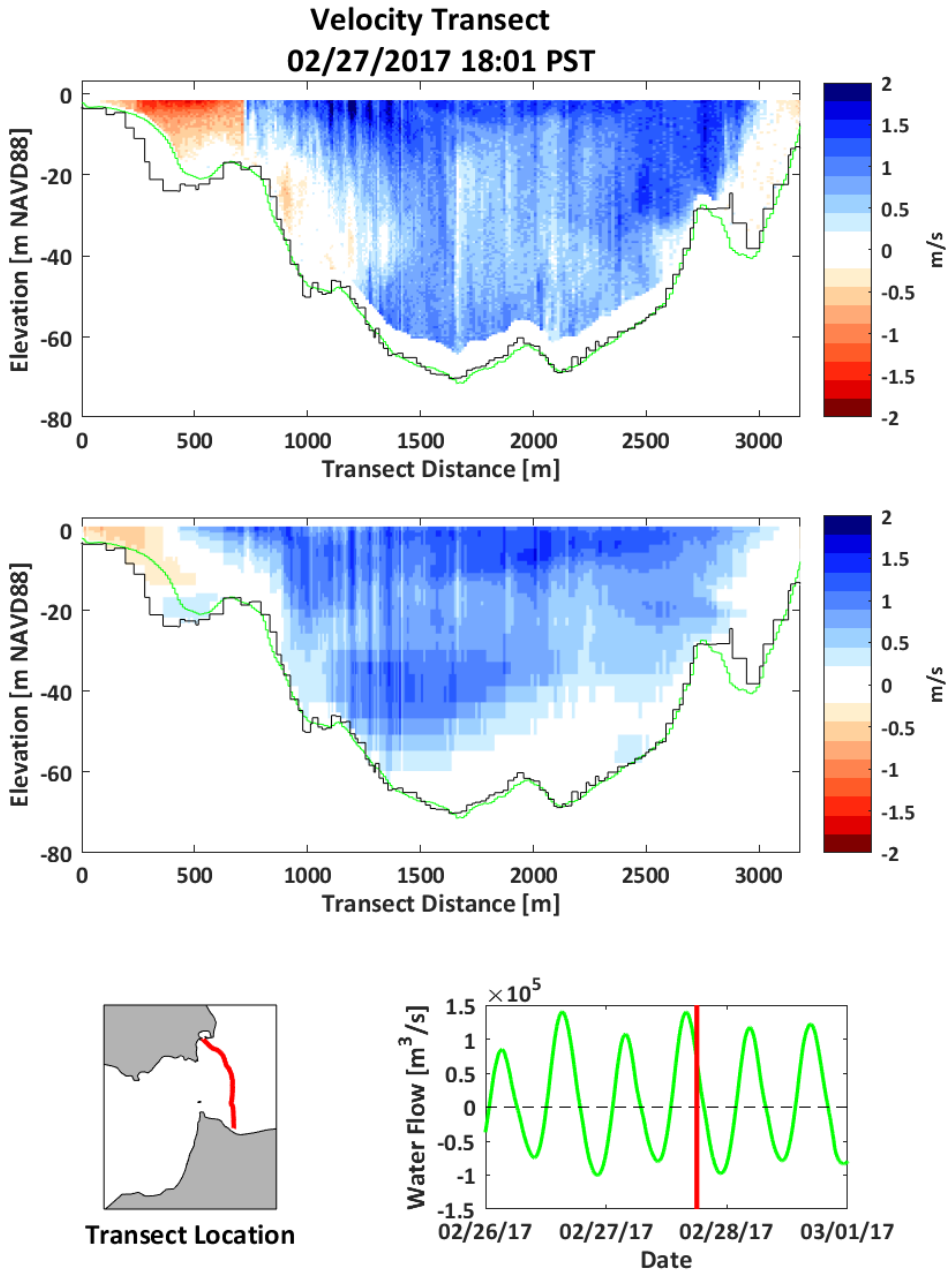

Notes: Figure shows velocities perpendicular to the boat track. Positive velocity is toward the west out of the Bay, and the left side of the upper panels corresponds to the southern end of the transect shown in the lower left panel. The lower right panel shows the water flow (positive out of the Bay). The seabed from the ADCP data is shown by the green line and from the model bathymetry by the black line.

Figure 4.1-5
Observed (top) and Predicted (middle) Velocity on February 27, 2017, Around 20:00 near Slack Water at the Start of Flood-Directed Flow

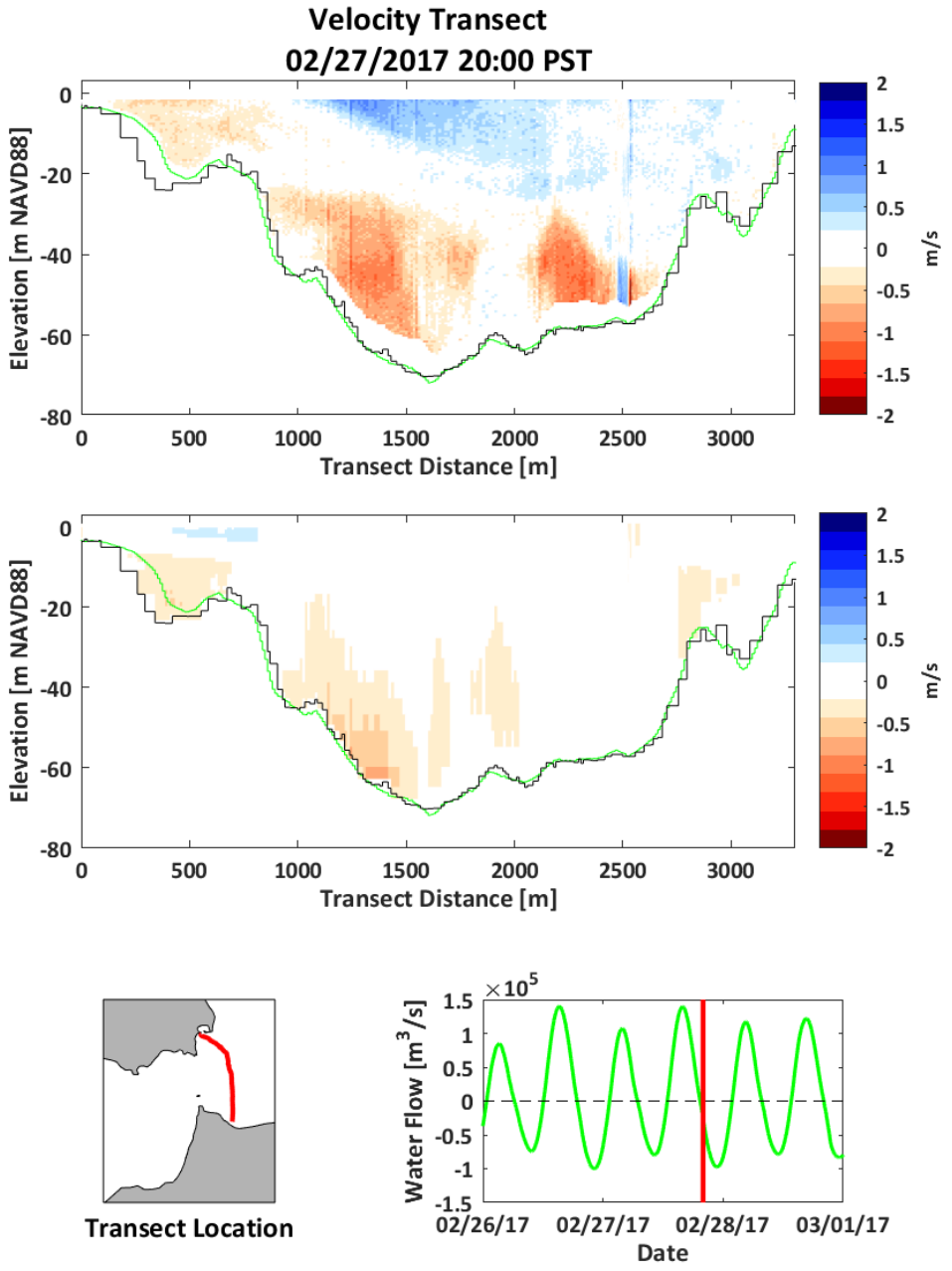

Notes: Figure shows velocities perpendicular to the boat track. Positive velocity is toward the west out of the Bay, and the left side of the upper panels corresponds to the southern end of the transect shown in the lower left panel. The lower right panel shows the water flow (positive out of the Bay). The seabed from the ADCP data is shown by the green line and from the model bathymetry by the black line.

Figure 4.1-6
Observed (top) and Predicted (middle) Velocity on February 27, 2017, Around 20:47 During Increasing Flood-Directed Flow

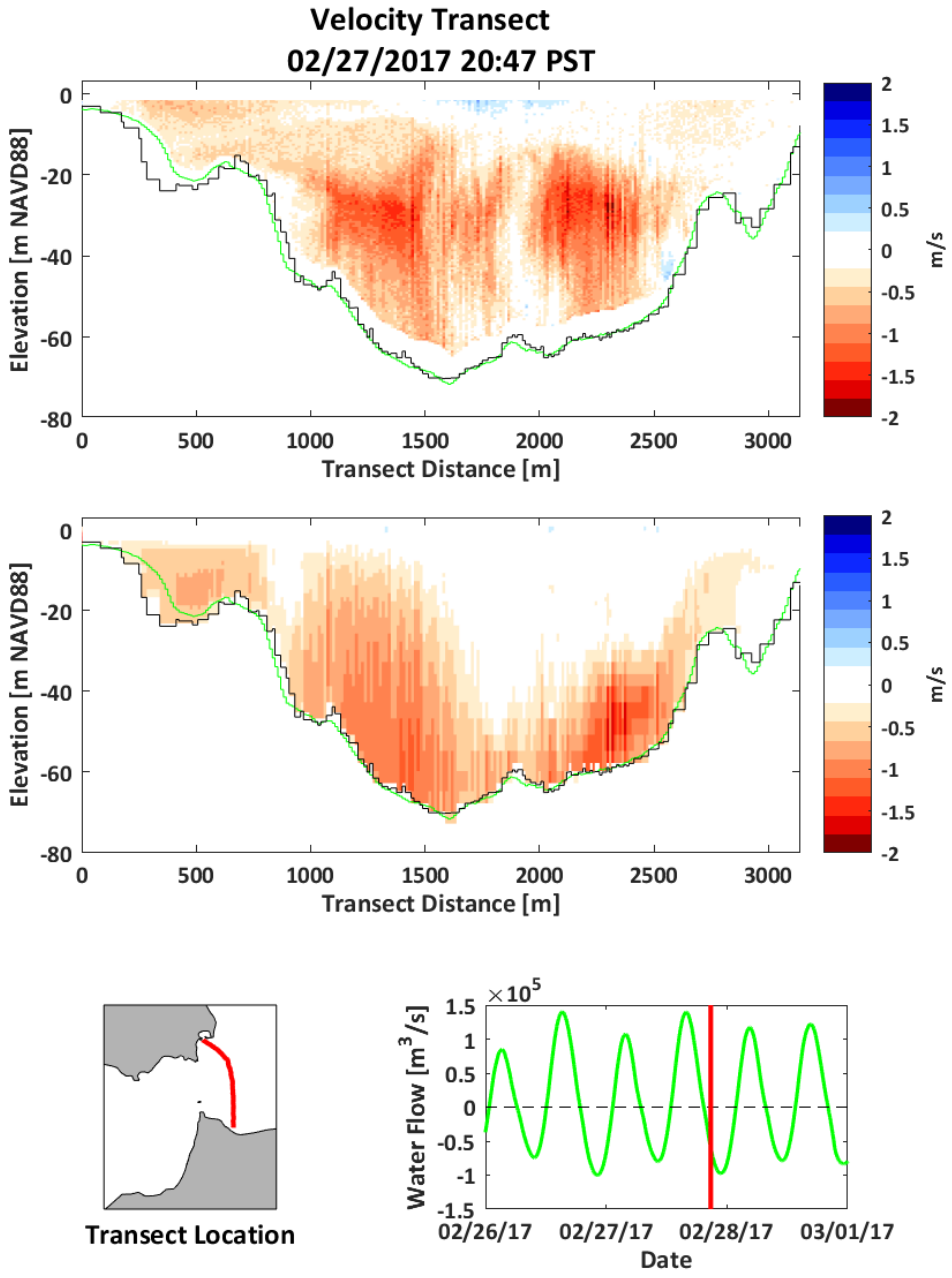

Notes: Figure shows velocities perpendicular to the boat track. Positive velocity is toward the west out of the Bay, and the left side of the upper panels corresponds to the southern end of the transect shown in the lower left panel. The lower right panel shows the water flow (positive out of the Bay). The seabed from the ADCP data is shown by the green line and from the model bathymetry by the black line.

Figure 4.1-7
Observed (top) and Predicted (middle) Velocity on February 27, 2017, Around 22:30 near Maximum Flood-Directed Flow

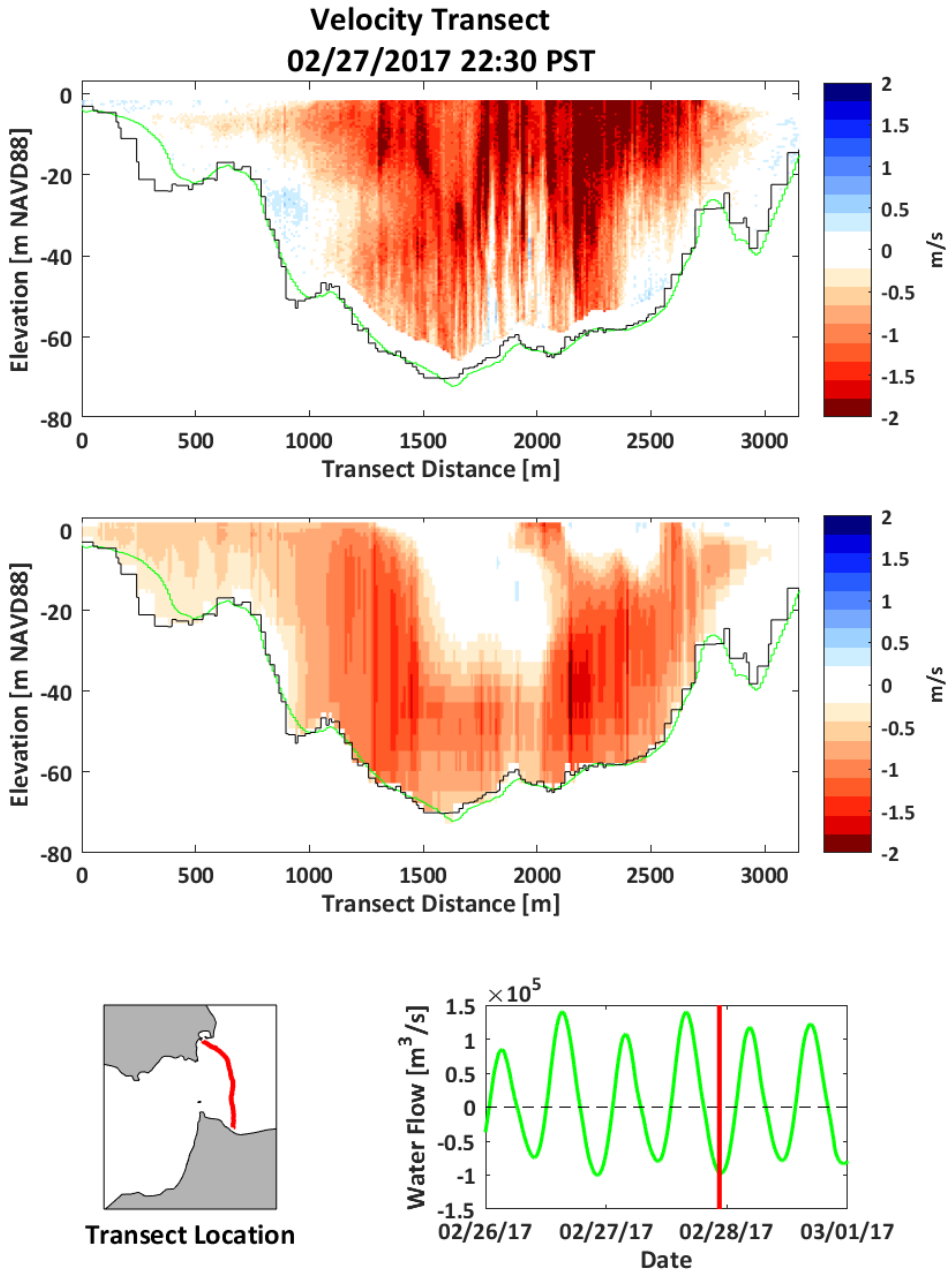

Notes: Figure shows velocities perpendicular to the boat track. Positive velocity is toward the west out of the Bay, and the left side of the upper panels corresponds to the southern end of the transect shown in the lower left panel. The lower right panel shows the water flow (positive out of the Bay). The seabed from the ADCP data is shown by the green line and from the model bathymetry by the black line.

Figure 4.1-8
Observed (top) and Predicted (middle) Velocity on February 28, 2017, Around 01:06 During Decreasing Flood-Directed Flow

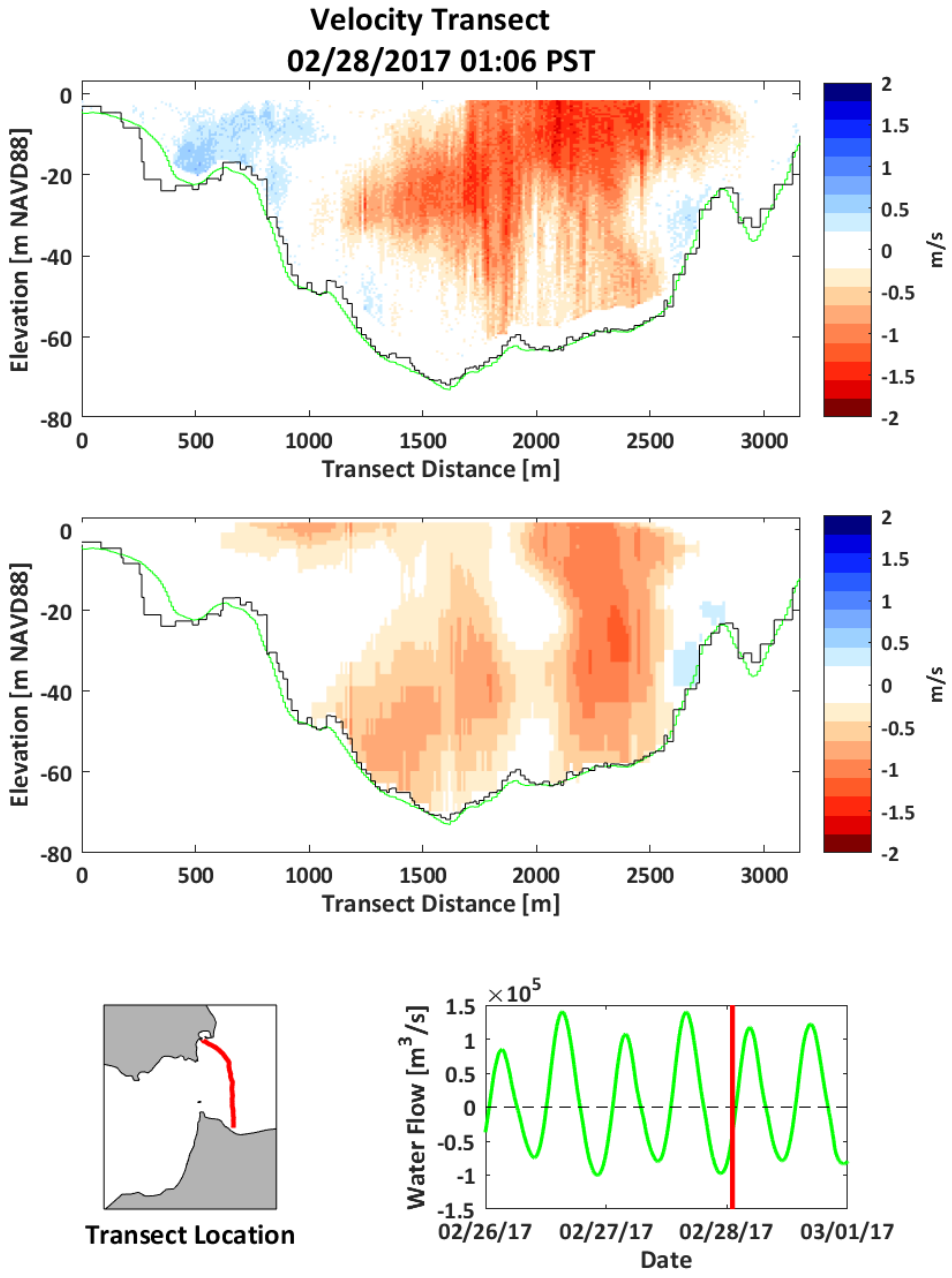

Notes: Figure shows velocities perpendicular to the boat track. Positive velocity is toward the west out of the Bay, and the left side of the upper panels corresponds to the southern end of the transect shown in the lower left panel. The lower right panel shows the water flow (positive out of the Bay). The seabed from the ADCP data is shown by the green line and from the model bathymetry by the black line.

4.2 SSC Cross Sections

Figures 4.2-1 through 4.2-8 compare the predicted SSC along the USGS transects to the corresponding SSC estimated from the ADCP data. The top panel is the observed SSC and the middle panel is the predicted SSC. The lower left panel is a map of the transect location and the lower right panel is the predicted water flow through the Golden Gate. Figures 4.2-1 through 4.2-8 span a complete tidal cycle and are representative of the 32 transects observed over the full sampling period. The cross section averaged SSC for each of the 32 transects was averaged to evaluate the overall average difference between the observed and predicted SSC. Predicted SSC matched the observed SSC very well when averaged over the 32 transects, with an average predicted SSC of 46.8 mg/L and average observed SSC of 47.9 mg/L.

Individual transects were further used to evaluate similarities and differences between the observed and predicted SSC. Near slack water at the start of ebb-directed flow, the observed and predicted SSC were relatively low, with the predicted SSC on average lower than the observed SSC (Figure 4.2-1). Both the observed and predicted SSC were higher on the northern end (right side of figure) of the transect than in the center. The observed and predicted SSC were also relatively well mixed throughout the water column. Observed and predicted SSC during increasing ebb-directed flow were similar to those near slack water (Figure 4.2-2). Observed and predicted SSC increased during maximum ebb-directed flow (Figure 4.2-3). The observed SSC at this time has more spatial variability than the predicted SSC. Predicted SSC continued to increase through decreasing ebb-directed flow (Figure 4.2-4) to near slack water before flood (Figure 4.2-5), yet the observed SSC decreased. Predicted and observed SSC were relatively similar during increasing flood-directed flow (Figure 4.2-6). However, during increasing flood-directed flow, the predicted SSC along the transect was decreasing through time while the observed SSC was increasing. Near peak flood-directed flow, the observed SSC was higher than the predicted SSC and had a large amount of vertical stratification in the SSC that was not captured by the predicted SSC (Figure 4.2-7). Observed and predicted SSC then decreased during decreasing flood-directed flow (Figure 4.2-8).

Overall, predicted SSC was similar magnitude to the observed SSC estimated from the ADCP backscatter data. Of the 32 ADCP transects, the predicted cross-sectional average SSC was within 5 mg/L of the observed SSC for seven transects. Predicted cross-sectional average SSC was more than 5 mg/L lower than the observed SSC for 16 transects and more than 5 mg/L higher than the observed SSC for nine transects. Predicted SSC reproduced some of the spatial and temporal patterns in the observed SSC but had less variability along each transect than the observed SSC. Observed SSC decreased abruptly around slack after ebb, which the predicted SSC did not capture. Observed SSC tended to be higher lower in the water column, while predicted SSC tended to be higher more toward the surface. This may result from the predicted SSC at the ADCP transect location increasing as fresher and relatively higher SSC water from in the Bay moves past the transect location on ebb tide.

Figure 4.2-1
Observed (top) and Predicted (middle) SSC on February 27, 2017, Around 12:59 near Slack Water at the Start of Ebb-Directed Flow

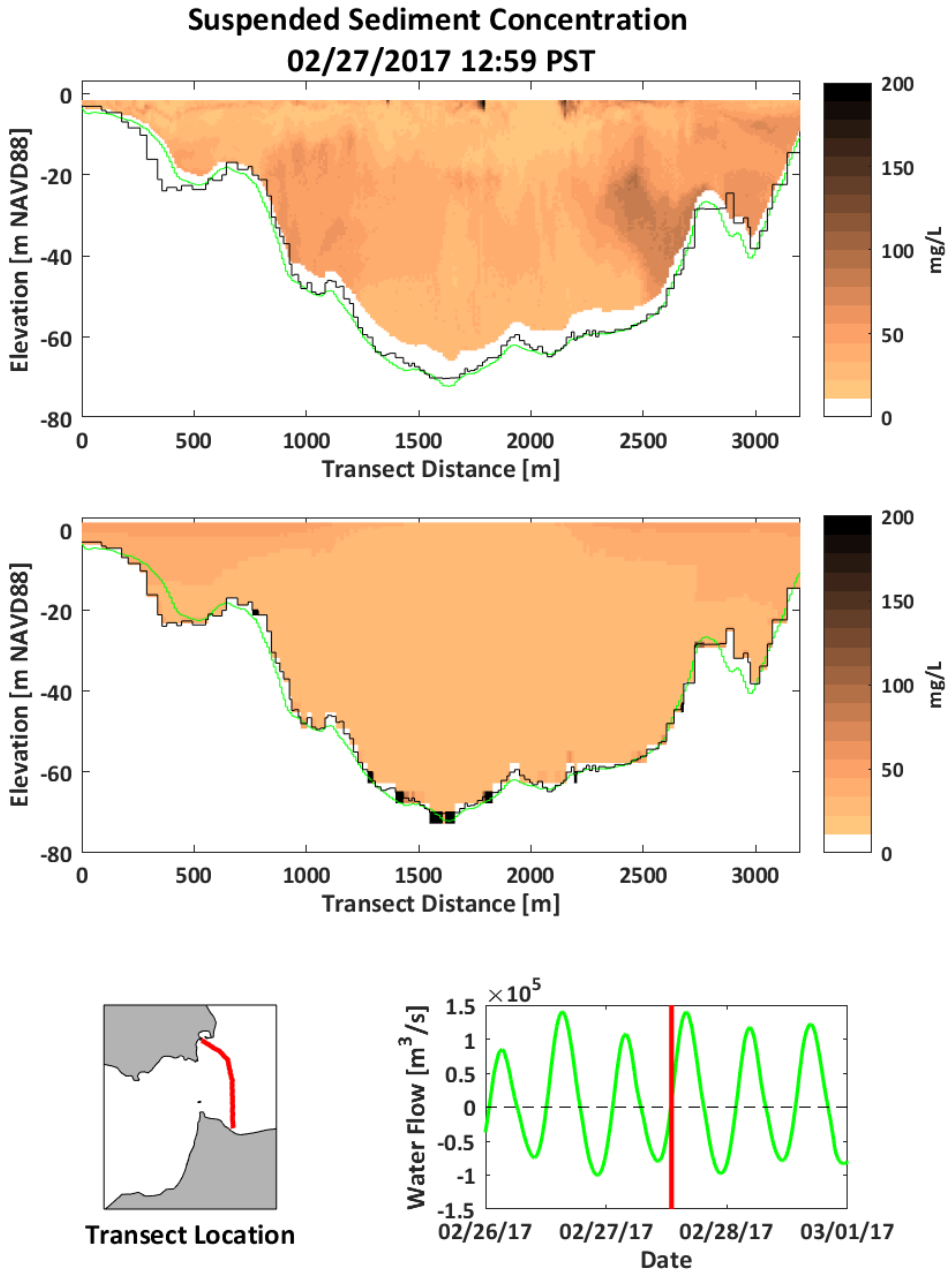

Notes: The left side of the upper panels corresponds to the southern end of the transect shown in the lower left panel. The lower right panel shows the water flow (positive out of the Bay). The seabed from the ADCP data is shown by the green line and from the model bathymetry by the black line.

Figure 4.2-2
Observed (top) and Predicted (middle) SSC on February 27, 2017, Around 14:16 During Increasing Ebb-Directed Flow

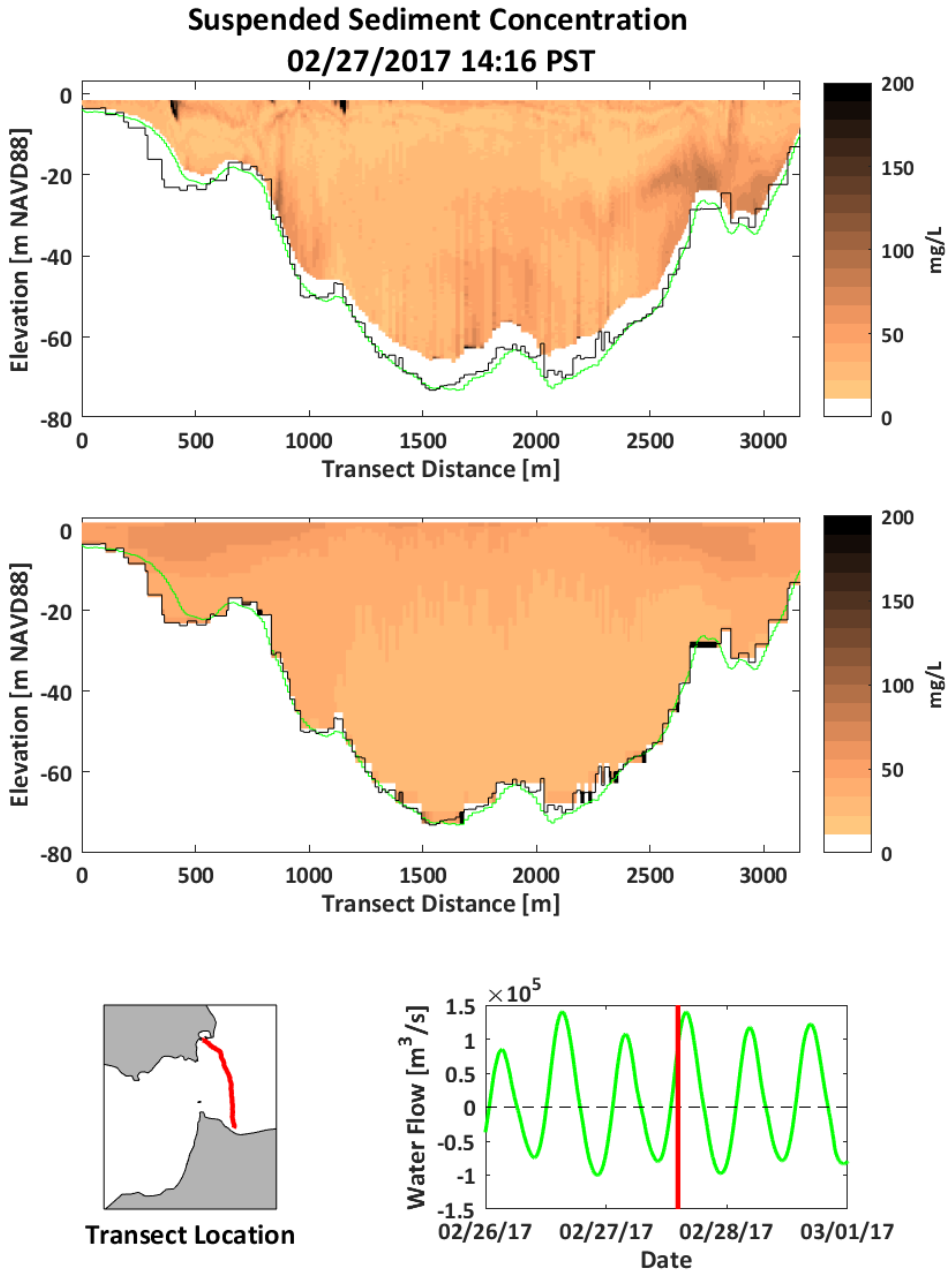

Notes: The left side of the upper panels corresponds to the southern end of the transect shown in the lower left panel. The lower right panel shows the water flow (positive out of the Bay). The seabed from the ADCP data is shown by the green line and from the model bathymetry by the black line.

Figure 4.2-3
Observed (top) and Predicted (middle) SSC on February 27, 2017, Around 15:28 near Maximum Ebb-Directed Flow

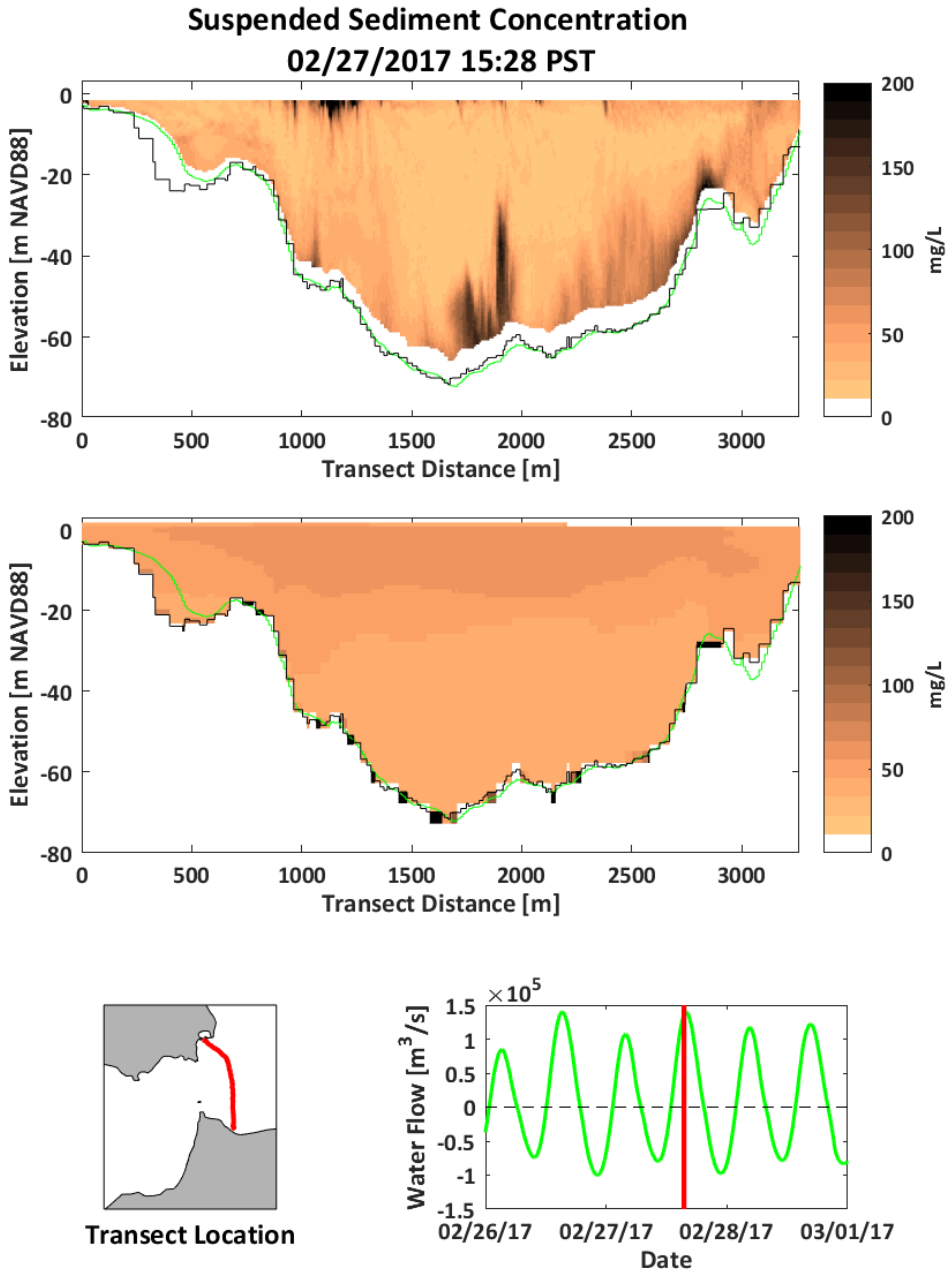

Notes: The left side of the upper panels corresponds to the southern end of the transect shown in the lower left panel. The lower right panel shows the water flow (positive out of the Bay). The seabed from the ADCP data is shown by the green line and from the model bathymetry by the black line.

Figure 4.2-4
Observed (top) and Predicted (middle) SSC on February 27, 2017, Around 18:01 During Decreasing Ebb-Directed Flow

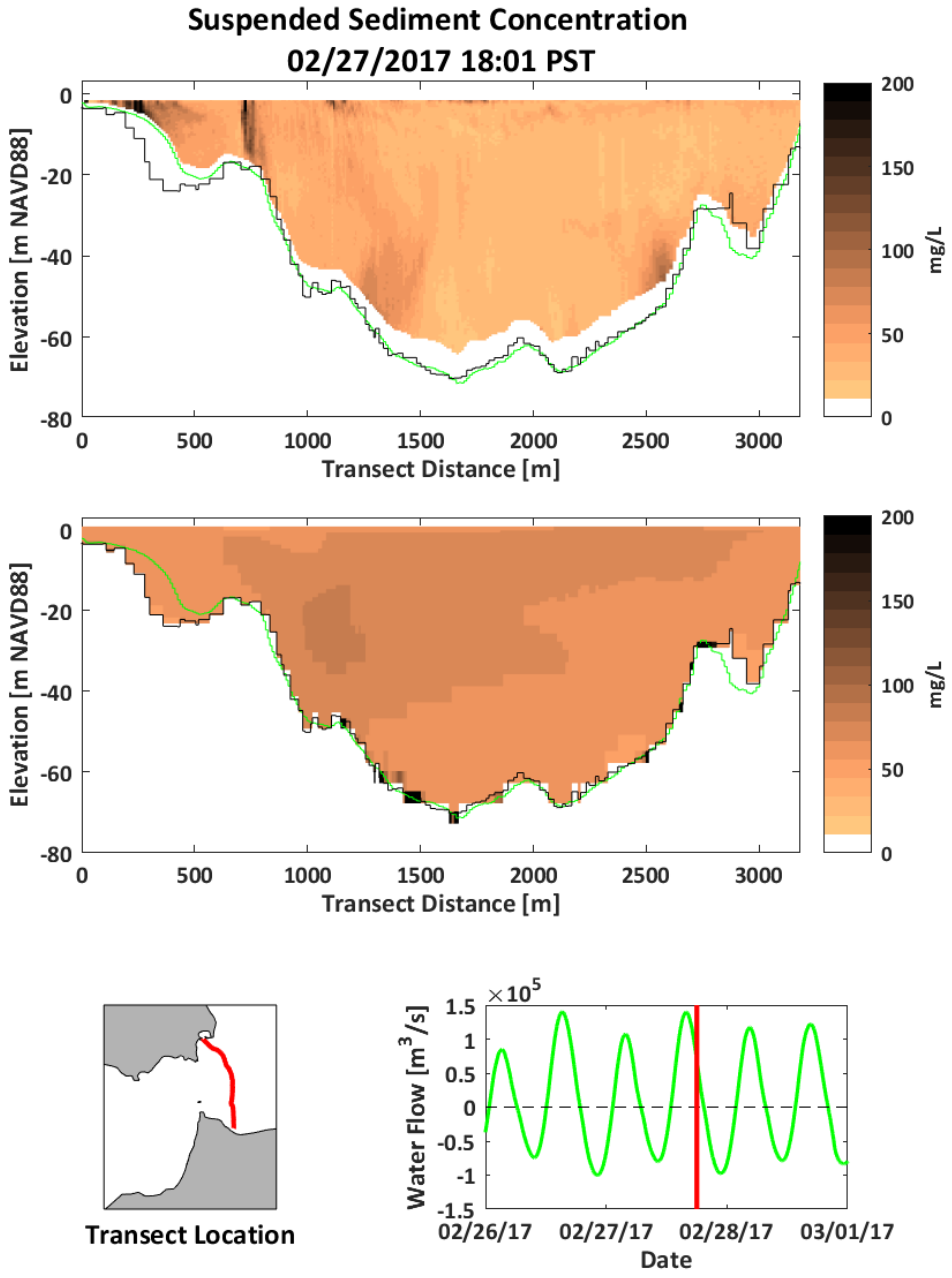

Notes: The left side of the upper panels corresponds to the southern end of the transect shown in the lower left panel. The lower right panel shows the water flow (positive out of the Bay). The seabed from the ADCP data is shown by the green line and from the model bathymetry by the black line.

Figure 4.2-5
Observed (top) and Predicted (middle) SSC on February 27, 2017, Around 20:00 near Slack Water at the Start of Flood-Directed Flow

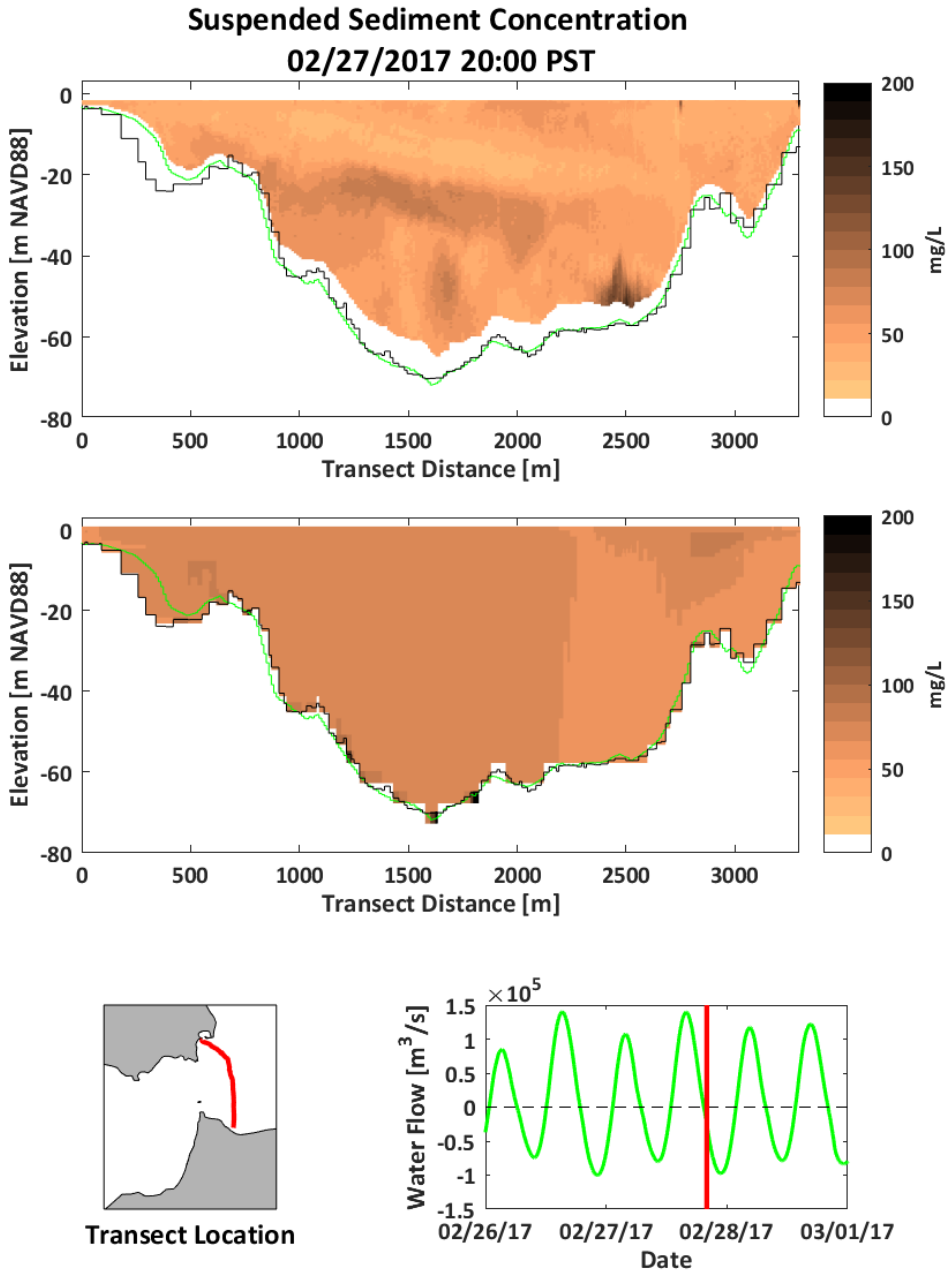

Notes: The left side of the upper panels corresponds to the southern end of the transect shown in the lower left panel. The lower right panel shows the water flow (positive out of the Bay). The seabed from the ADCP data is shown by the green line and from the model bathymetry by the black line.

Figure 4.2-6
Observed (top) and Predicted (middle) SSC on February 27, 2017, Around 20:47 During Increasing Flood-Directed Flow

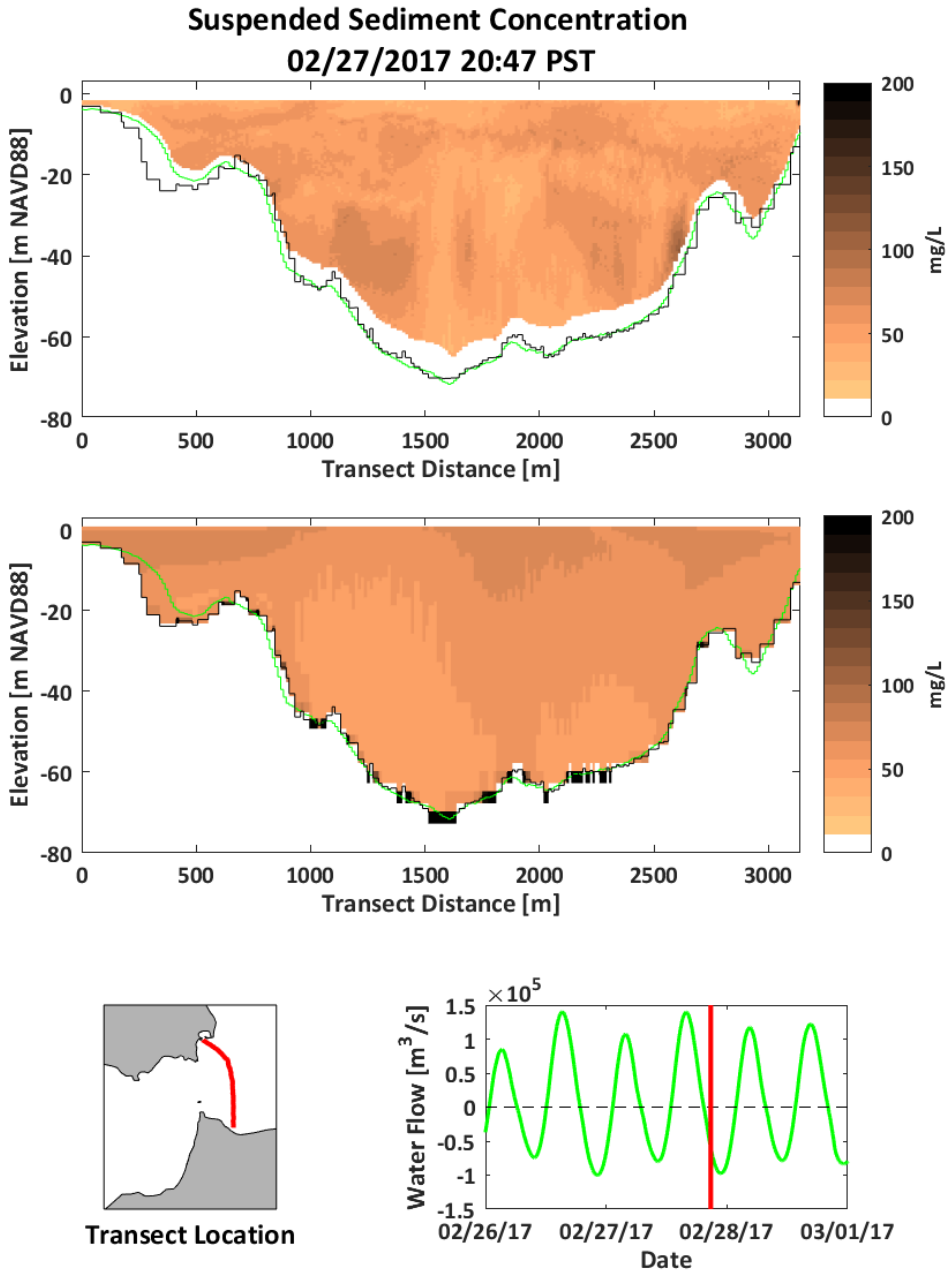

Notes: The left side of the upper panels corresponds to the southern end of the transect shown in the lower left panel. The lower right panel shows the water flow (positive out of the Bay). The seabed from the ADCP data is shown by the green line and from the model bathymetry by the black line.

Figure 4.2-7
Observed (top) and Predicted (middle) SSC on February 27, 2017, Around 22:30 near Maximum Flood-Directed Flow

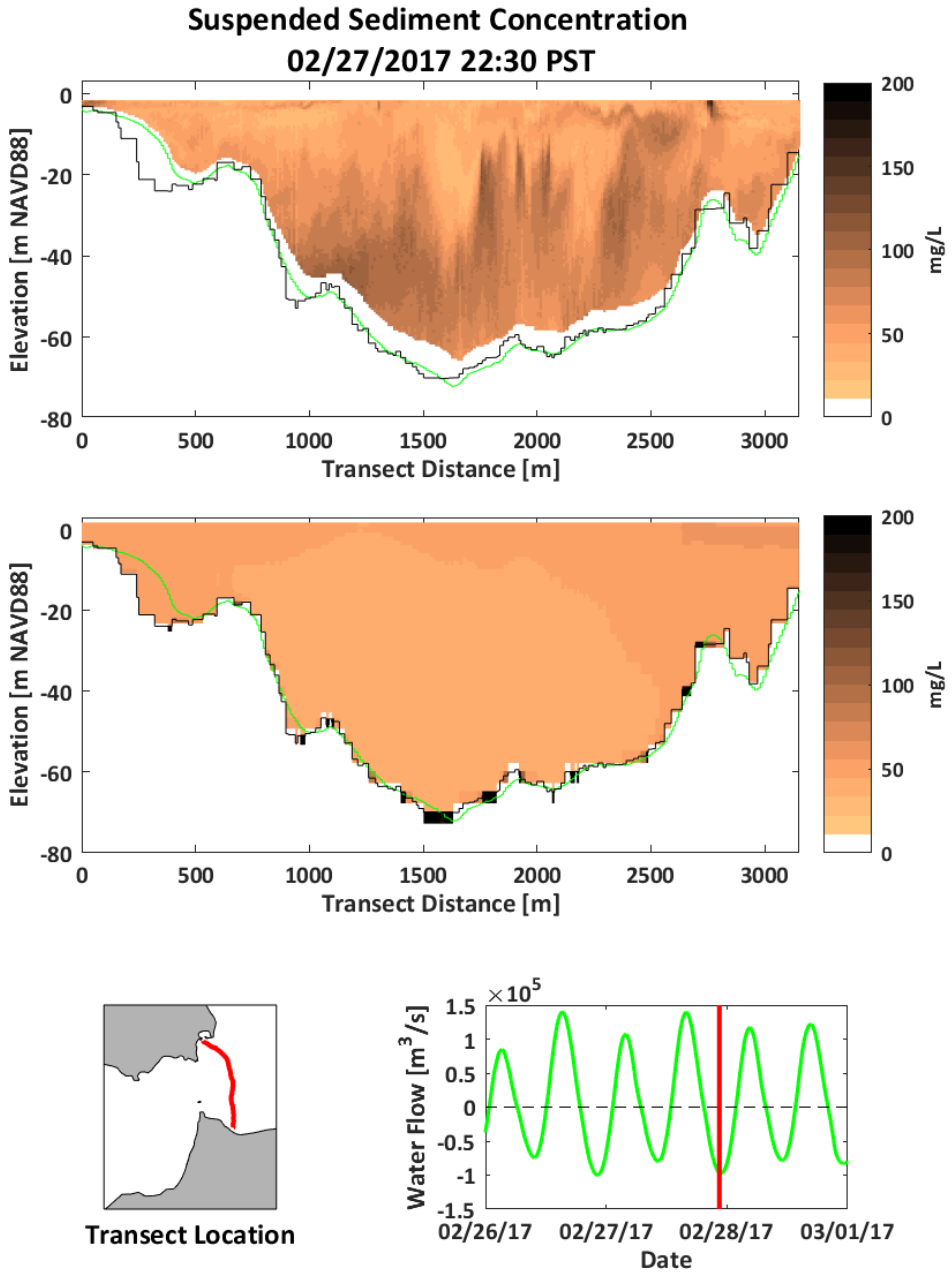

Notes: The left side of the upper panels corresponds to the southern end of the transect shown in the lower left panel. The lower right panel shows the water flow (positive out of the Bay). The seabed from the ADCP data is shown by the green line and from the model bathymetry by the black line.

Figure 4.2-8
Observed (top) and Predicted (middle) SSC on February 28, 2017, Around 01:06 During Decreasing Flood-Directed Flow

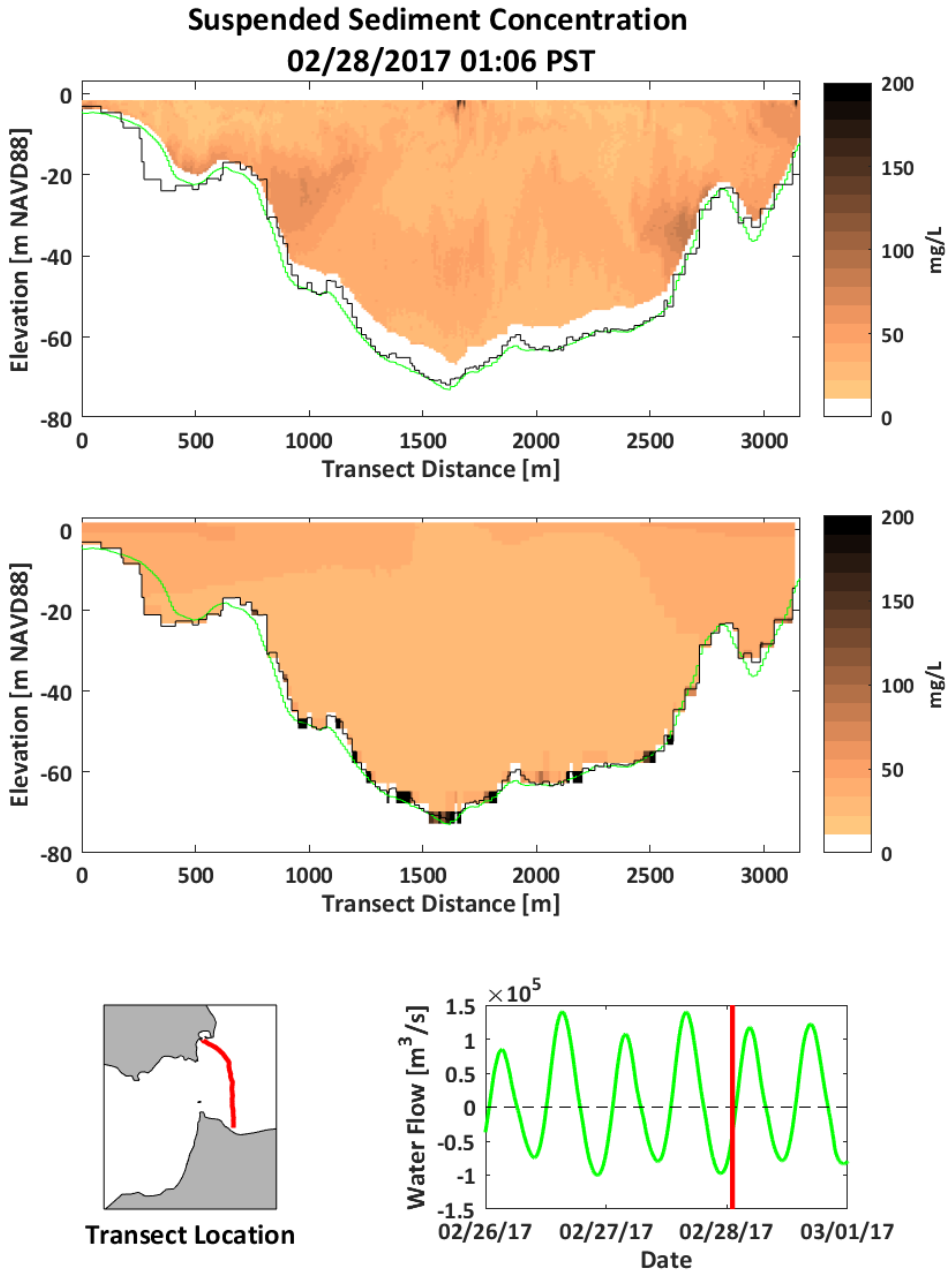

Notes: The left side of the upper panels corresponds to the southern end of the transect shown in the lower left panel. The lower right panel shows the water flow (positive out of the Bay). The seabed from the ADCP data is shown by the green line and from the model bathymetry by the black line.

4.3 Comparison of Water and Sediment Fluxes

The predicted model-based ADCP water flux was compared to the data-based ADCP water flux from USGS to determine if there were meaningful differences between the two estimates of water flux through the Golden Gate. The predicted model-based ADCP water flux matched the observed data-based flux well, with the peaks in the ebb- and flood-directed water fluxes matching in time and the magnitude of the water fluxes generally matching (Figures 4.3-1 and 4.3-2). The r^2 between the two water fluxes was high at 0.98 (Figure 4.3-2). The model-based ADCP water flux underpredicted the data-based ADCP water flux during peak flood (negative) flows. The total predicted water flux during ebb tide from the model-based ADCP estimate was 1.9×10^9 m^3, which was within 5% of the water flux during ebb tide of 2.0×10^9 m^3 estimated from the USGS ADCP measurements (Table 4-1). The total predicted water flux during flood tide from the model-based ADCP estimate was 1.4×10^9 m^3, which was 13% lower than the water flux during flood tide of 1.6×10^9 m^3 estimated from the USGS ADCP measurements (Table 4-1).

The predicted model-based ADCP sediment flux was compared to the data-based ADCP sediment flux from the USGS to determine the degree to which the model-based ADCP sediment flux matched that estimated from the data. The predicted model-based ADCP sediment flux was correlated to the observed data-based ADCP flux, with an $r^2=0.83$ (Figures 4.3-3 and 4.3-4). The overall magnitudes of the model-based sediment fluxes agreed with the data-based sediment fluxes. The predicted sediment flux from the model was greater than the data-based sediment flux estimates during ebb-directed flux and less than the data-based sediment flux estimates during flood-directed flux (Figure 4.3-3). The total predicted sediment flux during ebb tide from the model-based ADCP estimate was 10.5×10^7 kg, which was 52% more than the sediment flux during ebb tide of 6.9×10^7 kg estimated from the USGS ADCP measurements (Table 4-1). The total predicted sediment flux during flood tide from the model-based ADCP estimate was 6.4×10^7 kg, which was 30% lower than the sediment flux during flood tide of 9.1×10^7 kg estimated from the USGS ADCP measurements (Table 4-1).

Overall, the similarity in the model-based and data-based estimates of water and sediment fluxes, in terms of both their relative magnitudes (Table 4-1) and temporal variability (Figure 4.3-1 through Figure 4.3-4), demonstrates the UnTRIM Bay-Delta model is a useful tool for examining water and sediment fluxes through the Golden Gate.

Table 4-1
Predicted and Observed Total Ebb and Flood Fluxes Calculated from the ADCP-Based Fluxes from Each Transect

Tidal Stage	Water Flow (m^3)		Sediment Flux (kg)	
	Observed	Predicted	Observed	Predicted
Ebb	2.0×10^9	1.9×10^9	6.9×10^7	10.5×10^7
Flood	1.6×10^9	1.4×10^9	9.1×10^7	6.4×10^7

Note:
Observed values calculated based on updated ADCP-based fluxes provided by USGS.

Figure 4.3-1
Time Series of Data-Based and Model-Based ADCP Water Flux

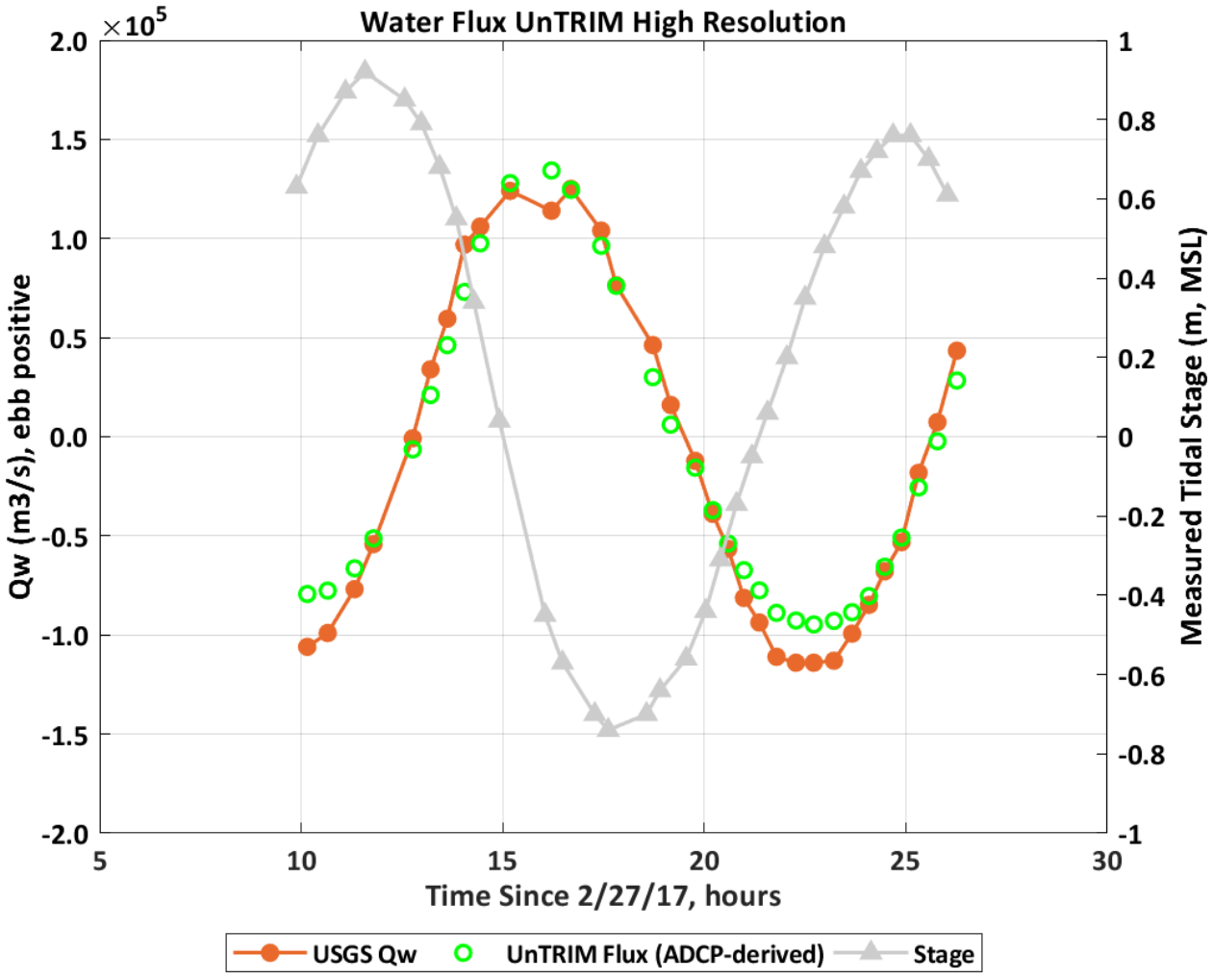

Notes: Figure recreated based on Figure 17 in Downing-Kunz et al. (2017) using updated water fluxes provided by USGS. USGS Qw is the data-based ADCP water flux, and the UnTRIM Flux (ADCP-derived) is the model-based ADCP water flux.

Figure 4.3-2
Scatter Plot of Data-Based and Model-Based ADCP Water Fluxes

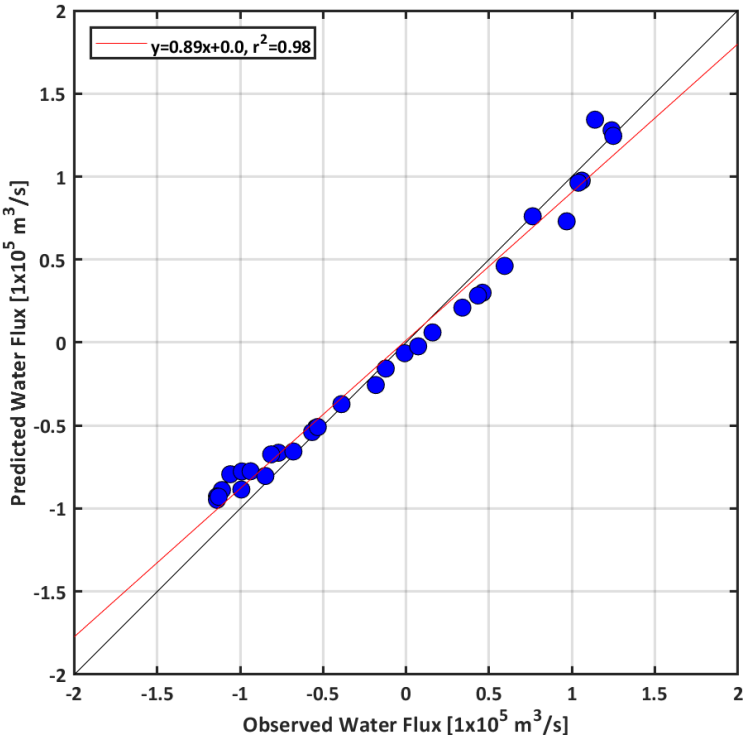

Note: Figure uses updated water fluxes provided by USGS and compares the data-based and model-based ADCP water fluxes. Positive values are ebb directed.

Figure 4.3-3
Time Series of Data-Based and Model-Based ADCP Sediment Fluxes

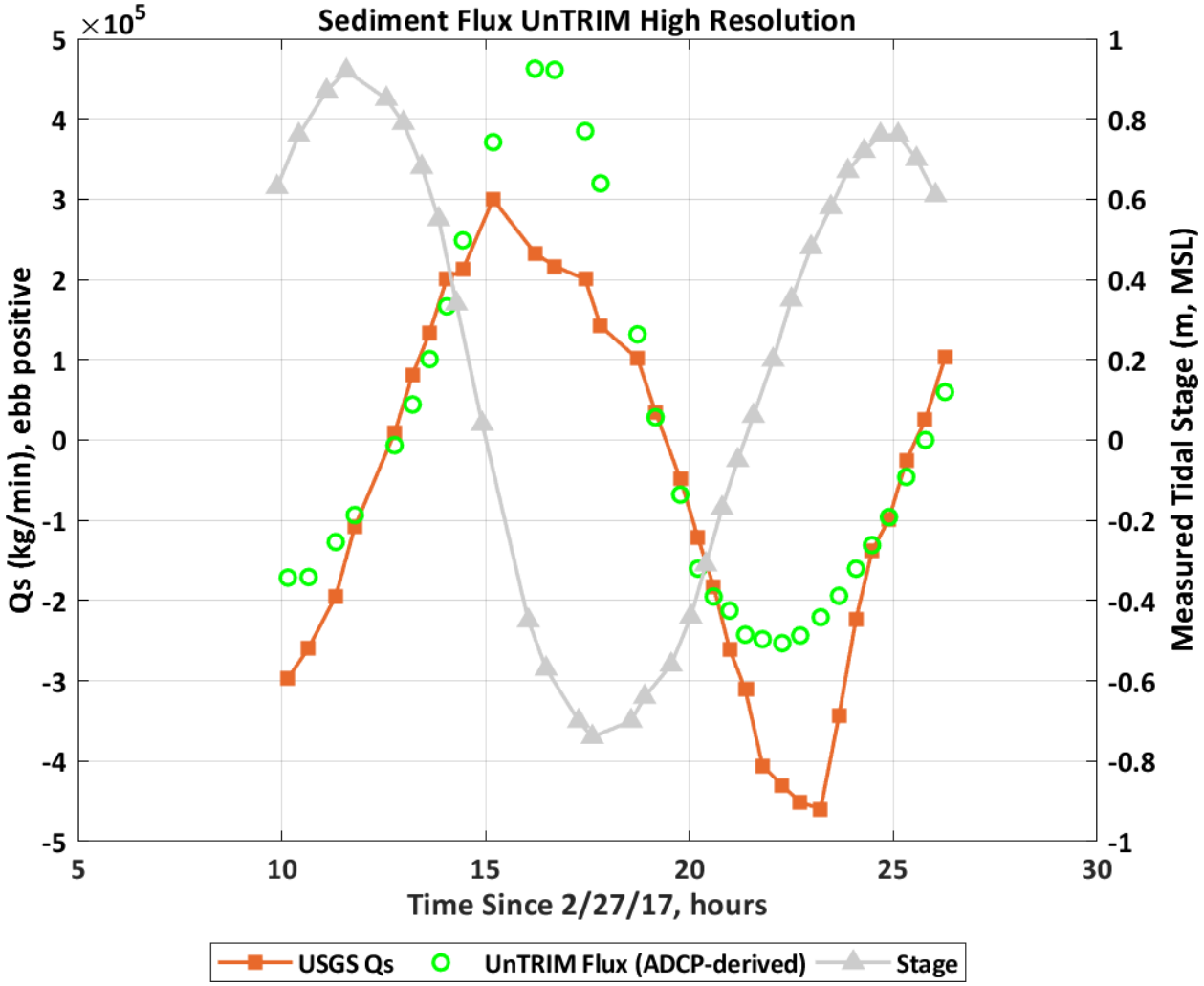

Notes: Figure recreated based on Figure 17 in Downing-Kunz et al. (2017) using updated sediment fluxes provided by USGS. USGS Qs is the data-based ADCP sediment flux, and the UnTRIM Flux (ADCP-derived) is the model-based ADCP sediment flux.

Figure 4.3-4
Scatter Plot of Data-Based and Model-Based ADCP Sediment Fluxes

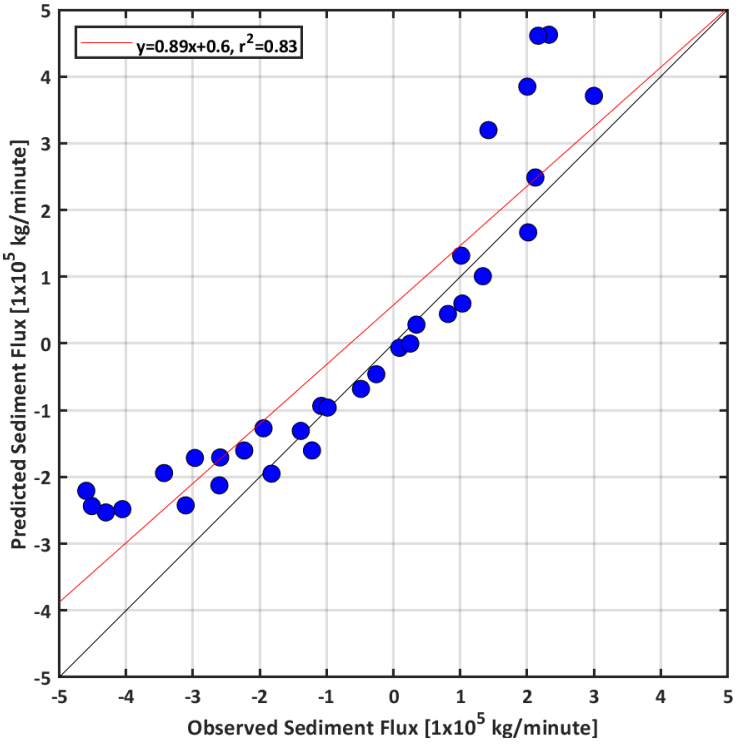

Note: Figure uses updated sediment fluxes provided by USGS and compares the data-based and model-based ADCP sediment fluxes. Positive values are ebb directed.

5 Predicted Sediment Flux

This section provides the predicted sediment fluxes between the different subembayments of the Bay and examines differences between the model-based ADCP sediment flux and the predicted cross-sectional sediment flux through a cross section at the Golden Gate.

5.1 Sediment Flux Between Embayments

The net sediment flux was calculated at five cross sections to summarize the predicted sediment flux between the Delta and the Bay, between the subembayments of San Francisco Bay, and between the Bay and the Pacific Ocean (Figure 5.1-1). Net sediment fluxes were calculated over three time periods, corresponding roughly to before, during, and after the 2017 high Delta outflow period (Table 5-1). Predicted sediment fluxes between the embayments were higher during the 2017 high Delta outflow period than before and after the high Delta outflows.

Before the 2017 high Delta outflow period, predicted sediment flux decreased between Chipps Island and Carquinez Bridge (net deposition) and increased between Carquinez Bridge and Point San Pablo (net erosion). Central Bay was predicted to be net depositional over this time period. Note that Central Bay is represented by the Point San Pablo, Golden Gate, and Bay Bridge control volume. During the 2017 high Delta outflow period, predicted net sediment flux was similar between Chipps Island and Carquinez Bridge (slightly net erosional) and increased from Carquinez Bridge to Point San Pablo (net erosion). Central Bay was predicted to be net depositional during this time period. Following the 2017 high Delta outflow period, predicted net sediment flux increased from Chipps Island to Carquinez Bridge (net erosion) and increased from Carquinez Bridge to Point San Pablo (net erosion). Central Bay was predicted to be net erosional over this time period. The finding that Suisun Bay between Chipps Island and Carquinez Bridge was net depositional before the period of high Delta outflow and net erosional during and following the large Delta outflow agrees with the findings from Ganju and Schoellhamer (2009). Predicted sediment flux at the Bay Bridge cross section was into the South Bay during the 2017 high Delta outflow period (negative value in Table 5-1) but out of the South Bay before and after the high Delta outflows (Table 5-1).

Table 5-1
Predicted Sediment Flux at Cross Section Between Embayments of San Francisco Bay

Cross Section Location	Sediment Flux (kg/day)		
	December 1, 2016, to January 3, 2017	January 4, 2017, to March 12, 2017	March 13, 2017, to April 15, 2017
Chipps Island	9.37×10^6	6.67×10^7	1.93×10^7
Carquinez Bridge	7.43×10^6	6.78×10^7	2.23×10^7
Point San Pablo	1.42×10^7	1.23×10^8	2.78×10^7
Golden Gate	1.40×10^7	1.05×10^8	2.97×10^7
Bay Bridge	4.12×10^6	-5.32×10^6	9.04×10^5

Note:
Positive sediment flux is toward the ocean.

Figure 5.1-1
Locations of Cross Sections Used for Evaluating Sediment Fluxes

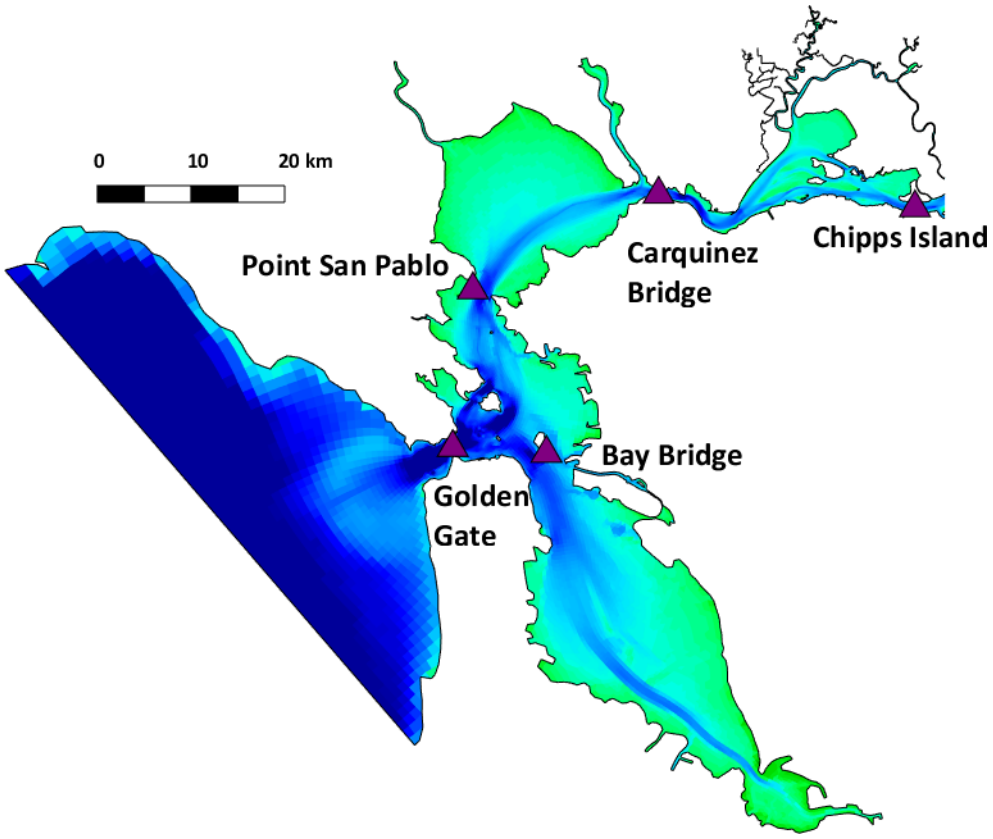

5.2 Water Flow and Sediment Flux Through the Golden Gate

The predicted cross-sectional water flow and sediment flux at each model time step through a cross section at the Golden Gate was used to compare to the fluxes derived from sampling the model along the ADCP transects presented in Section 4.3. Differences between the predicted cross-sectional and ADCP-based fluxes could indicate that the method of estimating the water and sediment fluxes from the velocity and SSC is creating a bias in the ADCP-based fluxes or that the ADCP transect location is missing important features of the water flow or sediment flux through the Golden Gate. The predicted cross-sectional water flow matched the model-based ADCP water flow very well (Figure 5.2-1). This suggests that the method of processing the ADCP data does not introduce a bias into the ADCP-based water flows and that the ADCP transect location is adequately capturing the water flow and sediment flux. The predicted cross-sectional sediment flux matched the model-based ADCP sediment flux very well (Figure 5.2-2). This suggests that the method of processing the ADCP data does not introduce a bias into the ADCP-based sediment fluxes. Comparing the predicted cross-sectional water flow and sediment flux to the model-based ADCP values demonstrates that the predicted cross-sectional fluxes can be used to further investigate the modeled water flow and sediment flux through the Golden Gate and relate findings back to the data-based ADCP fluxes from the USGS data collection. A large benefit of the predicted cross-sectional water flow and sediment flux is that it can be analyzed over the full 4.5 months of the analysis period, not simply the half tidal cycle of the ADCP data collection.

Figure 5.2-1
Time Series of Data-Based ADCP Water Fluxes, Model-Based ADCP Water Fluxes, and the Predicted Cross-Sectional Water Flux Through the Cross Section at the Golden Gate

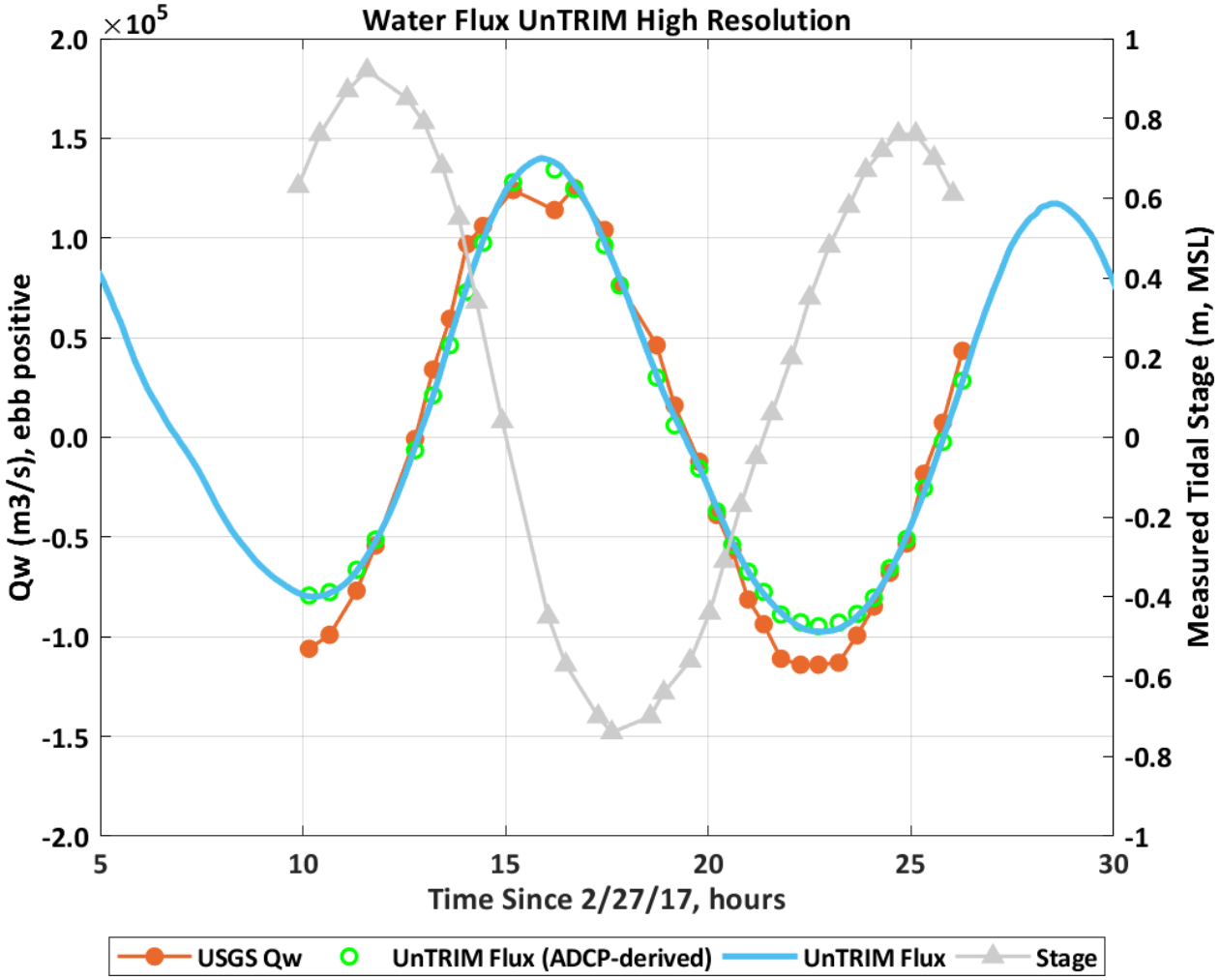

Notes: Figure recreated based on Figure 17 in Downing-Kunz et al. (2017) using updated water fluxess provided by USGS. USGS Qw is the data-based ADCP water flux, UnTRIM Flux (ADCP-derived) is the model-based ADCP water flux, and UnTRIM Flux is the predicted cross-sectional water flux at the Golden Gate every model time step.

Figure 5.2-2
Time Series of Data-Based ADCP Sediment Fluxes, Model-Based ADCP Sediment Fluxes, and the Predicted Cross-Sectional Sediment Flux Through the Cross Section at the Golden Gate

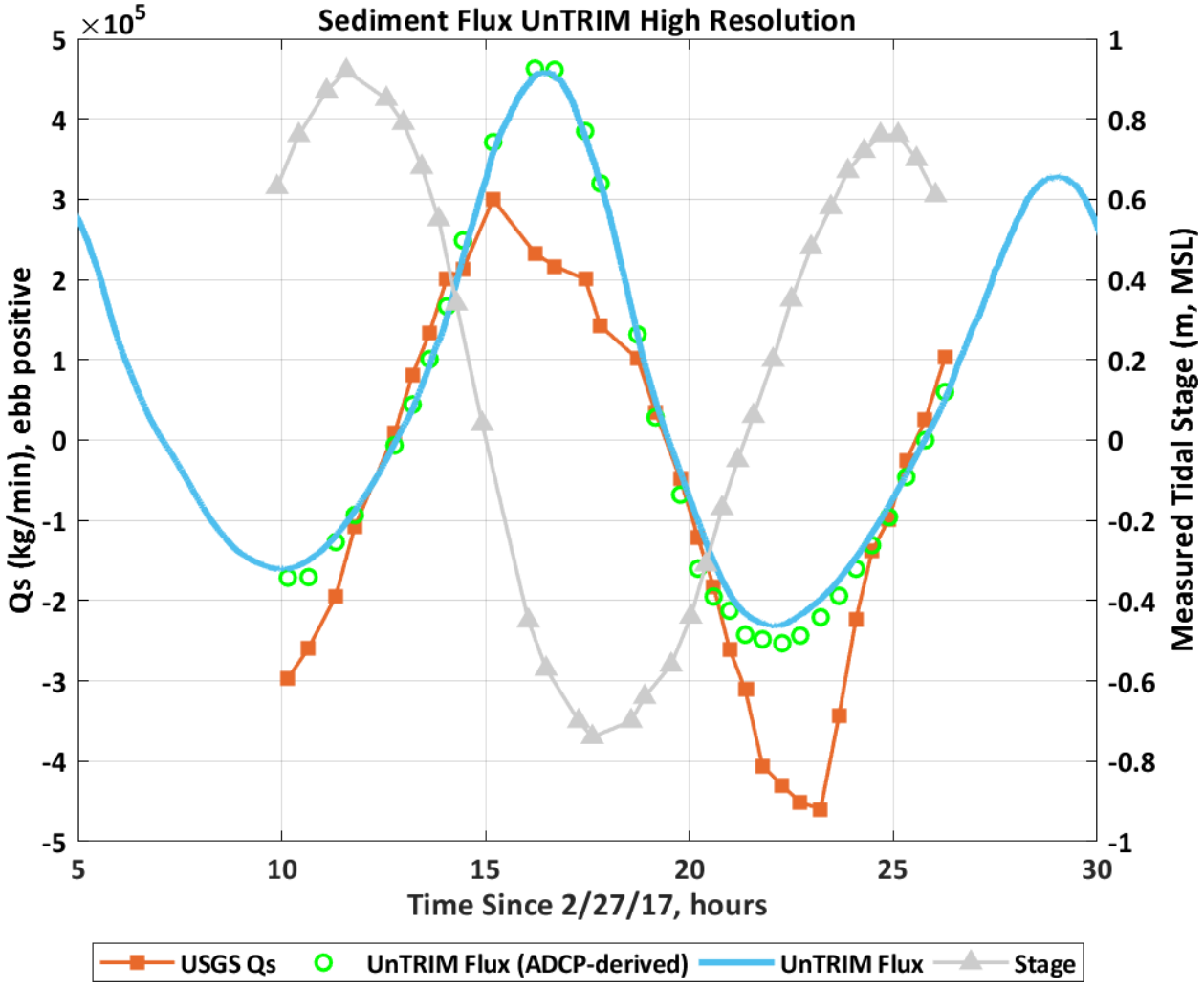

Notes: Figure recreated based on Figure 17 in Downing-Kunz et al. (2017) using updated sediment fluxes provided by USGS. USGS Qs is the data-based ADCP sediment flux, UnTRIM Flux (ADCP-derived) is the model-based ADCP sediment flux, and UnTRIM Flux is the predicted cross-sectional sediment flux at the Golden Gate every model time step.

The predicted cross-sectional water flow and sediment flux was summed over flood and ebb tides to determine the total fluxes during each tide. The values were summed during individual flood and ebb tides (sum of one flood and one ebb tide) and as the sum of a complete mixed semidiurnal tidal cycle (two consecutive flood or ebb tides of different magnitudes). Summing over only one flood and one ebb results in a large oscillation between consecutive flood and ebb tides because of the asymmetry in the tidal water levels and thus asymmetry in water flows through the Golden Gate. This can be thought of as evaluating half of the mixed semidiurnal tidal cycle, because the asymmetry of the flood and ebb tides is not captured. Here a half tidal cycle is considered one flood and ebb, while

the complete tidal cycle is considered both floods and ebbs in the mixed semidiurnal tidal cycle. Summing over a complete tidal cycle (two flood or two ebb tides) removes the oscillation in the total fluxes and can be better used to evaluate net sediment fluxes than examining half tidal cycles. As an alternative to summing over a complete tidal cycle, the instantaneous values could be tidally averaged to visualize the net water flow and sediment flux. However, summing over the complete tidal cycle facilitates comparison to the ADCP-based method where only half the tidal cycle was observed.

The predicted total water flow through the Golden Gate oscillates more in the ebb direction than the flood direction (Figure 5.2-3 upper). On any given day and for any given flood/ebb pair, the flood-directed water flow can be larger than the ebb-directed water flow, even during periods of high Delta outflow. However, when two flood and two ebb tides are considered, the total ebb-directed water flow was higher than the total flood-directed water flow during most of the analysis period, except during early and late December when Delta outflow (Figure 3.1-1) was very low (Figure 5.2-3 middle). During times of low Delta outflow, the net water flow over a tidal cycle can be in the flood direction (Figure 5.2-3 lower). This is most likely due to spring-neap cycles in the tidal water levels and corresponding spring-neap cycles in the water flow through the Golden Gate or other ephemeral processes. During periods of elevated Delta outflow, the net water flow over a tidal cycle is consistently in the ebb direction out of the Bay.

Figure 5.2-3
Time Series of Total Water Flow Through the Golden Gate over Half Tidal Cycles (upper), over Complete Tidal Cycles (middle), and the Net Water Flow over Complete Tidal Cycles (lower)

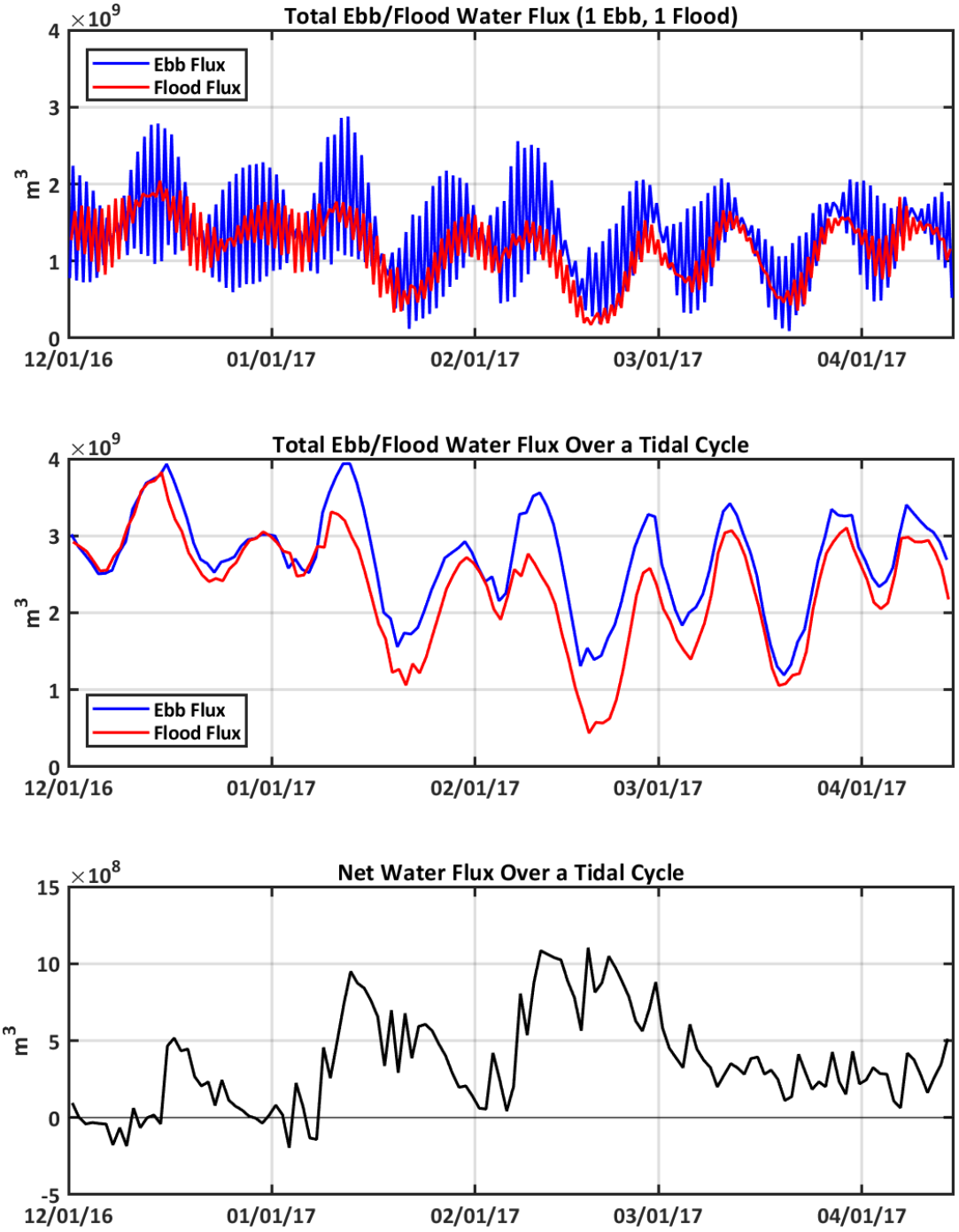

Note: Sign convention for the flood direction is taken to be positive in the top two panels of this figure to overlay the ebb- and flood-directed values. On the bottom panel, positive values indicate the ebb direction.

The predicted sediment flux over half of a tidal cycle has a similar pattern to the water flow, with an oscillation in the fluxes between consecutive floods and ebbs and a variation in the magnitude of the fluxes based on the spring-neap cycle (Figure 5.2-4). Predicted net sediment flux over individual half tidal cycles can also be in the flood direction, dependent on the water flows and SSC in the Bay and Pacific Ocean. Net flood-directed half tidal cycles are predicted to occur more often during the period of low Delta outflow before the 2017 high Delta outflow period than during or following the high Delta outflows. The predicted net ebb- and flood-directed sediment fluxes over a complete tidal cycle are relatively low before the 2017 high Delta outflow period, increase during the high Delta outflows and then decrease again following the high Delta outflows (Figures 5.2-4 and 5.2-5 third panels). The predicted net sediment flux over a complete tidal cycle is relatively low before the 2017 high Delta outflow period, increases during the high Delta outflows, and then decreases following the high Delta outflows (Figures 5.2-4 and 5.2-5 lower panels). Similar to the predicted net water flow, the net sediment flux over a complete tidal cycle is always in the ebb direction out of the Bay after the 2017 high Delta outflow period.

There are two periods during the 2017 high Delta outflow period where the ebb-directed sediment flux is decreasing while the flood-directed flux is increasing. The periods are shown on Figure 5.2-4 (third panel) around January 29, 2017, and February 26, 2017. Around January 29, 2017, the predicted net sediment flux is relatively low (Figure 5.2-4 lower panel) as a result of the flood-directed flux lagging the ebb-directed flux and the two fluxes approaching each other. Around February 26, 2017, the predicted net sediment flux remains relatively large in the ebb direction, even though the flood-directed flux is increasing while the ebb-directed flux is decreasing.

Figure 5.2-4
Time Series of Total Sediment Flux Through the Golden Gate over Half Tidal Cycles (upper panel), Net Sediment Flux over Half Tidal Cycles (second panel), Total Sediment Flux over Complete Tidal Cycles (third panel), and Net Sediment Flux over Complete Tidal Cycles (lower panel)

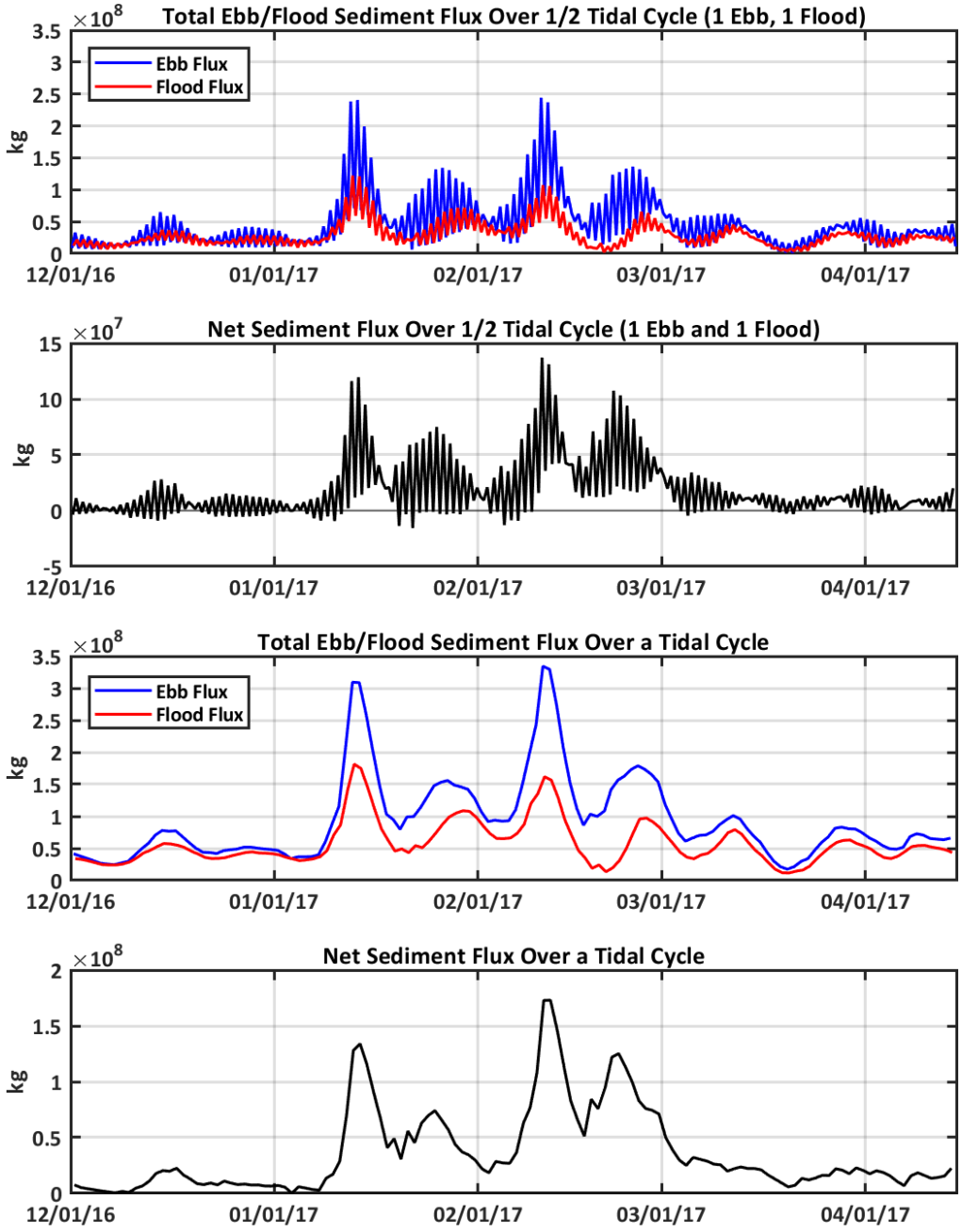

Note: Sign convention for the flood direction is taken to be positive in the first and third panels of this figure to overlay the ebb- and flood-directed values. On the second and fourth panels, positive values indicate the ebb direction.

Figure 5.2-5
Time Series of Total Water Through the Golden Gate over Complete Tidal Cycles (upper panel), Net Water Flow over Complete Tidal Cycles (second panel), Total Sediment Flux over Complete Tidal Cycles (third panel), and Net Sediment Flux over Complete Tidal Cycles (lower panel)

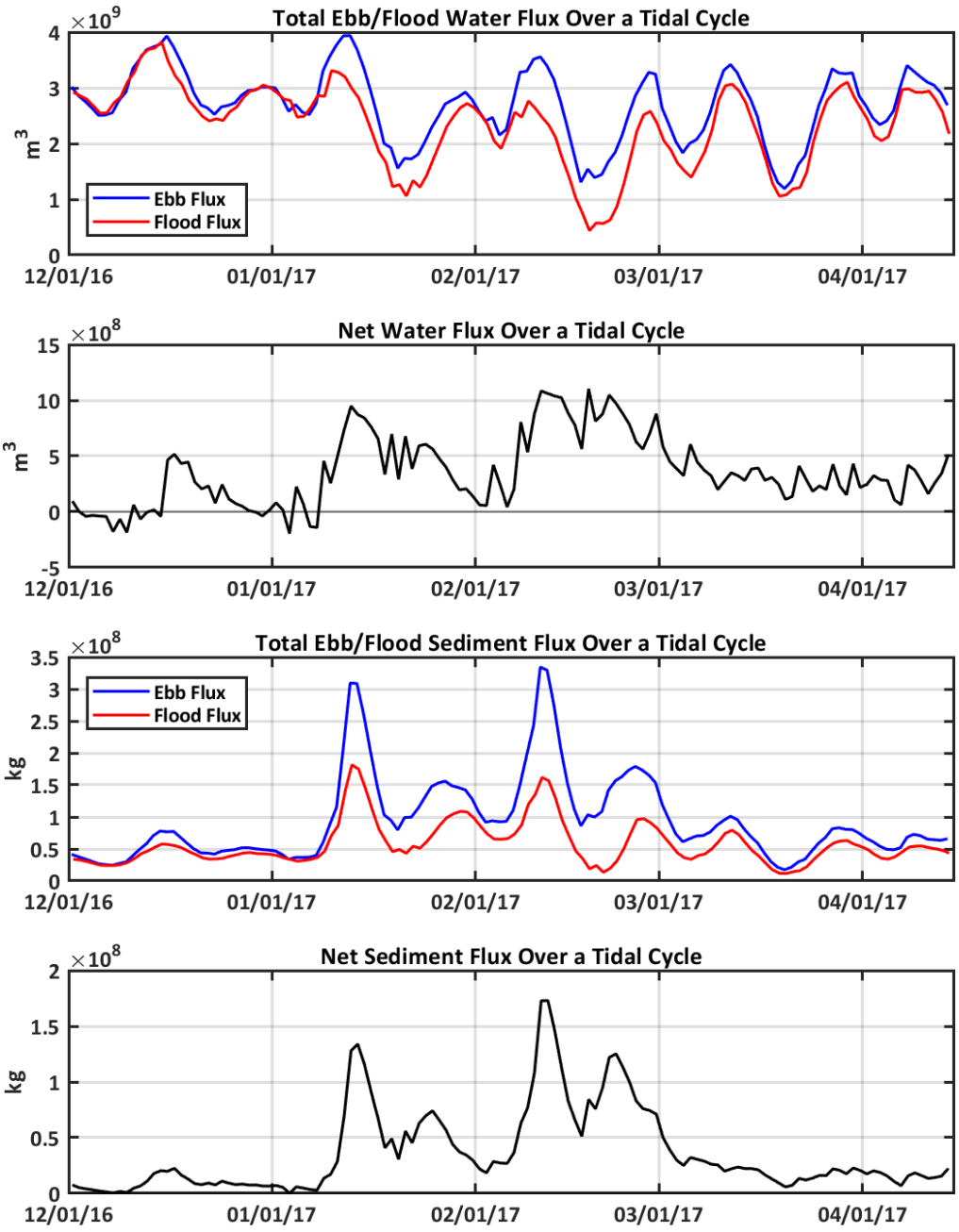

Note: Sign convention for the flood direction is taken to be positive in the first and third panels of this figure to overlay the ebb- and flood-directed values. On the second and fourth panels, positive values indicate the ebb direction.

5.3 Investigation of the Differences between Observed and Predicted Fluxes

Additional analysis was conducted to investigate the differences between the observed and predicted fluxes. First, two hybrid sediment flux estimates were calculated using a combination of the observed and predicted velocity and SSC along the transects to investigate whether the source of the differences in computed sediment flux could be attributed to differences in water flux or differences in SSC. Second, additional analysis was conducted to assess the effect of the region of flood-directed velocity in the ADCP data during five of the transects during ebb tide and whether this eddy, which was not predicted to be as strong in the model, was resulting in a reduction in the ebb-directed flux in the data-based ADCP sediment flux relative to the model-based ADCP sediment flux. A third short analysis was conducted to examine whether the water column had salinity stratification present during the data collection period.

5.3.1 Investigating the Source of the Differences Between Observed and Predicted Sediment Flux

To investigate the differences between the observed and model-predicted sediment fluxes, two hybrid sediment flux estimates were calculated using a combination of the observed and predicted velocity and SSC along the transects. One estimate of sediment flux used the predicted velocity along the transects with the observed SSC along the transects. The second estimate of sediment flux used the observed velocity along the transects with the predicted SSC along the transects. These hybrid sediment flux estimates were used to evaluate whether the difference between the model-based and data-based sediment fluxes was due primarily to differences in velocity along the transect or differences in the SSC along the transect.

The sediment flux estimates using the predicted velocity and observed SSC decrease relative to the model-based (UnTRIM) ADCP sediment flux and match the data-based ADCP sediment flux well during ebb (positive)-directed fluxes (Figure 5.3-1). Using the predicted velocity and observed SSC, the sediment flux was increased relative to the model-based (UnTRIM) ADCP sediment flux on flood-directed fluxes but was still lower magnitude than the data-based ADCP sediment flux. The sediment flux estimates using observed velocity and predicted SSC decrease relative to the model-based (UnTRIM) ADCP sediment flux and are more similar to the model-based ADCP sediment flux during ebb-directed fluxes than when using the modeled velocity (Figure 5.3-1). Using the observed velocity and predicted SSC, the sediment flux was increased relative to the model-based (UnTRIM) ADCP sediment flux on flood-directed fluxes, but was still lower than the data-based ADCP sediment flux. Analyses for the hybrid sediment flux estimates suggest that the difference in the data-based and model-based ADCP sediment fluxes is largely from differences between observed and predicted SSC and less from differences between observed and predicted velocity.

Figure 5.3-1
Time Series of ADCP Sediment Fluxes with Mixed Observed and Predicted Water Velocity and SSC

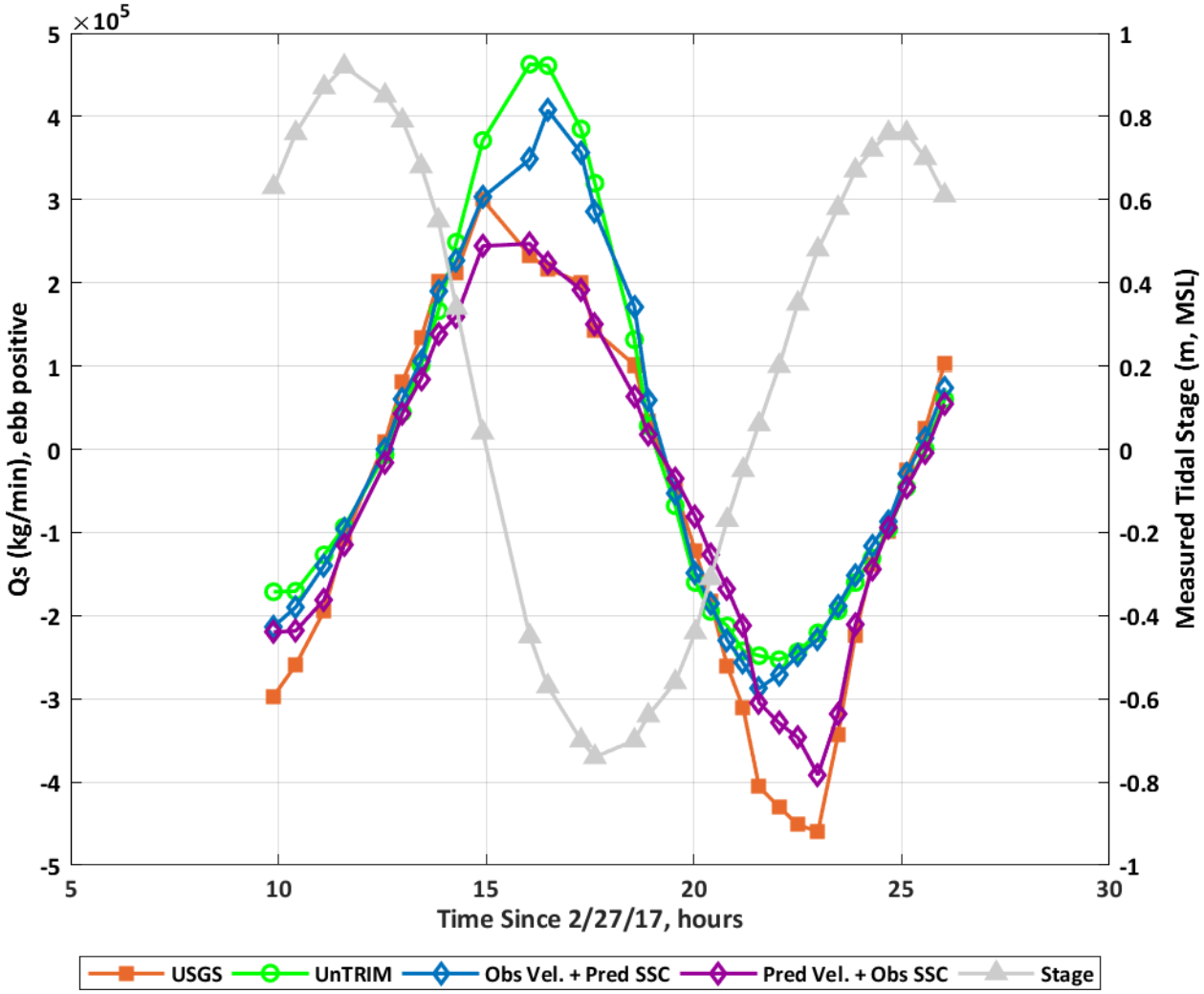

Notes: Figure recreated based on Figure 17 in Downing-Kunz et al. (2017) using updated sediment fluxes provided by USGS. USGS is the data-based ADCP sediment flux, UnTRIM is the model-based ADCP sediment flux, Obs Vel. + Pred SSC is calculated using the USGS observed velocity, and the UnTRIM-predicted SSC. Pred Vel. + Obs SSC is calculated using the UnTRIM-predicted velocity and the observed SSC.

5.3.2 Effect of Observed Eddy on Water Flow and Sediment Flux

The observed velocity data show a consistent portion of the transect with flood-directed velocity during periods of overall ebb-directed velocity in five of the 32 USGS transects that is also captured in the predicted velocity (e.g., Figure 4.1-4). This flood-directed velocity occurred on the southern end of the transects during and following the maximum ebb-directed water flow. It is believed the region of flood velocity during ebb tides results from a recirculating horizontal eddy at the southern

end of the transect near the San Francisco shoreline. The ADCP data was analyzed to determine the effect of the flood-directed velocity in the eddy on the ADCP-based water flow and sediment flux. This analysis was to determine if the flood-directed velocity in the data was contributing to the difference between the model-based and data-based ADCP water flow and sediment flux during ebb-directed fluxes. The portion of the cross section with the flood-directed velocity was removed from the ADCP data and the data reprocessed to estimate new water flows and sediment fluxes without the portion of the transect with the strongly flood-directed velocity.

Figure 5.3-3 shows the ADCP-based water flows with and without the portion of the transects with the strongly flood-directed velocity. Figure 5.3-4 shows the ADCP-based sediment fluxes with and without the portion of the transects with the strongly flood-directed velocity. Removing the portion of the transects with strongly flood-directed velocity increases the ebb-directed flows slightly but overall has very little effect on the water flows (Figure 5.3-2). Removing the portion of the transects with strongly flood-directed velocity increases the ebb-directed sediment fluxes slightly but overall has very little effect on the sediment fluxes (Figure 5.3-3). This demonstrates that the portion of the transect that has strongly flood-directed velocity during overall ebb-directed flow only very slightly effects the data-based ADCP water flows and sediment fluxes and does not meaningfully contribute to the differences between the data-based and model-based ADCP water flows and sediment fluxes.

Figure 5.3-2
Data-Based ADCP Water Flows with and without the Portion of the Transects with Strongly Flood-Directed Velocity

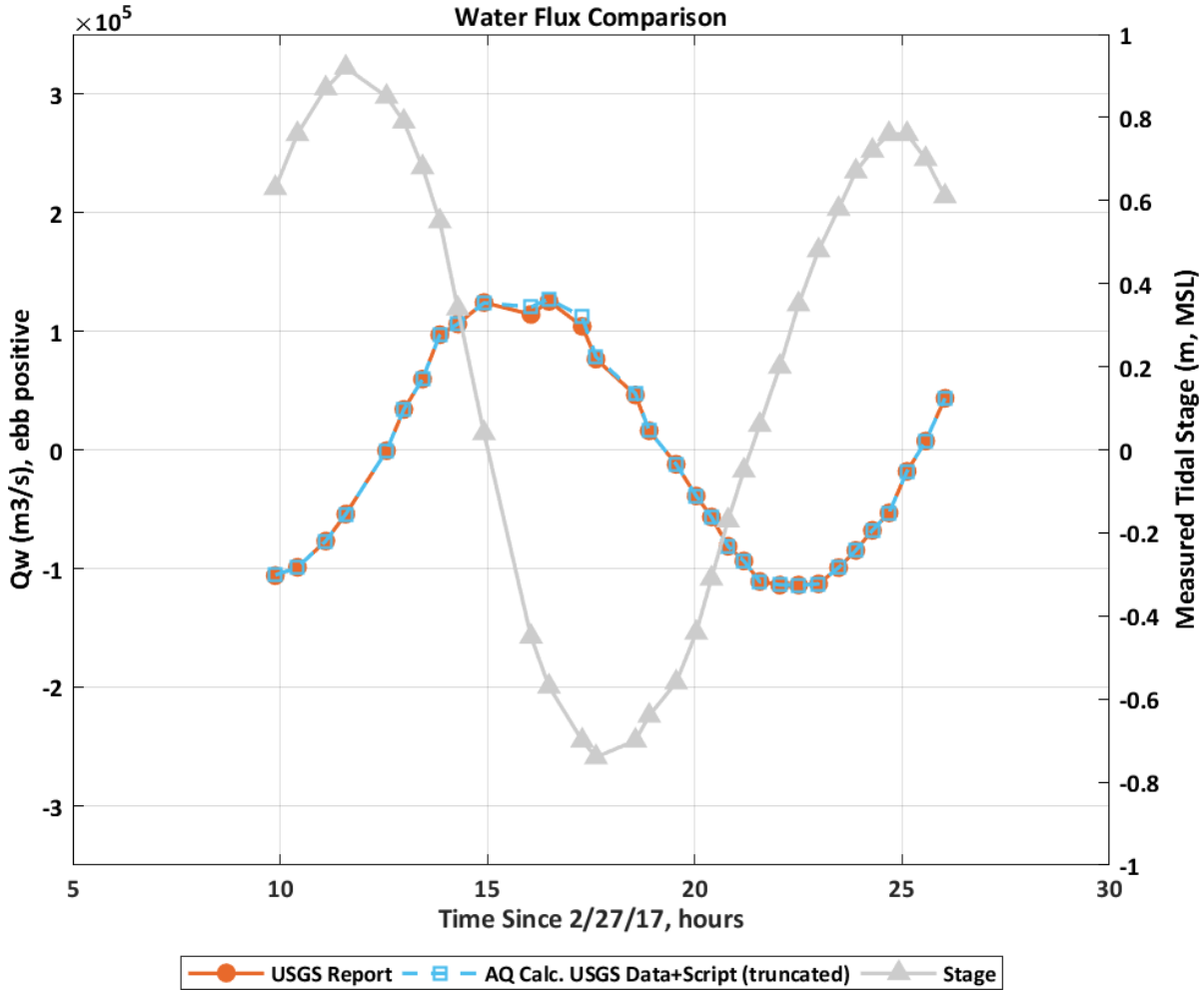

Notes: Figure recreated based on Figure 17 in Downing-Kunz et al. (2017) using updated water flows provided by USGS. USGS Report is the data-based ADCP sediment flux, and AQ Calc. USGS Data+Script (truncated) is the recalcualtion of the water flow without the portion of each transect with strongly flood-directed velocity.

Figure 5.3-3
Data-Based ADCP Sediment Fluxes with and without the Portion of the Transects with Strongly Flood-Directed Velocity

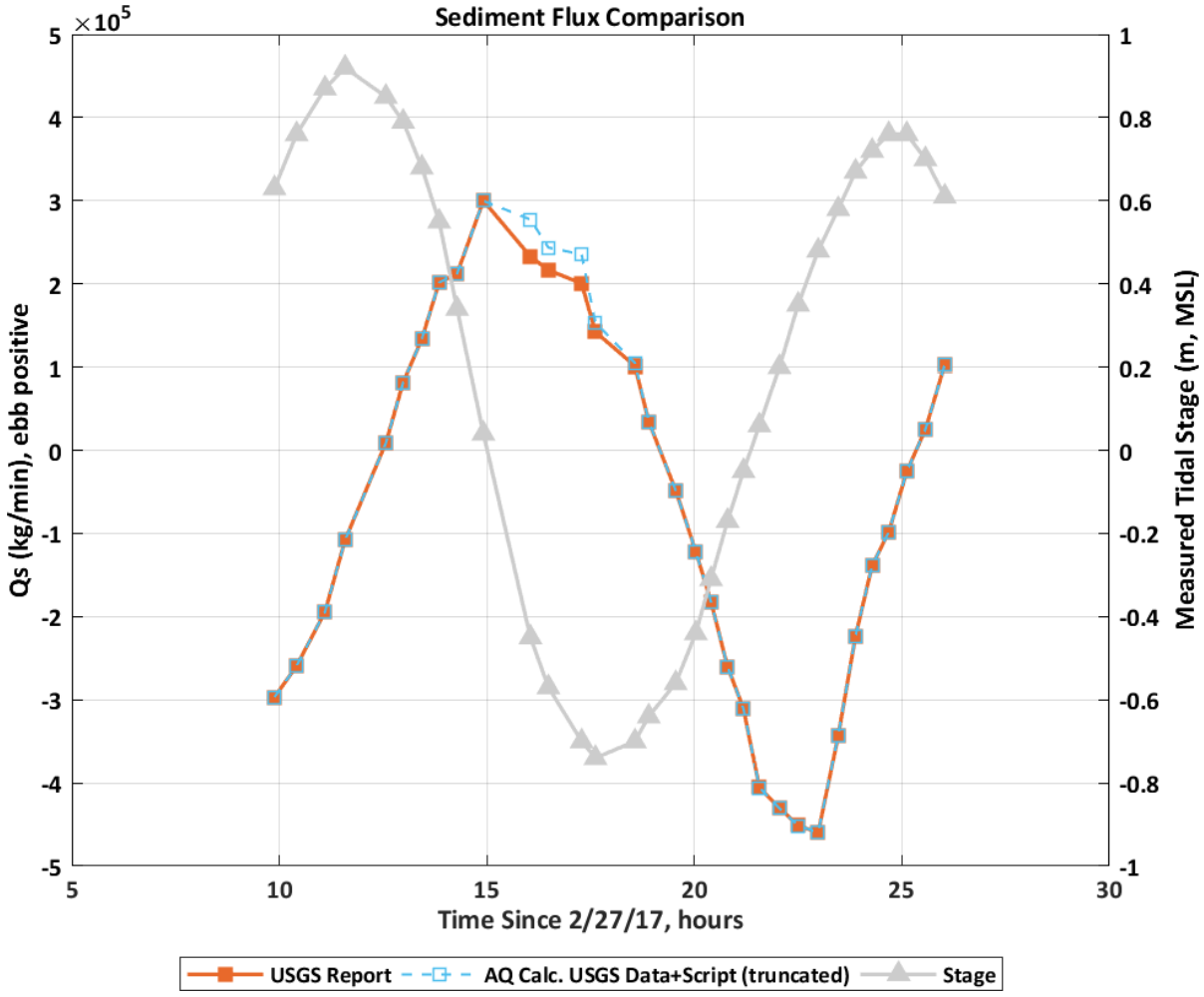

Notes: Figure recreated based on Figure 17 in Downing-Kunz et al. (2017) using updated sediment fluxes provided by USGS. USGS Report is the is the data-based ADCP sediment flux, and AQ Calc. USGS Data+Script (truncated) is the recalcualtion of the sediment fluxes without the portion of each transect with strongly flood-directed velocity.

5.3.3 Salinity Stratification

Downing-Kunz et al. (2017) noted that if stratification was present it could influence the use of SSC at the Alcatraz data collection location for surrogate sediment flux estimates. They also noted that the ADCP signal attenuation varies with suspended sediment size, which means the backscatter to SSC conversion varies with sediment size. The sediment grain size distribution and ratio of flocculated to single particles suspended in the water column at the data collection location could be affected by water column stratification, along with other factors.

Predicted salinity along the ADCP transects was examined to evaluate whether salinity stratification was predicted at the time of the data collection. Predicted salinity showed strong stratification during ebb-directed flow, with stratification decreasing during flood-directed flow (Figure 5.3-4). Comparison of predicted salinity to observed salinity at Alcatraz shows the predicted salinity was lower than observed at this time period but that the observed salinity was also quite low during ebb flow. This suggests that stratification was present during the data collection period, especially nearing the end of ebb flow.

Figure 5.3-4
Predicted Salinity During Ebb Flow (Top) and Flood Flow (Bottom)

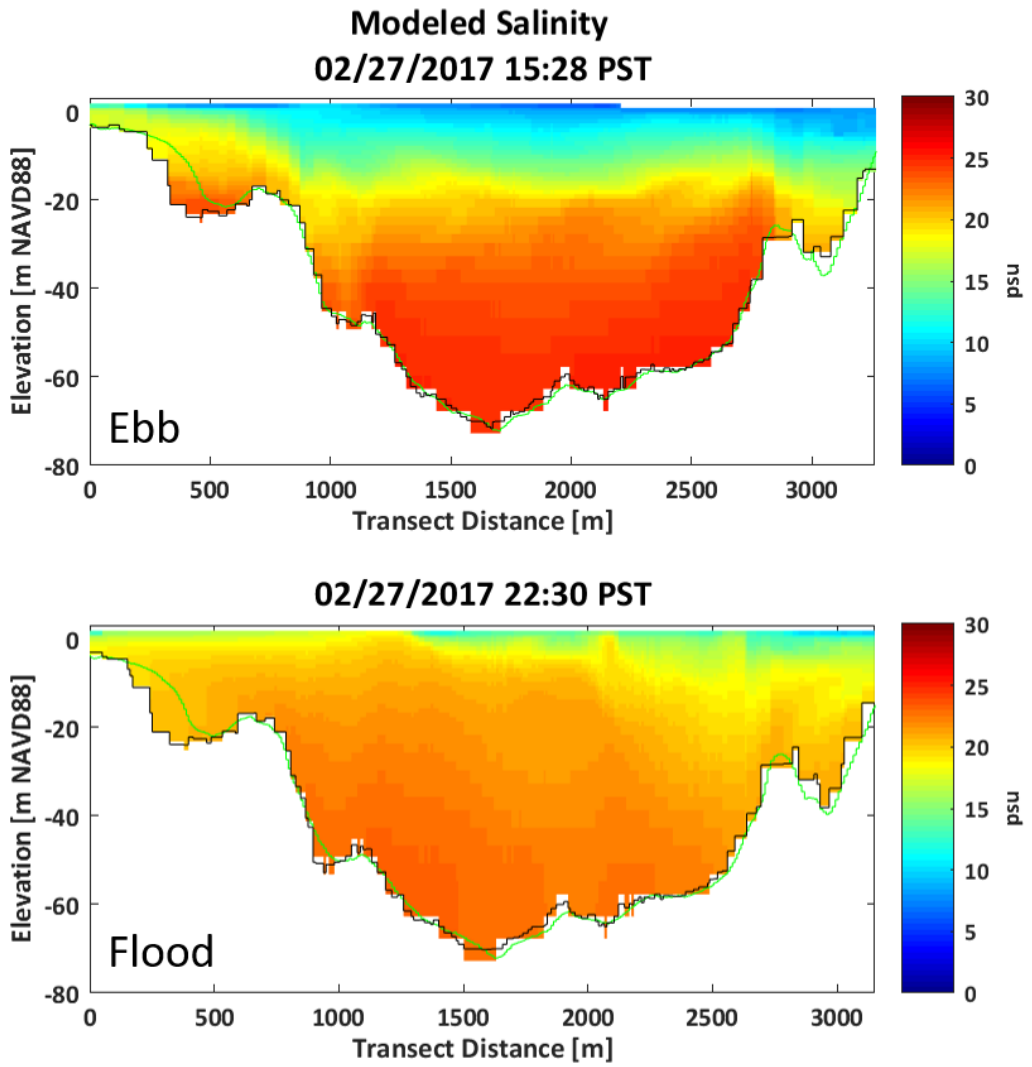

5.4 Summary of Water Flow and Sediment Flux Through the Golden Gate

During any individual half tidal cycle (one flood and the following ebb), the net water flow can be into or out of the Bay dependent on tidal asymmetry and the freshwater inflow to the Bay (Figure 5.2-3). The net water flow over a complete tidal cycle (two floods and two ebbs) can be either into the Bay or out of the Bay during periods of low freshwater inflow to the Bay and likely alternates between into and out of the Bay based on spring-neap cycles. During periods of elevated freshwater inflow to the Bay, such as during the 2017 high Delta outflow period, the net water flow over complete tidal cycles is out of the Bay. The net water flow decreased following the 2017 high Delta outflow period but remained out of the Bay because of the higher Delta outflow following the 2017 high Delta outflow period than before.

Analysis of the model results suggests that the sediment flux through the Golden Gate can be in either the flood or ebb direction, dependent on tidal asymmetry and the duration of the analysis period. When evaluating sediment flux over a half tidal cycle (one flood and one ebb tide), the predicted sediment flux was often in the flood direction. However, the predicted sediment flux was always in the ebb direction when evaluated over a complete tidal cycle (two flood and two ebb tides). The predicted sediment flux also had two periods when the net flood-directed flux was increasing while the net ebb-directed flux was decreasing, resulting in the flood- and ebb-directed sediment fluxes becoming closer in magnitude. Since the USGS data collection spanned half a tidal cycle (one flood and one ebb tide) and occurred during a period when the predicted flood and ebb-directed fluxes were becoming closer in magnitude, either the short data collection period or the decrease in the difference in the net flood- and ebb-directed fluxes could be resulting in the USGS observed sediment flux in the flood (into the Bay) direction. However, there could also be other factors or physical processes influencing the sediment fluxes calculated from the ADCP data. Another data collection study that spanned a complete tidal cycle during both periods with large asymmetry in the tides and with minimal asymmetry in the tides would provide valuable information for further evaluating the periodic nature of the predicted sediment flux into the Bay.

Due to the model-based ADCP sediment flux being more ebb directed than the data-based ADCP sediment flux, there is some additional uncertainty in the predicted cross-sectional sediment flux above that inherent in sediment transport modeling. The model-data comparison suggests that the predicted sediment flux through the Golden Gate is biased in the ebb (out of the Bay) direction, at least during the data collection. This suggests that during the trailing end of the period of high Delta outflow the net sediment flux out of the Bay could be overpredicted. With the single data collection period, it is not possible to directly evaluate uncertainty in the predicted sediment flux during different conditions (i.e., during the peaks in Delta outflow).

6 Surrogate Measurements for Estimating Sediment Flux Through the Golden Gate

Predicted water flow and SSC were used in combination with observed data to evaluate whether surrogate measurements can be used to estimate a continuous time series of sediment flux through the Golden Gate—that is, whether observed or analytically calculated measurements of water flow and SSC can be used to estimate the sediment flux through the Golden Gate. Multiple estimates of water flow and SSC were used to estimate a sediment flux based on surrogate measurements over the study analysis period (December 1, 2016, through April 15, 2017). These surrogate sediment fluxes were then compared to the predicted cross-sectional sediment flux through the Golden Gate to determine how well the surrogate sediment flux from each water flow and SSC combination recreated the predicted cross-sectional sediment flux. A benefit of conducting this analysis using sediment transport model output is that the total predicted cross-sectional sediment flux that the surrogate estimates are meant to reproduce is known, and thus the accuracy of the surrogate sediment flux can be directly evaluated.

6.1 Surrogates for Water Flow Through the Golden Gate

Two estimates of water flow through the Golden Gate were used to estimate sediment fluxes. The first water flow was the predicted cross-sectional water flow through the Golden Gate from the UnTRIM model. Using the predicted cross-sectional water flow through the Golden Gate and time series SSC at a discrete location to calculate a surrogate sediment flux evaluates whether the SSC at that location can be used as a surrogate SSC for estimating sediment flux.

The second water flow was a 6-minute estimate of water flow based on a National Oceanic and Atmospheric Administration (NOAA)-predicted velocity near the Golden Gate. Predicted velocity near the Golden Gate (Figure 6.1-1) is available from the NOAA Tides and Currents webpage (station SFB1202; NOAA 2020). This velocity is predicted based on tidal harmonics and does not directly provide an estimate of water flow. The NOAA-predicted velocity was compared to the UnTRIM-predicted water flow through the Golden Gate to develop a simple relationship between the NOAA velocity and water flow through the Golden Gate. A parabolic equation was fit to the velocity versus water flow in order to estimate water flow through the Golden Gate from the NOAA-predicted velocity (Figure 6.1-2). This is a relatively simple relationship, and possible improvements are discussed in Section 6.3. The Golden Gate water flow predicted from the NOAA velocity has the main drawback of not including net flows through the Golden Gate based on freshwater inflows to the Bay and possibly to a lesser extent net flow resulting from atmospheric forcing.

Figure 6.1-1
Locations of NOAA-Predicted Velocity and Time Series SSC Used as Surrogate Measurements for Estimating Sediment Flux

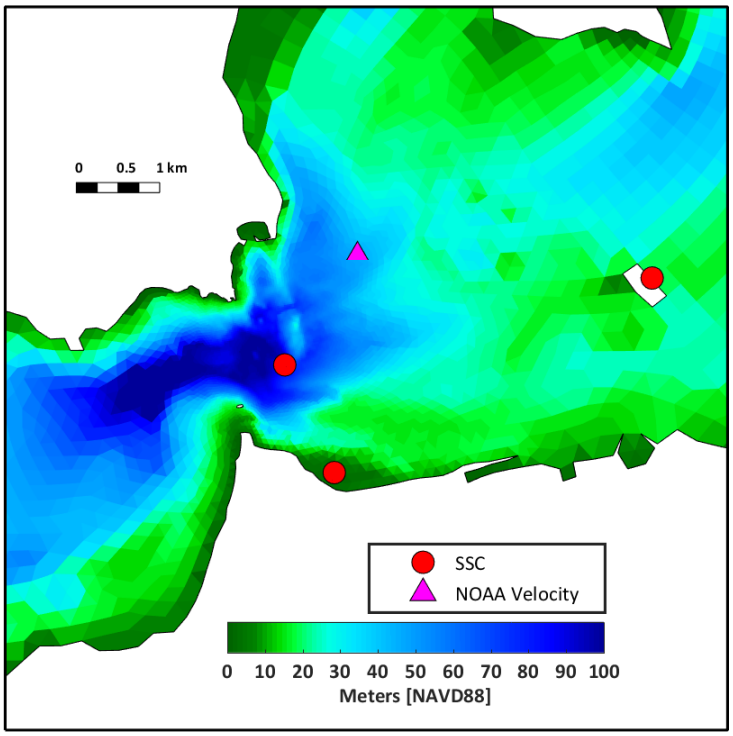

Figure 6.1-2
Relationship Between NOAA-Predicted Velocity and UnTRIM-Predicted Water Flow Through the Golden Gate

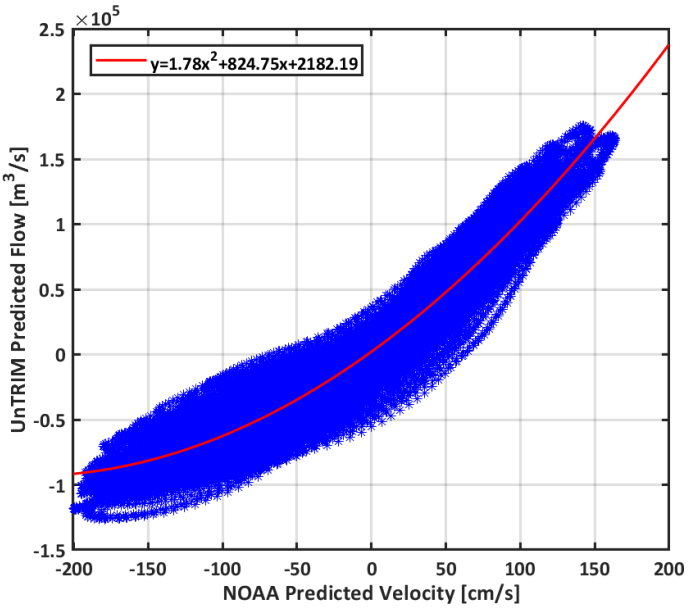

6.2 Surrogates for SSC at the Golden Gate

There is currently no observed SSC at the Golden Gate, which necessitates using SSC at some other location to estimate a surrogate sediment flux. Time series SSC at three locations were extracted from the model for use as surrogate SSC measurements (Figure 6.1-1). The first location was east of the Golden Gate at a depth of about 20 m below the surface. A location at the Golden Gate was not used in this analysis because we wanted to evaluate SSC from near the Golden Gate but not right at the Golden Gate, and SSC at the Golden Gate would likely not be a good evaluation of surrogate measurements, as the water flow and SSC are then collocated at the location of interest. The second location was close to the shoreline near San Francisco, an assumed relatively easy area to install instrumentation to observe SSC. The third location was at the Alcatraz continuous monitoring location at the same depth as the current instrumentation. The observed SSC at Alcatraz available from USGS (2020a) was also used as a fourth SSC time series.

6.3 Surrogate Estimates of Sediment Flux Through the Golden Gate

The two estimates of water flow through the Golden Gate were multiplied by the four time series of SSC, resulting in eight surrogate estimates of the sediment flux through the Golden Gate. These surrogate sediment fluxes were compared to the predicted cross-sectional sediment flux through the Golden Gate to evaluate the difference between the two sediment flux estimates. Scatter plots were used to compare the different estimates of sediment flux. These plots compare the instantaneous

values of each of the different estimates of sediment flux and as such generally evaluate the large range in sediment flux that occurs over a tidal cycle. The different estimates of sediment flux were also compared using the tidal-averaged sediment flux to better evaluate the net sediment fluxes.

Using the predicted cross-sectional water flow through the Golden Gate, the predicted cross-sectional sediment flux was generally well predicted by the surrogate sediment flux (Figure 6.3-1). Using the predicted SSC near the Golden Gate, the surrogate sediment flux nearly equaled the predicted cross-sectional sediment flux. Using the SSC near San Francisco, the slope of the best fit line increased relative to using the SSC near the Golden Gate. Although the r^2 remained very high at 0.97 when using the predicted SSC farther from the Golden Gate at Alcatraz, the slope of the best fit line further increased. This increase in the slope of the best fit line likely results from generally higher SSC at the discrete Alcatraz monitoring location than the cross-sectional average SSC at the Golden Gate. This analysis using the predicted SSC suggests that the closer to the Golden Gate an SSC continuous monitoring sensor can be placed the better the sediment flux estimates will be and that using locations in the Bay farther from the Golden Gate could result in an overprediction of the instantaneous sediment fluxes. Using the observed SSC at Alcatraz to predict a surrogate sediment flux resulted in more variability about the best fit line and a lower r^2 than using the predicted SSC at Alcatraz. The larger magnitude but short duration increases in the observed SSC at Alcatraz contributed to the larger scatter about the best fit line and lower r^2, as short-duration increases in SSC at Alcatraz do not necessarily correspond to similar increases in SSC at the Golden Gate.

The tidal-averaged (net) sediment flux over the tidal cycles is more important for a surrogate sediment flux estimate to capture than the instantaneous sediment flux, as the net fluxes are what result in sediment export from, or supply to, the Bay. Even though the four SSC time series all resulted in generally satisfactory surrogate estimates of the instantaneous Golden Gate sediment flux, they did not all result in accurate surrogate estimates of the tidal-averaged (net) sediment flux. Using the SSC near the Golden Gate, the tidal-averaged predicted cross-sectional sediment flux was very accurately estimated by the surrogate sediment flux (Figure 6.3-2). Using the SSC near San Francisco, the tidal-averaged flux during periods of lower Delta outflow were not that well represented by the surrogate sediment flux, and the increase in the sediment flux as a result of the 2017 high Delta outflow period was not well represented by the surrogate sediment flux. Using the predicted SSC at Alcatraz, the tidal-averaged sediment flux was well represented by the surrogate sediment flux, although the surrogate sediment flux generally underestimated the tidal-averaged predicted cross-sectional sediment flux. Using the observed SSC at Alcatraz, the tidal-averaged sediment flux was very poorly represented by the surrogate sediment flux. This analysis suggests that the net sediment flux through the Golden Gate can likely be estimated from surrogate measurements of SSC, as long as those measurements are representative of the conditions at the Golden Gate.

Surrogate estimates of sediment flux through the Golden Gate were also calculated using the time series of water flow through the Golden Gate developed using the NOAA-predicted velocity. The surrogate sediment fluxes reproduced the instantaneous predicted cross-sectional sediment flux to similar accuracy as when the predicted cross-sectional water flow was used (Figure 6.3-3). When using the predicted SSC, the r^2 was generally high (0.83 or greater). The slope of the best fit line was near 1 when using SSC near the Golden Gate but gets larger with increasing distance from the Golden Gate to the SSC location. There was also generally a little more scatter about the best fit line when using the water flow predicted from the NOAA velocity than when using the predicted cross-sectional water flow. Using the observed SSC at Alcatraz results in a similar comparison of the predicted cross-sectional and surrogate sediment fluxes as when the predicted cross-sectional water flow was used; the scatter about the best fit line increased and the slope of the best fit line decreased.

Using the surrogate water flow from the NOAA velocity and SSC from near the Golden Gate, the tidal-averaged predicted cross-sectional sediment flux is generally well represented by the surrogate sediment flux (Figure 6.3-4). There are two notable differences between the two fluxes. The first is the surrogate sediment flux lagged the predicted cross-sectional sediment flux during the two smaller increases in sediment flux during the 2017 high Delta outflow period (around January 29, 2017, and February 26, 2017). The second is the larger spring-neap signal in the surrogate sediment flux following the 2017 high Delta outflow period. Using the predicted SSC near San Francisco, the predicted cross-sectional sediment flux was generally represented by the surrogate sediment flux before the 2017 high Delta outflow period, but the increase in the net sediment flux during high Delta outflow was not captured by the surrogate sediment flux. Using the predicted SSC at Alcatraz, the tidal-averaged sediment flux was moderately well represented by the surrogate sediment flux. However, the surrogate sediment flux overestimated the magnitude of the sediment flux from the small increase in Delta outflow in December 2016. Similar to using the SSC from near the Golden Gate, the surrogate sediment flux underestimated the sediment flux during the two smaller increases in sediment flux and overestimated the spring-neap signal following the 2017 high Delta outflow period. Using the observed SSC at Alcatraz, the surrogate sediment flux moderately well represented the tidal-averaged predicted cross-sectional sediment flux before the 2017 high Delta outflow period but underestimated the sediment flux during and following the high Delta outflows.

It is interesting to note that the two largest peaks in tidal-averaged sediment flux through the Golden Gate during the 2017 high Delta outflow period were well represented using the surrogate sediment flux based on the NOAA velocity and predicted SSC near the Golden Gate and at Alcatraz. However, the surrogate sediment flux lagged the predicted cross-sectional sediment flux for the two smaller increases during the 2017 high Delta outflow period. This suggests that the physical processes driving the larger versus smaller increases in sediment flux during the 2017 high Delta outflow period are likely the result of tidal asymmetries that repeat with the spring-neap cycle in

combination with elevated Delta outflow. The larger peaks likely are strongly influenced by tidal asymmetry, because these are captured using the surrogate water flow that does not include any effects of Delta outflow on the net water flow through the Golden Gate. The smaller peaks likely then are strongly influenced by a combination of tidal asymmetry and net water outflow through the Golden Gate, because these smaller increases in sediment flux are not as well captured by the surrogate sediment flux that does not include any effects of Delta outflow on the net water flow through the Golden Gate.

The Golden Gate water flow predicted from the NOAA velocity has the main drawback of not including net flows through the Golden Gate based on freshwater inflows to the Bay, and possibly to a lesser extent net flows resulting from atmospheric forcing. The NOAA-predicted velocity to the Golden Gate water flow relationship could be improved by evaluating a longer time period and incorporating a metric for freshwater flow to the Bay (possibly Delta outflow) to better capture net water flows through the Golden Gate. A lag time between the NOAA-predicted velocity and water flow at the Golden Gate could be evaluated to potentially improve the instantaneous predictions of water flow. Both including more variables (such as Delta outflow) in the velocity to Golden Gate water flow relationship and evaluating lag times between the velocity and Golden Gate water flow could be evaluated using longer model simulations that include a wide range of conditions.

Figure 6.3-1
Scatter Plots of the Predicted Cross-Sectional Sediment Flux and the Surrogate Sediment Flux Using the Predicted Cross-Sectional Water Flow

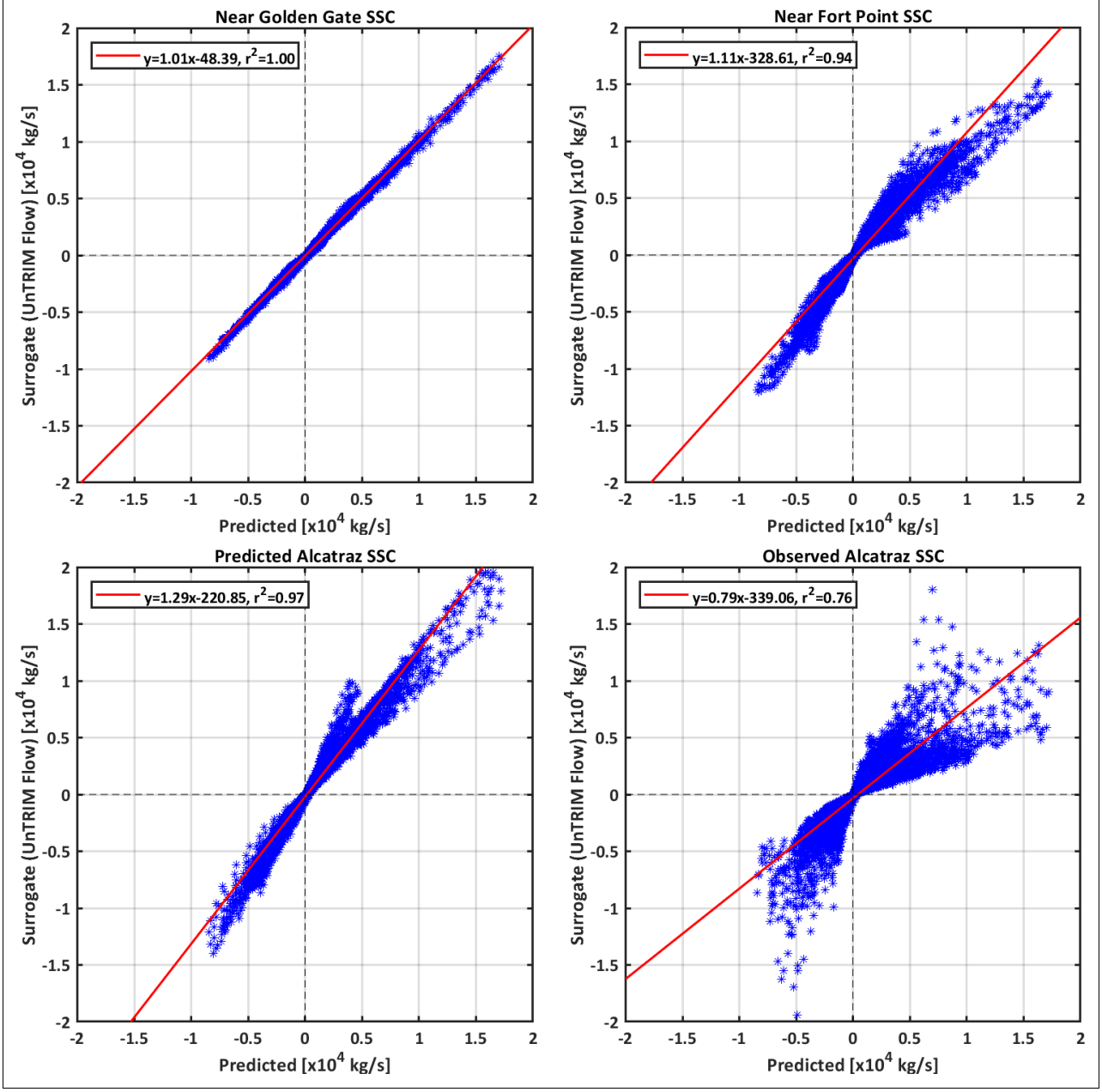

Figure 6.3-2
Tidal-Averaged Sediment Flux Through the Golden Gate Using the Predicted Cross-Sectional Water Flow

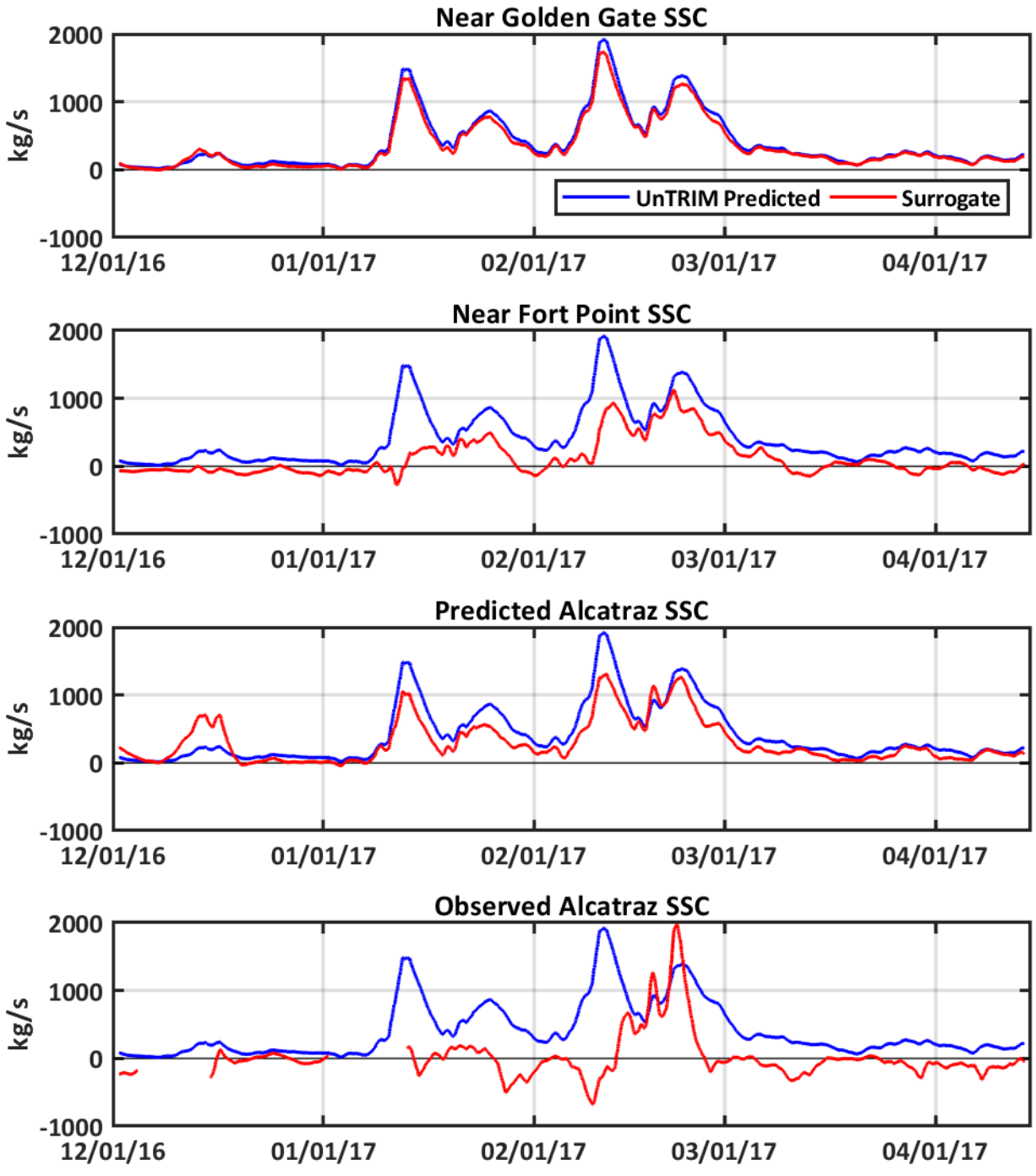

Figure 6.3-3
Scatter Plots of the Predicted Cross-Sectional Sediment Flux and the Surrogate Sediment Flux Using the NOAA Velocity to Estimate Water Flow

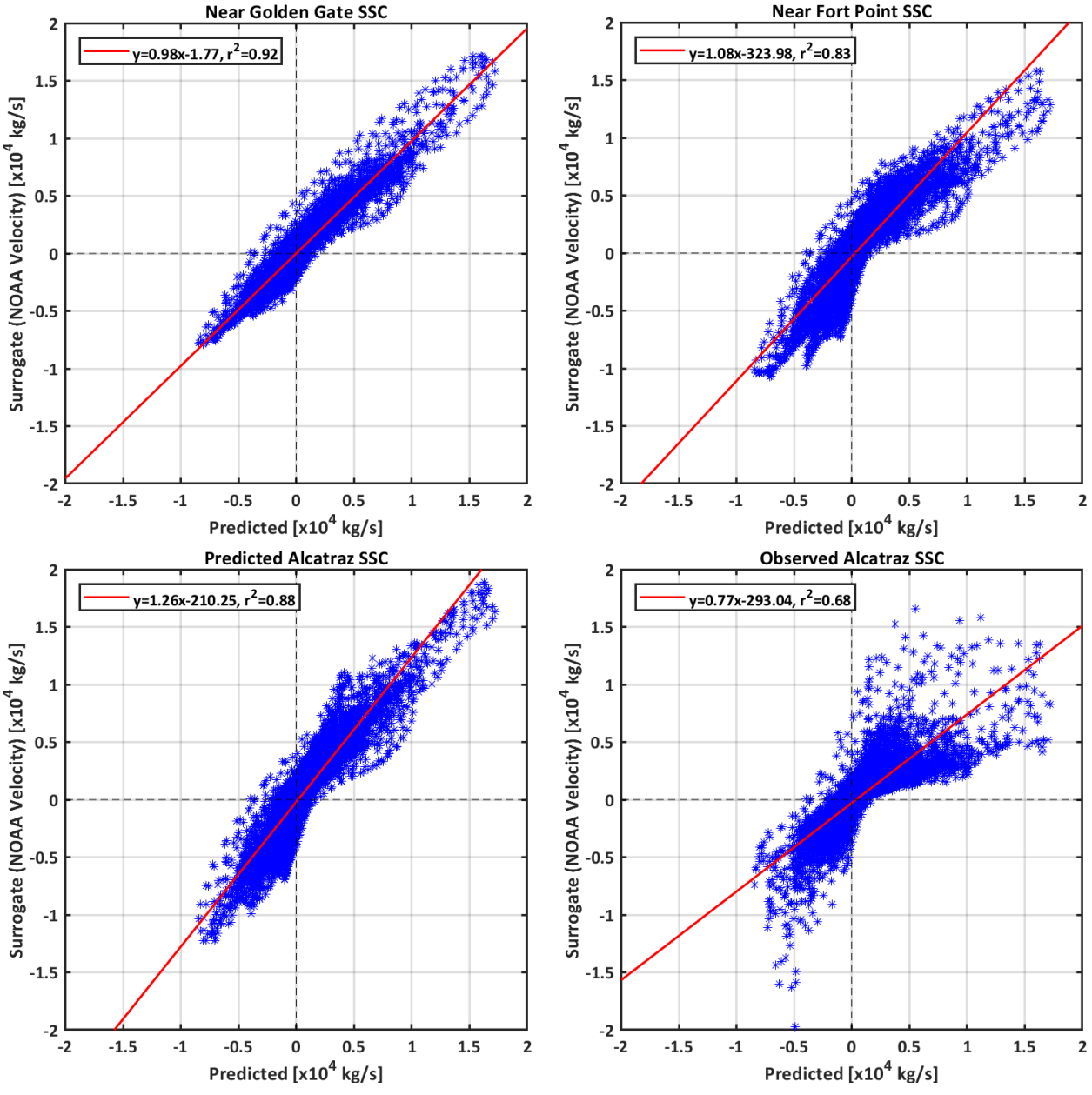

Figure 6.3-4
Tidal-Averaged Sediment Flux Through the Golden Gate Using the NOAA Velocity to Estimate Water Flow

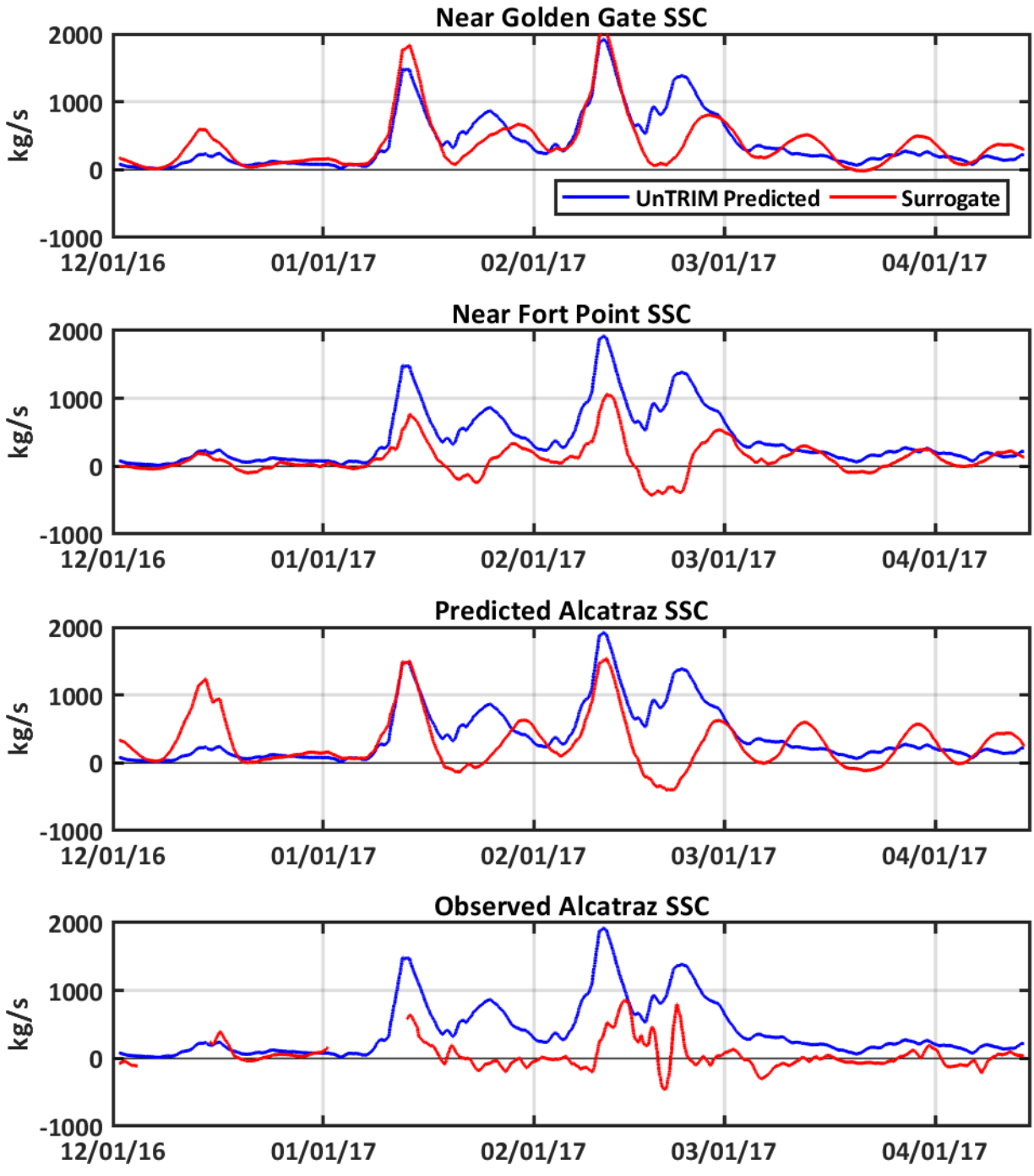

7 Summary and Conclusions

There is significant uncertainty in the quantity and timing of the sediment flux between the Bay and the Pacific Ocean through the constriction at the Golden Gate. A better understanding of the sediment flux through the Golden Gate is needed to better quantify sediment budgets for the Bay. USGS conducted a boat-based data collection to estimate the sediment flux through the Golden Gate during 2016 and again during the high Delta outflow in 2017 (Downing-Kunz et al. 2017). The results of the 2017 sampling over a 16.5-hour period spanning a half tidal cycle suggested sediment flux into the Bay over a tidal cycle during the trailing off of the 2017 high Delta outflow period. Based on the measurements collected during this single flood and ebb tide, USGS estimated a net sediment flux into the Bay (Downing-Kunz et al. 2017), which is inconsistent with the expected net flux of sediment from the Bay to the Pacific Ocean. One of the goals of this analysis was to simulate the period spanning the 16.5-hour USGS data collection period to better understand how this single observed ebb tide and flood tide sediment flux fit into the larger context of sediment flux across the longer high flow period.

The high-resolution UnTRIM Bay-Delta model was used to simulate hydrodynamics, waves, and sediment transport throughout the Bay and the Delta as part of a set of modeling studies overseen by SFEI and funded through the Bay RMP and the Nutrient Management Strategy. The goal of this Bay RMP sediment modeling study was to predict sediment flux through the Golden Gate over the entire 2017 high Delta outflow period and relate findings from the model simulation to the data-based estimates of sediment flux from USGS.

Validation of the predicted velocity and SSC at the locations of the USGS data collection showed the velocity along the transects was accurately predicted. The overall magnitude of the observed SSC was well predicted. However, some of the temporal and spatial variability in the observed SSC was not captured in the predicted SSC, notably the abrupt decrease in observed SSC near slack after ebb. The water fluxes through the transects were accurately predicted. The predicted sediment flux from the model was greater than the data-based sediment flux estimates during ebb-directed flux and less than the data-based sediment flux estimates during flood-directed flux. Overall, the similarity in the model-based and data-based estimates of water and sediment fluxes, in terms of both their relative magnitudes (Table 4-1) and temporal variability (Figures 4.2-1 through 4.2-4), demonstrates the UnTRIM Bay-Delta model is a useful tool for examining water and sediment fluxes through the Golden Gate. The predicted sediment flux was more ebb-directed than the data-based sediment flux, which adds some uncertainty to the predicted net sediment flux around the period of data collection.

During any individual half of the mixed semidiurnal tidal cycle (one flood and the following ebb), the model simulations demonstrate that the net water flow can be into or out of the Bay depending on tidal asymmetry and the freshwater inflow to the Bay (Figure 5.2-3). The model simulations also

confirm that the net water flow over a complete tidal cycle (two floods and two ebbs) can be either into the Bay or out of the Bay during periods of low freshwater inflow to the Bay and likely alternates between into and out of the Bay based on spring-neap cycles. During periods of elevated freshwater inflow to the Bay, such as during the 2017 high Delta outflow period, the net water flow over complete tidal cycles is out of the Bay. The net water flow decreased following the high Delta outflows in 2017 but remained out of the Bay because of the higher Delta outflow following the 2017 high Delta outflow period than before.

Analysis of the model results suggests that the sediment flux through the Golden Gate can be in either the flood or ebb direction, dependent on tidal asymmetry and the duration of the analysis period. When evaluating sediment flux over a half of the mixed semidiurnal tidal cycle (one flood and one ebb tide), the predicted sediment flux was often in the flood direction. However, the predicted sediment flux was always in the ebb direction when evaluated over a complete tidal cycle (two flood and two ebb tides). The predicted sediment flux also had two periods during the 2017 high Delta outflow period when the net flood-directed flux was increasing while the net ebb-directed flux was decreasing, resulting in the flood- and ebb-directed sediment fluxes becoming closer in magnitude. Since the USGS data collection spanned half a tidal cycle (one flood and one ebb tide) and occurred during a period when the predicted flood and ebb-directed fluxes were becoming closer in magnitude, either or a combination of the short data collection period and the decrease in the difference in the net flood- and ebb-directed fluxes could be resulting in the USGS-observed sediment flux in the flood (into the Bay) direction. However, there could also be other factors or physical processes influencing the sediment fluxes calculated from the ADCP data. Another data collection study that spanned a complete tidal cycle consisting of two flood and two ebb tides during both periods with large asymmetry in the tides and with minimal asymmetry in the tides would provide valuable information for further evaluating the periodic nature of the predicted sediment flux into the Bay.

An initial hypothesis was that the USGS ADCP-based sediment flux was into the Bay due to the timing of the data collection at the trailing end of the period of high Delta outflow and that if the data collection had occurred closer to the peaks in Delta outflow the USGS data-based ADCP sediment flux would have been directed out of the Bay. The overestimation of the model-based ADCP sediment flux in the ebb direction relative to the data-based ADCP sediment flux limits the ability for the model predictions to confirm or refute this hypothesis. However, the predicted ebb-directed net sediment flux was higher during the peaks in Delta outflow than during the data collection period. This suggests that had the data collection occurred during the peaks in Delta outflow, the data-based ADCP sediment flux would have been more likely to be directed out of the Bay, even when sampling only half the mixed semidiurnal tidal cycle.

Surrogate measurements of water flow through the Golden Gate and SSC were used to calculate surrogate estimates of sediment flux through the Golden Gate. These surrogate estimates of sediment flux were compared to the predicted cross-sectional sediment flux through the Golden Gate to evaluate the accuracy of the surrogate sediment fluxes. This comparison evaluated how well each surrogate sediment flux estimates represented the modeled sediment flux. This analysis showed that the predicted cross-sectional sediment flux could be moderately well represented using water flow at the Golden Gate derived from the publicly available NOAA-predicted velocity and SSC near the Golden Gate. The accuracy of the surrogate sediment flux decreased as the distance from the Golden Gate to the location of the SSC increased. For example, using predicted SSC at Alcatraz resulted in a surrogate sediment flux that did not match the predicted flux as well as surrogate sediment fluxes calculated using point measures of SSC located closer to the Golden Gate. This analysis suggests that the closer to the channel at the Golden Gate the SSC can be observed, the better the surrogate estimates of sediment flux will be.

The Golden Gate water flow predicted from the NOAA velocity using the simple relationship developed in this study has the main drawback of not including net flows through the Golden Gate based on freshwater inflows to the Bay, and possibly to a lesser extent net flows resulting from atmospheric forcing. The NOAA-predicted velocity to Golden Gate water flow relationship could be improved by evaluating a longer time period and incorporating a metric for freshwater flow to the Bay (possibly Delta outflow) to better capture net water flows through the Golden Gate. Overall, this analysis suggests that it may be possible to reasonably estimate sediment flux through the Golden Gate using the harmonically predicted tidal currents and an estimate of net water outflow if continuous backscatter data can be collected near the Golden Gate. However, a more detailed analysis would be needed to develop relationships for flow and sediment flux using this data to build on the preliminary investigation of developing a surrogate for sediment flux that was presented in this report.

Acknowledgements

This study was conducted as part of a set of modeling studies overseen by SFEI and funded through the Bay RMP. The authors would like to thank Scott Dusterhoff (SFEI) and Melissa Foley (SFEI) for their oversight of the study. We would also like to thank Maureen Downing-Kunz (USGS) and Paul Work (USGS) for sharing their data and ADCP processing script and for their helpful and constructive feedback on our approach and analysis during the course of this study. We thank those who reviewed an earlier draft of this report for their constructive comments, including Bruce Jaffe, David Schoellhamer, Jessica Lacy, Lester McKee, Melissa Foley, Patricia Wiberg, Paul Work, and Scott Dusterhoff. The UnTRIM code was developed by Professor Vincenzo Casulli (University of Trento, Italy). The SediMorph model was originally developed at the German Federal Waterways Engineering and Research Institute in Hamburg (BAW-Hamburg) by Andreas Malcherek. The SediMorph model was provided through a collaboration agreement with the BAW.

References

Anchor QEA (Anchor QEA, LLC), 2017. *Influence of Observed Decadal Declines in Wind Speed and Sediment Supply on Turbidity in the San Francisco Estuary*. Prepared for the Metropolitan Water District of Southern California. June 2017.

Barnard, P.L., A.C. Foxgrover, E.P.L. Elias, L.H. Erikson, J.R. Hein, M. McGann, K. Mizell, R.J. Rosenbauer, P.W. Swarzenski, R.K. Takesue, F. Wong, and D.L. Woodrow, 2013. "Integration of Bed Characteristics, Geochemical Tracers, Current Measurements, and Numerical Modeling for Assessing the Provenance of Beach Sand in the San Francisco Bay Coastal System." *Marine Geology* 336:120–145. Available at: http://dx.doi.org/10.1016/j.margeo.2013.08.007.

BAW (Bundesanstalt für Wasserbau [Federal Waterways Engineering and Research Institute]), 2005. *Mathematical Module SediMorph*. Validation Document, Version 1.1.

Bever, A.J., and M.L. MacWilliams, 2013. "Simulating Sediment Transport Processes in San Pablo Bay Using Coupled Hydrodynamic, Wave, and Sediment Transport Models." *Marine Geology* 345:235–253. Available at: https://doi.org/10.1016/j.margeo.2013.06.012.

Bever, A.J., and M.L. MacWilliams, 2014. *South San Francisco Bay Sediment Transport Modeling*. Prepared for the U.S. Army Corps of Engineers, San Francisco District. July 15, 2014.

Bever, A.J., M.L MacWilliams, F. Wu, L. Andes, and C.S. Conner, 2014. *Numerical Modeling of Sediment Dispersal Following Dredge Material Placements to Examine Possible Augmentation of the Sediment Supply to Marshes and Mudflats, San Francisco Bay, USA*. 33rd PIANC World Congress (San Francisco, California); June 2014.

Bever, A.J., M.L. MacWilliams, and D.K. Fullerton, 2018. "The Influence of an Observed Decadal Decline in Wind Speed on Turbidity in the San Francisco Estuary." *Estuaries and Coasts* 41:1943–1967. Available at: https://doi.org/10.1007/s12237-018-0403-x.

CDWR (California Department of Water Resources), 1995. *Estimation of Delta Island Diversions and Return Flows*. Modeling Support Branch, Division of Planning. February 1995.

Cheng, R.T., V. Casulli, and J.W. Gartner, 1993. "Tidal Residual Intertidal Mudflat (TRIM) Model and Its Applications to San Francisco Bay, California." *Estuarine, Coastal and Shelf Science* 369:235–280. Available at: http://dx.doi.org/10.1006/ecss.1993.1016.

Delta Modeling Associates (Delta Modeling Associates, Inc.), 2014. *Evaluation of Effects of Prospect Island Restoration on Sediment Transport and Turbidity: Phase 2 Alternatives. Final Report: Prospect Island Tidal Habitat Restoration Project.* Prepared for the California Department of Water Resources and Wetlands and Water Resources, Inc. March 6, 2014.

Delta Modeling Associates, 2015. *Analysis of the Effect of Project Depth, Water Year Type and Advanced Maintenance Dredging on Shoaling Rates in the Oakland Harbor Navigation Channel, Central San Francisco Bay 3-D Sediment Transport Modeling Study, Final Report*. Prepared for the U.S. Army Corps of Engineers, San Francisco District. March 2015.

Downing-Kunz, M., D. Schoellhamer, and P. Work, 2017. *Water and Suspended-Sediment Flux Measurements at the Golden Gate, 2016–2017*. SFEI Document Number 856. December 2017.

Downing-Kunz, M., D. Schoellhamer, and P. Work, 2018. *ADCP Data in Support of Water and Suspended-Sediment Flux Measurements at the Golden Gate, 2016–2017*. U.S. Geological Survey Data Release. 2018. Available at: https://doi.org/10.5066/F7639P1N.

Eisma, D., 1986. "Flocculation and De-Flocculation of Suspended Matter in Estuaries." *Netherlands Journal of Sea Research* 20:183–199. Available at: http://dx.doi.org/10.1016/0077-7579(86)90041-4.

Fugate, D.C., and C.T. Friedrichs, 2003. "Controls on Suspended Aggregate Size in Partially Mixed Estuaries." *Estuarine, Coastal and Shelf Science* 58:389–404. Available at: http://dx.doi.org/10.1016/S0272-7714(03)00107-0.

Funakoshi, Y., S.C. Hagen, and P. Bacopoulos, 2008. "Coupling of Hydrodynamic and Wave Models: Case Study for Hurricane Floyd (1999) Hindcast." *Journal of Waterway, Port, Coastal, and Ocean Engineering* 134(6):321–335. Available at: https://doi.org/10.1061/(ASCE)0733-950X(2008)134:6(321).

Ganju, N.K., and D.H. Schoellhamer, 2009. "Calibration of an Estuarine Sediment Transport Model to Sediment Fluxes as an Intermediate Step for Simulation of Geomorphic Evolution." *Continental Shelf Research* 29: 148–158. Available at: https://doi.org/10.1016/j.csr.2007.09.005.

Gross, E.S., M.L. MacWilliams, and W.J. Kimmerer, 2010. "Three-Dimensional Modeling of Tidal Hydrodynamics in the San Francisco Estuary." *San Francisco Estuary and Watershed Science*. 7(2). Available at: https://escholarship.org/uc/item/9rv243mg.

Haidvogel, D.B., H. Arango, W.P. Budgell, B.D. Coruelle, E. Curshitser, E.D. Lorenzo, K. Fennel, W.R. Geyer, A.J. Hermann, L. Lanerolle, J. Levin, J.C. McWilliams, A.J. Miller, A.M. Moore, T.M. Powell, A.F. Schepetkin, C.R. Sherwood, R.P. Signell, J.C. Warner, and J. Wilkin, 2008. "Regional Ocean Forecasting in Terrain-Following Coordinates: Model Formulation and Skill Assessment." *Journal of Computational Physics* 227:3595–3624. Available at: https://doi.org/10.1016/j.jcp.2007.06.016.

Hill, P.S., and I.N. McCave, 2001. "Suspended Particle Transport in Benthic Boundary Layers." *The Benthic Boundary Layer*. Editors, B.P. Boudreau and B.B. Jorgensen. Oxford, England: Oxford University Press; pp. 78–103.

Hofmann, E.E., B. Cahill, K. Fennel, M.A.M. Friedrichs, K. Hyde, C. Lee, A. Mannino, R.G. Najjar, J.E. O'Reilly, J. Wilkin, and J. Xue, 2011. "Modeling the Dynamics of Continental Shelf Carbon." *Annual Review of Marine Science* 3:93–122. Available at: https://doi.org/10.1146/annurev-marine-120709-142740.

Huzzey, L.M., J.E., Cloern, and T.M. Powell, 1990. "Episodic Changes in Lateral Transport and Phytoplankton Distribution in South San Francisco Bay." *Limnology and Oceanography* 35:472–478.

Jenkins, C.J., 2010. *dbSEABED: An Information Processing System for Marine Substrates*. Available at: http://instaar.colorado.edu/~jenkinsc/dbseabed/.

Jolliff, J.K., J.C. Kindle, I. Shulman, B. Penta, M.A.M. Friedrichs, R. Helber, and R.A. Arnone, 2009. "Summary Diagrams for Coupled Hydrodynamic-Ecosystem Model Skill Assessment." *Journal of Marine Systems* 76:64–82. Available at: https://doi.org/10.1016/j.jmarsys.2008.05.014.

Kineke, G.C., and R.W. Sternberg, 1989. "The Effect of Particle Settling Velocity on Computed Suspended Sediment Concentration Profiles." *Marine Geology* 90:159–174. Available at: http://dx.doi.org/10.1016/0025-3227(89)90039-X.

MacWilliams, M.L., and R.T. Cheng, 2007. *Three-Dimensional Hydrodynamic Modeling of San Pablo Bay on an Unstructured Grid.* 7th International Conference on Hydroscience and Engineering (Philadelphia, Pennsylvania); September 10–13, 2007.

MacWilliams, M.L., and E.S. Gross, 2007. *UnTRIM San Francisco Bay-Delta Model Calibration Report, Delta Risk Management Study*. Prepared for the California Department of Water Resources. March 2007.

MacWilliams, M.L., E.S. Gross, J.F. DeGeorge, and R.R. Rachiele, 2007. *Three-Dimensional Hydrodynamic Modeling of the San Francisco Estuary on an Unstructured Grid*. 32nd Congress of the International Association of Hydro-Environment Engineering and Research (Venice, Italy); July 1–6, 2007.

MacWilliams, M.L., F.G. Salcedo, and E.S. Gross, 2008. *San Francisco Bay-Delta UnTRIM Model Calibration Report, POD 3-D Particle Tracking Modeling Study*. Prepared for the California Department of Water Resources. December 19, 2008.

MacWilliams, M.L., F.G. Salcedo, and E.S. Gross, 2009. *San Francisco Bay-Delta UnTRIM Model Calibration Report, Sacramento and Stockton Deep Water Ship Channel 3-D Hydrodynamic and Salinity Modeling Study*. Prepared for the U.S. Army Corps of Engineers, San Francisco District. July 14, 2009.

MacWilliams, M.L., and E.S. Gross, 2010. *UnTRIM San Francisco Bay-Delta Model Sea Level Rise Scenario Modeling Report, Bay Delta Conservation Plan*. Final Report. Prepared for Science Applications International Corporation and the California Department of Water Resources. July 16, 2010.

MacWilliams, M.L., N.E. Kilham, and A.J. Bever, 2012a. *South San Francisco Bay Long Wave Modeling Report*. Prepared for the U.S. Army Corps of Engineers, San Francisco District. 2012.

MacWilliams, M.L., A.J. Bever, and E.S. Gross, 2012b. *Three-Dimensional Sediment Transport Modeling for San Francisco Bay RDMMP*. Prepared for the U.S. Army Corps of Engineers, San Francisco District. November 21, 2012.

MacWilliams, M.L., and E.S. Gross, 2013. "Hydrodynamic Simulation of Circulation and Residence Time in Clifton Court Forebay." *San Francisco Estuary and Watershed Science* 11(2):30. Available at: https://escholarship.org/uc/item/4q82g2bz.

MacWilliams M.L., P.F. Sing, F. Wu, and N. Hedgecock, 2014. *Evaluation of the Potential Salinity Impacts Resulting from the Deepening of the San Francisco Bay to Stockton Navigation Improvement Project*. 33rd PIANC World Congress (San Francisco, California); June 2014.

MacWilliams, M.L., A.J. Bever, E.S. Gross, G.A. Ketefian, and W.J. Kimmerer, 2015. "Three-Dimensional Modeling of Hydrodynamics and Salinity in the San Francisco Estuary: An Evaluation of Model Accuracy, X2, and the Low Salinity Zone." *San Francisco Estuary and Watershed Science* 13(1):37. Available at: http://dx.doi.org/10.15447/sfews.2015v13iss1art2.

MacWilliams, M.L., A.J. Bever, and E. Foresman, 2016. "3-D Simulations of the San Francisco Estuary with Subgrid Bathymetry to Explore Long-Term Trends in Salinity Distribution and Fish Abundance." *San Francisco Estuary and Watershed Science* 14(2). Available at: http://escholarship.org/uc/item/5qj0k0m6.

Mikkelsen, O.A., P.S. Hill, and T.G. Milligan, 2006. "Single Grain, Microfloc and Macrofloc Volume Variations Observed with a LISST-100 and a Digital Floc Camera." *Journal of Sea Research* 55(2): 87–102. Available at: http://dx.doi.org/10.1016/j.seares.2005.09.003.

NOAA (National Oceanic and Atmospheric Administration), 2020. "Golden Gate Currents – Station ID: SFB1202." Accessed September 30, 2020. Available at: https://tidesandcurrents.noaa.gov/stationhome.html?id=SFB1202.

Pratt, T.C., H.A. Benson, A.M. Teeter, and J.V. Letter, 1994. *San Francisco Bay Long Term Management Strategy (LTMS) for Dredging and Disposal Report 4 Field Data Collection*. Technical Report HL-94-1994. 1994.

Ralston, D.K., W.R. Geyer, and J.A. Lerczak, 2010. "Structure, Variability, and Salt Flux in a Strongly Forced Salt Wedge Estuary." *Journal of Geophysical Research* 115. Available at: http://dx.doi.org/10.1029/2009JC005806.

Schoellhamer, D.H., N.K. Ganju, P.R. Mineart, and M.A. Lionberger, 2008. "Sensitivity and Spin Up Times of Cohesive Sediment Transport Models Used to Simulate Bathymetric Change." *Marine Science* 9:463–475. Available at: http://dx.doi.org/10.1016/S1568-2692(08)80033-2.

Sea Engineering, 2008. "Aquatic Transfer Facility Sediment Transport Analysis." *Technical Studies for the Aquatic Transfer Facility*: *Hamilton Wetlands Restoration Project*. Editors, D.A. Cacchione and P.A. Mull.

Smith, S.J., and C.T. Friedrichs, 2011. "Size and Settling Velocities of Cohesive Flocs and Suspended Sediment Aggregates in a Trailing Suction Hopper Dredge Plume." *Continental Shelf Research* 31(10):550–563. Available at: http://dx.doi.org/10.1016/j.csr.2010.04.002.

Stacey, M.T., 1996. *Turbulent Mixing and Residual Circulation in a Partially Stratified Estuary*. PhD Thesis. Stanford, California. Stanford University; Department of Civil Engineering.

SWAN Team (Simulating WAves Nearshore Team), 2009a. *SWAN User Manual Version 40.72*. Delft, Netherlands: Delft University of Technology.

SWAN Team, 2009b. *SWAN Scientific and Technical Documentation 40.72*. Delft, Netherlands: Delft University of Technology.

USGS (U.S. Geological Survey), 2020a. "USGS Water Data for California." *National Water Information System*. Accessed February 2020. Available at: http://waterdata.usgs.gov/ca/nwis/.

USGS, 2020b. "Water Quality of San Francisco Bay." Accessed February 2020. Available at: https://sfbay.wr.usgs.gov/access/wqdata/.

van der Wegen, M., B.E. Jaffe, and J.A. Roelvink, 2011. "Process-Based, Morphodynamic Hindcast of Decadal Deposition Patterns in San Pablo Bay, California, 1856–1887." *Journal of Geophysical Research* 116:F2. Available at: http://dx.doi.org/10.1029/2009JF001614.

Wang, B., S.N. Giddings, O.B. Fringer, E.S. Gross, D.A. Fong, and S.G. Monismith, 2011. "Modeling and Understanding Turbulent Mixing in a Macrotidal Salt Wedge Estuary." *Journal of Geophysical Research* 116:C2(C02036). Available at: http://dx.doi.org/10.1029/2010JC006135.

Warner, J.C., W.R. Geyer, and J.A. Lerczak, 2005a. "Numerical Modeling of an Estuary: A Comprehensive Skill Assessment." *Journal of Geophysical Research* 110(C05001). Available at: http://dx.doi.org/10.1029/2004JC002691.

Warner J.C., C.S. Sherwood, H.G. Arango, and R.P. Signell, 2005b. "Performance of Four Turbulence Closure Models Implemented Using a Generic Length Scale Method." *Ocean Modeling* 8:81–113. Available at: http://dx.doi.org/10.1016/j.ocemod.2003.12.003.

Weilbeer, H., 2005. "Numerical Simulation and Analyses of Sediment Transport Processes in the Ems-Dollard Estuary with a Three-Dimensional Model." *Sediment and Ecohydraulics: INTERCOH 2005*. Editors, T. Kusuda, H. Yamanishi, J. Spearman, and J.Z. Gailani. Amsterdam, Netherlands: Elsevier.

Willmott, C.J., 1981. "On the Validation of Models." *Physical Geography* 2:184–194.

Wright, S. (U.S. Geological Survey), 2012. Personal communication with Aaron Bever and Michael MacWilliams (Delta Modeling Associates). 2012.

Wright, S.A., and D.H. Schoellhamer, 2005. "Estimating Sediment Budgets at the Interface Between Rivers and Estuaries with Application to the Sacramento-San Joaquin River Delta." *Water Resources Research* 4:W09428.

Appendix A
Model Validation

A. Model Validation

A.1 Summary

Because the UnTRIM Bay-Delta model has already been extensively validated, this appendix provides model validations SSC throughout the Bay during the period that the Golden Gate sediment flux was examined. Predicted SSC was compared to observed SSC using time series at discrete locations and transects of SSC vertical profiles spanning from the far South Bay to Rio Vista. Time series data were available from five locations through USGS (USGS 2020a). The vertical profiles of SSC were also available from USGS (USGS 2020b). Transects that only spanned a very short length of the Bay were excluded from the comparison.

A.2 Statistics Used for Model Validation

Following the approach used by MacWilliams et al. (2015), model skill and target diagrams were used to provide quantitative metrics for evaluating model accuracy. Willmott (1981) defined the predictive skill of a model based on the quantitative agreement between observations (*O*) and model predictions (*M*) as shown in Equation A-1.

Equation A-1

$$Skill = 1 - \left[\sum_{i=1}^{N} \left| X_{Mi} - X_{Oi} \right|^2 \right] / \left[\sum_{i=1}^{N} \left(\left| X_{Mi} - \overline{X_O} \right| + \left| X_{Oi} - \overline{X_O} \right| \right)^2 \right]$$

where:

X	=	the variable being compared
$\bar{X}$	=	time average of *X*
M_i	=	model value at time *i* of *N* total comparison times
O_i	=	observation at time *i*

Perfect agreement between model results and observations yields a skill of 1. Although the Willmott (1981) model skill metric has some shortcomings (Ralston et al. 2010), it has nevertheless been used for comparing model predictions to observed data in numerous hydrodynamic modeling studies (e.g., Warner et al. 2005a; Haidvogel et al. 2008; MacWilliams and Gross 2013; MacWilliams et al. 2015).

Jolliff et al. (2009) and Hofmann et al. (2011) provide detailed descriptions of target diagrams and their use in assessing model skill. This approach uses the *bias* and the unbiased root-mean-square

difference (*ubRMSD*) to assess the accuracy of the model predictions. The *bias* of the model estimates is calculated as shown in Equation A-2.

Equation A-2

$$bias = \frac{1}{N}\sum_{i=1}^{N} X_{Mi} - \frac{1}{N}\sum_{i=1}^{N} X_{Oi}$$

The *ubRMSD* is calculated as shown in Equation A-3.

Equation A-3

$$ubRMSD = \left(\frac{1}{N}\sum_{i=1}^{N} \left[\left(X_{Mi} - \overline{X_M} \right) - \left(X_{Oi} - \overline{X_O} \right) \right]^2 \right)^{0.5}$$

To indicate whether the modeled variability is greater than or less than the observed variability, the *ubRMSD* is multiplied by the sign of the difference in the modeled and observed standard deviations, as shown in Equation A-4.

Equation A-4

$$ubRMSD_2 = ubRMSD(\sigma_M - \sigma_O)/|\sigma_M - \sigma_O|$$

where:

σ_M	=	modeled standard deviation
σ_O	=	observed standard deviation

The *bias* and the *ubRMSD*$_2$ are normalized (denoted by subscript *N*) by the observed standard deviation to make their absolute values comparable among different variables and different sets of observed data, as shown in Equations A-5 and A-6.

Equation A-5

$$bias_N = bias/\sigma_O$$

Equation A-6

$$ubRMSD_N = ubRMSD_2/\sigma_O$$

On each target diagram, the $bias_N$ between modeled and observed values is plotted on the Y-axis, and the $ubRMSD_N$ is plotted on the X-axis. The radial distance from the origin to each data point is the normalized root-mean-square difference ($RMSD_N$), as shown in Equation A-7.

Equation A-7

$$RMSD_N = \sqrt{bias_N^2 + ubRMSD_N^2}$$

MacWilliams et al. (2015) provide a more detailed description of the model validation methods and suggest thresholds for the validation metrics that indicate model accuracy. These target diagram thresholds were adopted in this report to classify the model accuracy. Very accurate predictions are classified as those with an $RMSD_N$ of less than 0.25, and accurate predictions are classified as those with an $RMSD_N$ of less than 0.5. Acceptable predictions are indicated by an $RMSD_N$ of less than 1.0, and an $RMSD_N$ of greater than 1.0 indicates less accurate predictions.

A.3 Validation of Predicted SSC

Predicted SSCs were validated using continuous-monitoring time-series data at fixed locations in the Bay (Figure A-1). Time-series SSC was validated at five locations, with three locations having both upper and lower sensors. This resulted in a total of eight comparisons. The figures for comparing predicted and observed time series include upper panels that highlight the instantaneous predicted and observed SSC over relatively short time intervals, tidal-averaged predicted and observed SSC on the lower left panel over the complete analysis period, and a scatter plot on the lower right panel incorporating the complete analysis period. Two instantaneous top panels are shown. The uppermost panel is during the end of the 2017 high Delta outflow period to overlap with the USGS data collection period, while the second from the top panel is following the 2017 high Delta outflow period. This allows for evaluating the tidal timescale variability in the predicted and observed SSC both during and following the 2017 high Delta outflow period.

Using the thresholds for model accuracy from MacWilliams et al. (2015), SSC was acceptably predicted for five comparisons but the $RMSD_N$ was greater than 1.0 for three comparisons (Table A-1; Figure A-2). At the Alcatraz station, predicted SSC accurately captured the increase in SSC as a result

of the 2017 high Delta outflow period and then the decrease in SSC following elevated Delta outflows (Figure A-3). This suggests that the predicted SSC accurately captured the timing of the turbid pulse of water from elevated Delta outflow. However, the higher predicted SSC than observed suggests sediment supply to Central Bay from the Delta may have been overpredicted. The predicted SSC had larger tidal timescale variability during the 2017 high Delta outflow period than following, which matches the observed SSC. At the Pier 17 station, predicted SSC also accurately captured the increase in SSC as a result of the 2017 high Delta outflow period and then the decrease in SSC following the elevated Delta outflows (Figure A-4). Predicted SSC at Pier 17 underestimated the relatively short-duration large-magnitude spikes in the observed SSC at Pier 17.

At the Richmond San Rafael Bridge upper station, predicted SSC accurately captured the increase in SSC as a result of the 2017 high Delta outflow period and then the decrease in SSC following elevated Delta outflow (Figure A-5). Predicted SSC accurately captured the overall tidal timescale variability in the SSC both during and following the 2017 high Delta outflow period, but the model underestimated the relatively short-duration large-magnitude spikes in the observed SSC. The greater range in predicted SSC over a tidal cycle during the 2017 high Delta outflow period than following matches with the observed SSC. At the Richmond-San Rafael Bridge lower station, predicted SSC accurately captured the increase in SSC as a result of the 2017 high Delta outflow period and then the decrease in SSC following elevated Delta outflow (Figure A-6), although predicted SSC was lower than observed during the trailing end of the 2017 high Delta outflow period (around March 1 to 15, 2017). The tidal timescale variability in the predicted SSC was generally lower than in the observed SSC during the 2017 high Delta outflow period. Following the 2017 high Delta outflow period, predicted SSC accurately captured the overall tidal timescale variability in the SSC, but the model underestimated the relatively short-duration large-magnitude spikes in the observed SSC at the Richmond-San Rafael Bridge station.

At the Benicia Bridge upper station, predicted SSC was higher during the 2017 high Delta outflow period than following, matching the pattern in the data, but the model generally underpredicted the SSC during the 2017 high Delta outflow period at this station (Figure A-7). Predicted SSC accurately captured the overall tidal timescale variability in the SSC both during and following the 2017 high Delta outflow period. The greater range in predicted SSC over a tidal cycle during the 2017 high Delta outflow period than following matches with the observed SSC. At the Benicia Bridge lower station, predicted SSC was higher during the 2017 high Delta outflow period than following, matching the pattern in the data, but the model generally underpredicted the SSC during the 2017 high Delta outflow period at this station (Figure A-8). This may be a result of the predicted location of the turbidity maximum being slightly too far seaward. Predicted SSC accurately captured the overall tidal timescale variability in the SSC during the 2017 high Delta outflow period, but the model underpredicted the tidal timescale variability in SSC following elevated Delta outflow. Interestingly, at the Benicia Bridge lower station, the observed SSC has higher tidal timescale variability under lower

average SSC conditions following the 2017 high Delta outflow period than under elevated average SSC conditions during elevated Delta outflow.

At the USGS Dumbarton Bridge upper (Figure A-9) and lower (Figures A-10) stations, the predicted SSC was on average higher than the observed SSC. Neither the predicted nor observed SSC showed a strong signal of the 2017 high Delta outflow period at Dumbarton Bridge.

Modeled SSC accurately captured the increase in the time series SSC as a result of the 2017 high Delta outflow period and decrease in SSC following the elevated Delta outflow at the Central Bay and North Bay stations. Neither the predicted nor observed SSC showed a strong signal of the 2017 high Delta outflow period in the South Bay. Overall, the predicted SSC captured the spatial variability in the average observed SSC (Table A-1). In general, the underprediction of relatively short-duration large-magnitude spikes in SSC partially result in low r^2 and model skill values at some stations, even when the predicted and observed average SSC matches relatively well (i.e., Pier 17, Richmond-San Rafael Bridge). The $ubRMSD_N$ for seven of the eight comparisons was negative, indicating that the variability in the modeled SSC was lower than the variability in the observed SSC. At Alcatraz, the overprediction of SSC during the period of high Delta outflow results in a positive $ubRMSD_N$.

In addition to time series comparisons at fixed locations, predicted SSC was compared to observed SSC along a transect from the far South Bay to Rio Vista (Figures A-11 through A-15). Before the 2017 high Delta outflow period, the predicted SSC very accurately captured the pattern and magnitude in SSC along the transect, including the highest SSC near Dumbarton Bridge, quite low SSC in the Central Bay, and relatively uniform SSC along the transect from Carquinez Bridge to Rio Vista, with increasing SSC toward the bed (Figure A-11). During the 2017 high Delta outflow period, both the predicted and observed SSC show a pronounced turbidity maximum in the North Bay, but the predicted location of the highest SSC is shifted seaward relative to the observed SSC (Figures A-12 and A-14). This indicates that the modeled turbidity maximum was shifted seaward relative to the location suggested by the observed SSC. Immediately following the 2017 high Delta outflow period, the predicted and observed SSC was higher near Dumbarton Bridge and Rio Vista than along the rest of the transect, but the predicted SSC was higher than observed over a large portion of the transect (Figure A-15).

Overall, predicted and observed SSC along the transect running from the far South Bay to Rio Vista showed similar vertical and along-Bay structure. Both the predicted and observed SSC generally had higher concentrations near Carquinez Bridge and in the South Bay (Figures A-11 through A-15) than in the Central Bay during the dates of data collection. Observed SSC showed increasing concentration from the surface to the seabed at times, and the model reproduced this trend (Figure A-11). Predicted SSC tended to be higher than observed within the South Bay after the January 11, 2017 cruise (Figures A-13 and A-15).

Table A-1
Predicted and Observed SSC, Cross-Correlation Statistics, Model Skill, and Target Diagram Statistics for SSC Continuous Monitoring Stations for the 2017 Simulation

Station	Mean SSC		Cross Correlation		r^2	Skill	Target Diagram		
	Observed (mg/L)	Predicted (mg/L)	Amp Ratio	Lag (min)			$bias_N$	$ubRMSD_N$	$RMSD_N$
Alcatraz	33.2	45.8	0.703	NA	0.470	0.783	0.444	0.804	0.918
Pier 17	73.3	66.9	0.215	NA	0.164	0.552	-0.104	-0.923	0.929
Richmond-San Rafael Bridge (Upper)	59.0	72.9	0.306	NA	0.205	0.609	0.153	-0.919	0.932
Richmond-San Rafael Bridge (Lower)	107.6	99.4	0.232	NA	0.208	0.572	-0.058	-0.891	0.893
Benicia Bridge (Upper)	88.2	57.5	0.263	7	0.482	0.599	-0.701	-0.786	1.053
Benicia Bridge (Lower)	98.5	67.5	0.225	7	0.384	0.580	-0.662	-0.826	1.059
USGS Dumbarton Bridge (Upper)	94.7	147.4	0.138	NA	0.043	0.445	0.489	-1.081	1.186
USGS Dumbarton Bridge (Lower)	170.7	180.0	0.243	NA	0.166	0.593	0.068	-0.933	0.935

Note:
The cross correlation did not find a maximum r^2 within a lag of ±60 minutes (indicated as NA for not applicable).

Figure A-1
SSC Continuous Monitoring Stations Used for Model Validation

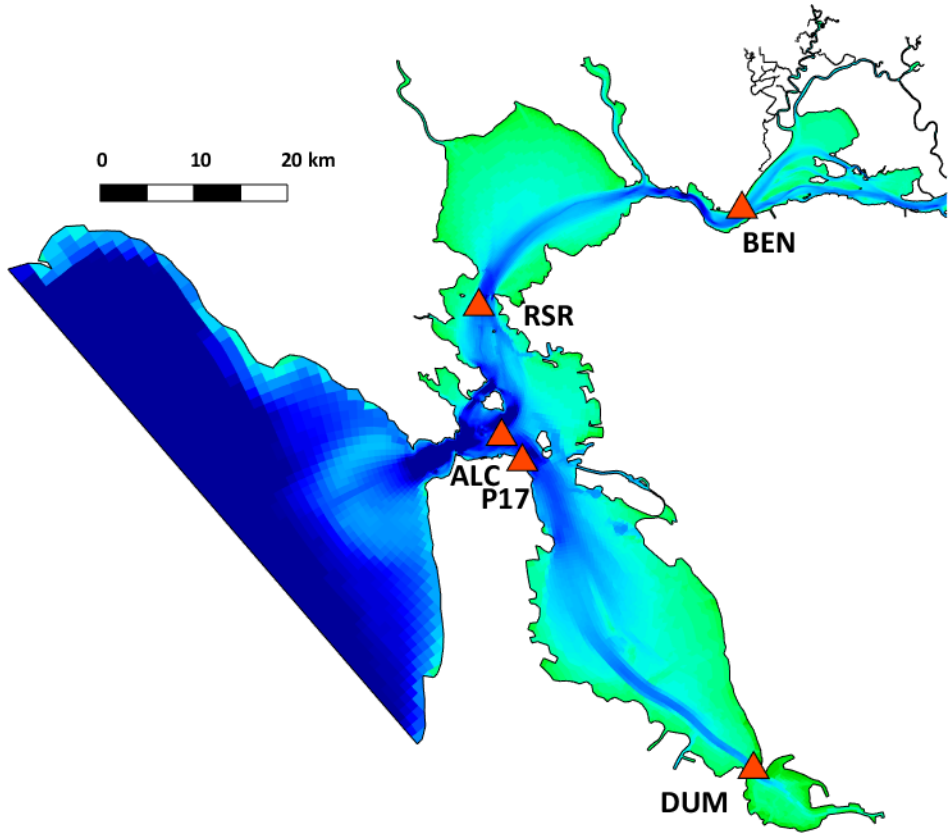

Dumbarton Bridge (DUM)
Pier 17 (P17)
Alcatraz (ALC)
Richmond-San Rafael Bridge (RSR)
Benicia Bridge (BEN)

Figure A-2
Target Diagram Showing the Model Validation Using the Time Series SSC for the 2017 Simulation Period

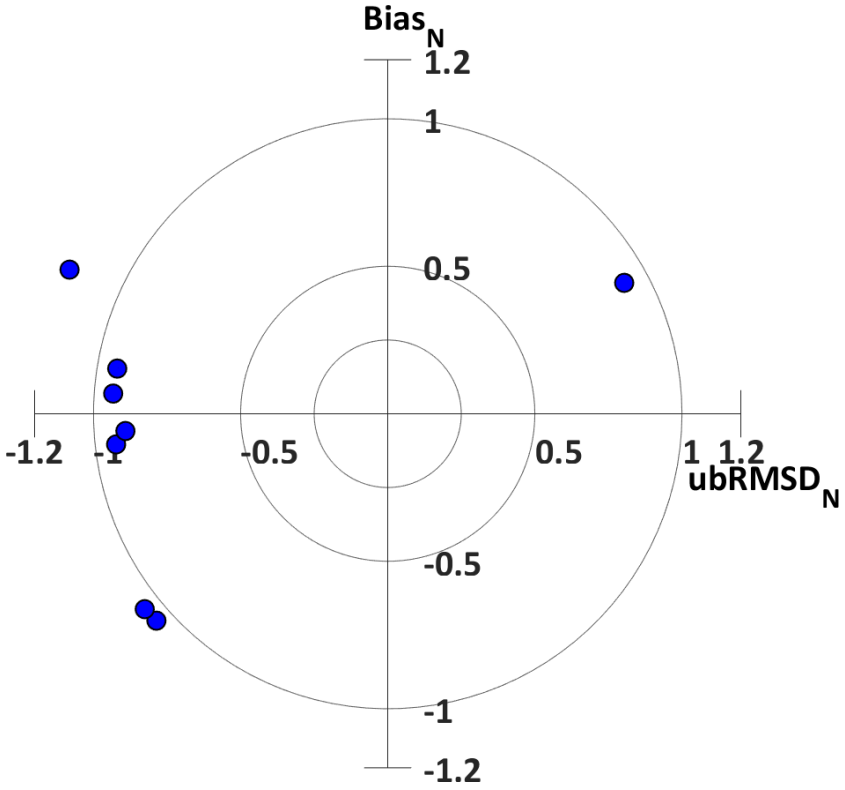

Figure A-3
Observed and Predicted SSC at Alcatraz

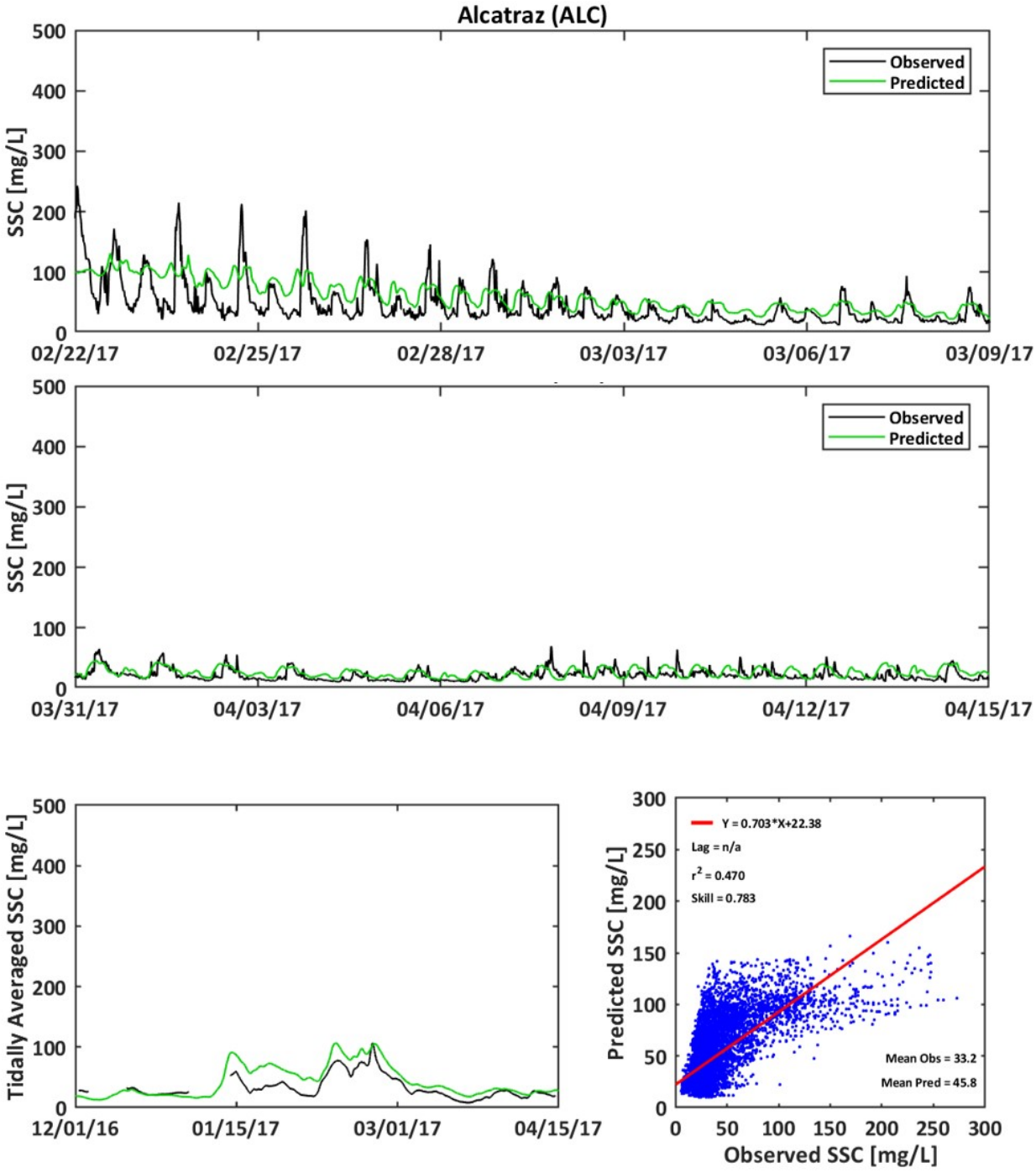

Figure A-4
Observed and Predicted SSC at Pier 17

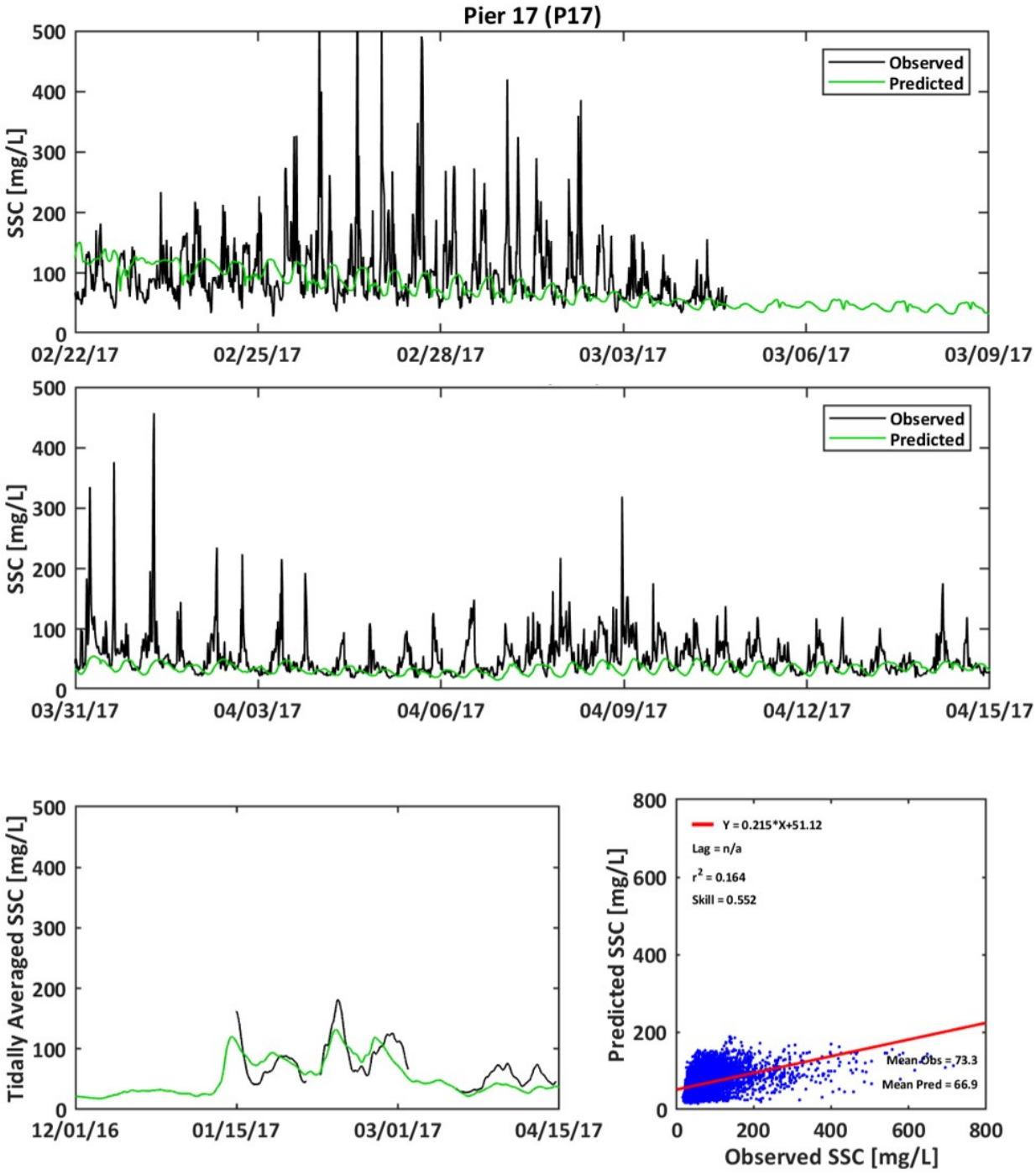

Figure A-5
Observed and Predicted SSC at Richmond-San Rafael Bridge (upper)

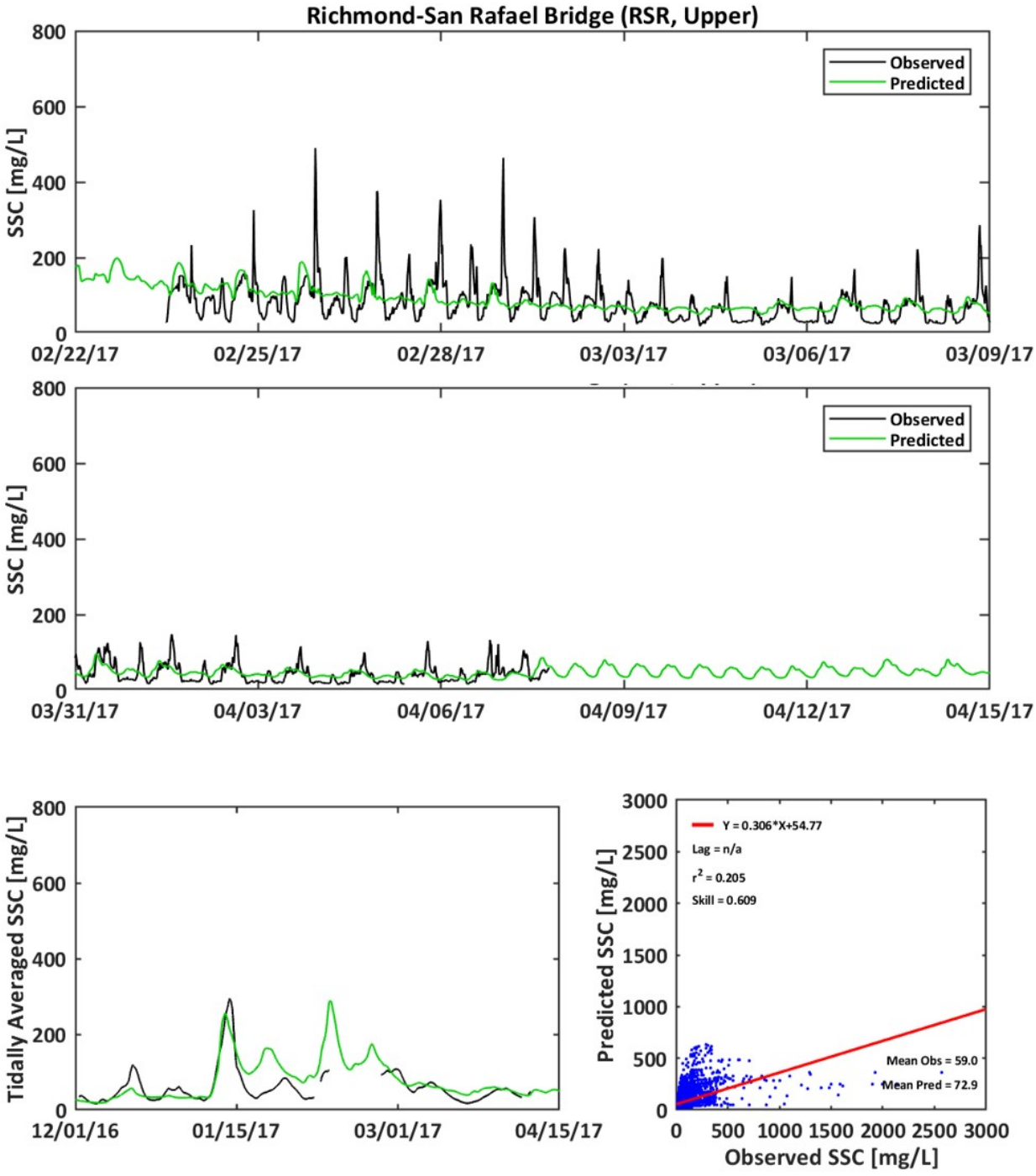

Figure A-6
Observed and Predicted SSC at Richmond-San Rafael Bridge (lower)

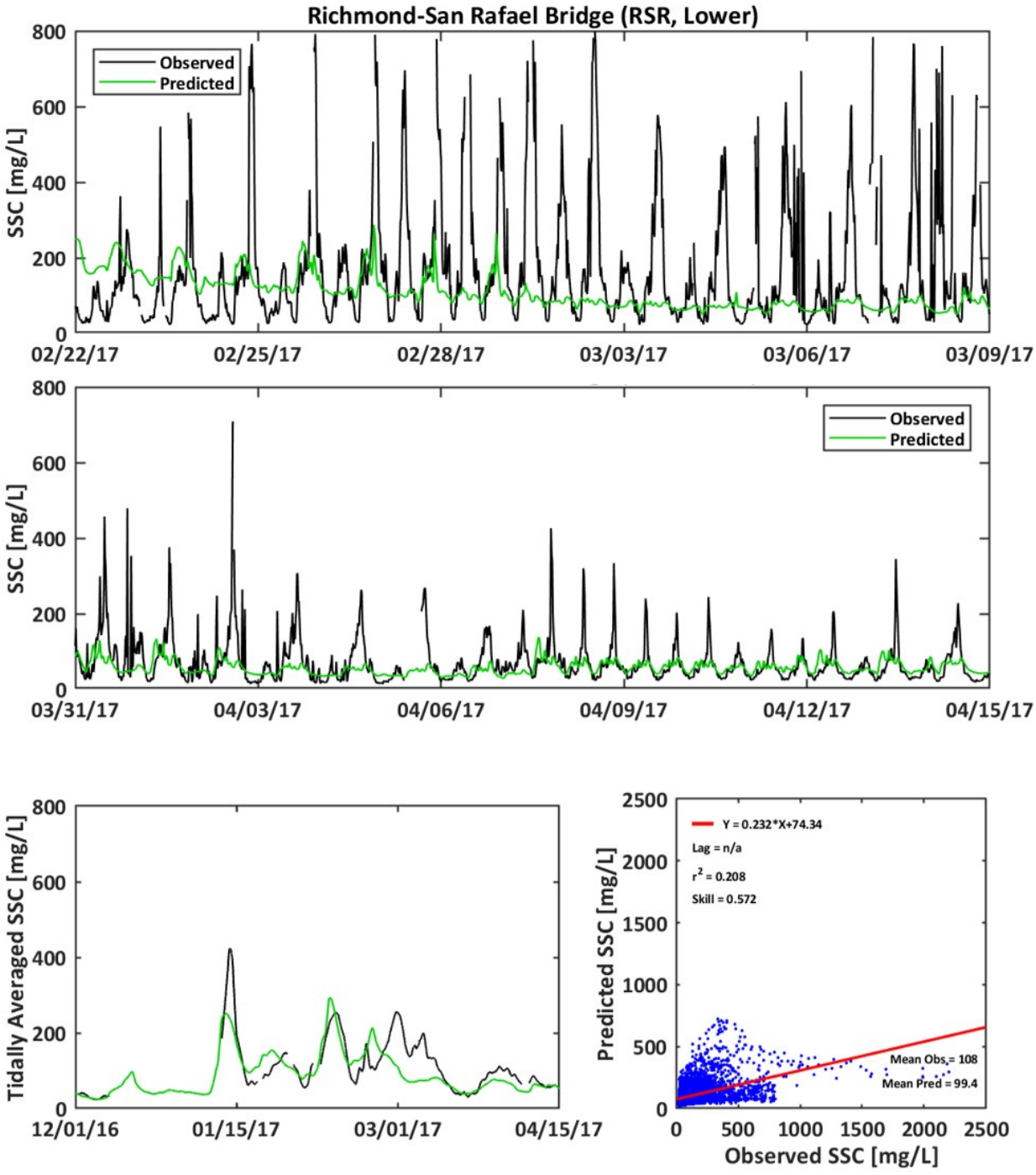

Figure A-7
Observed and Predicted SSC at Benicia Bridge (upper)

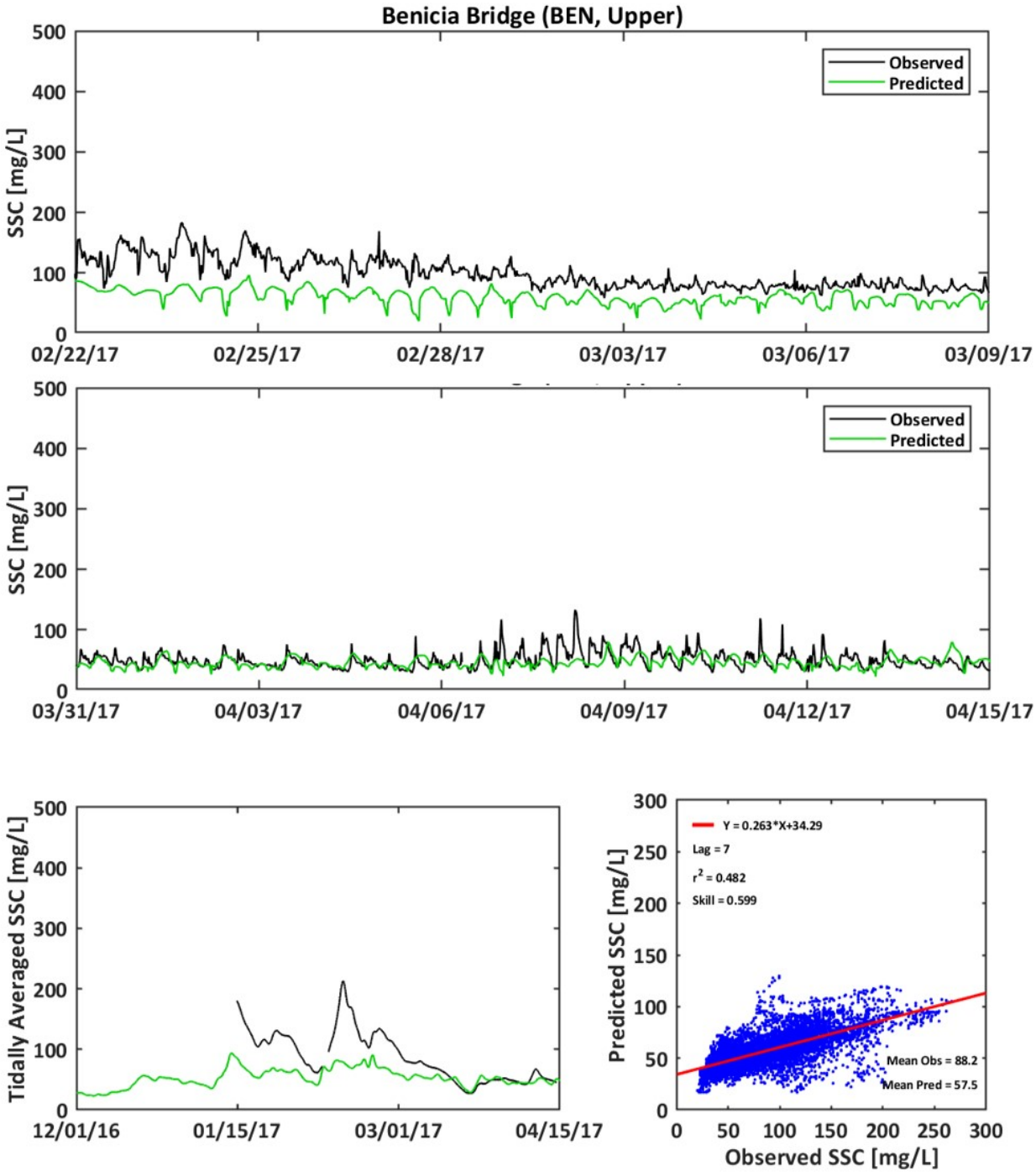

Figure A-8
Observed and Predicted SSC at Benicia Bridge (lower)

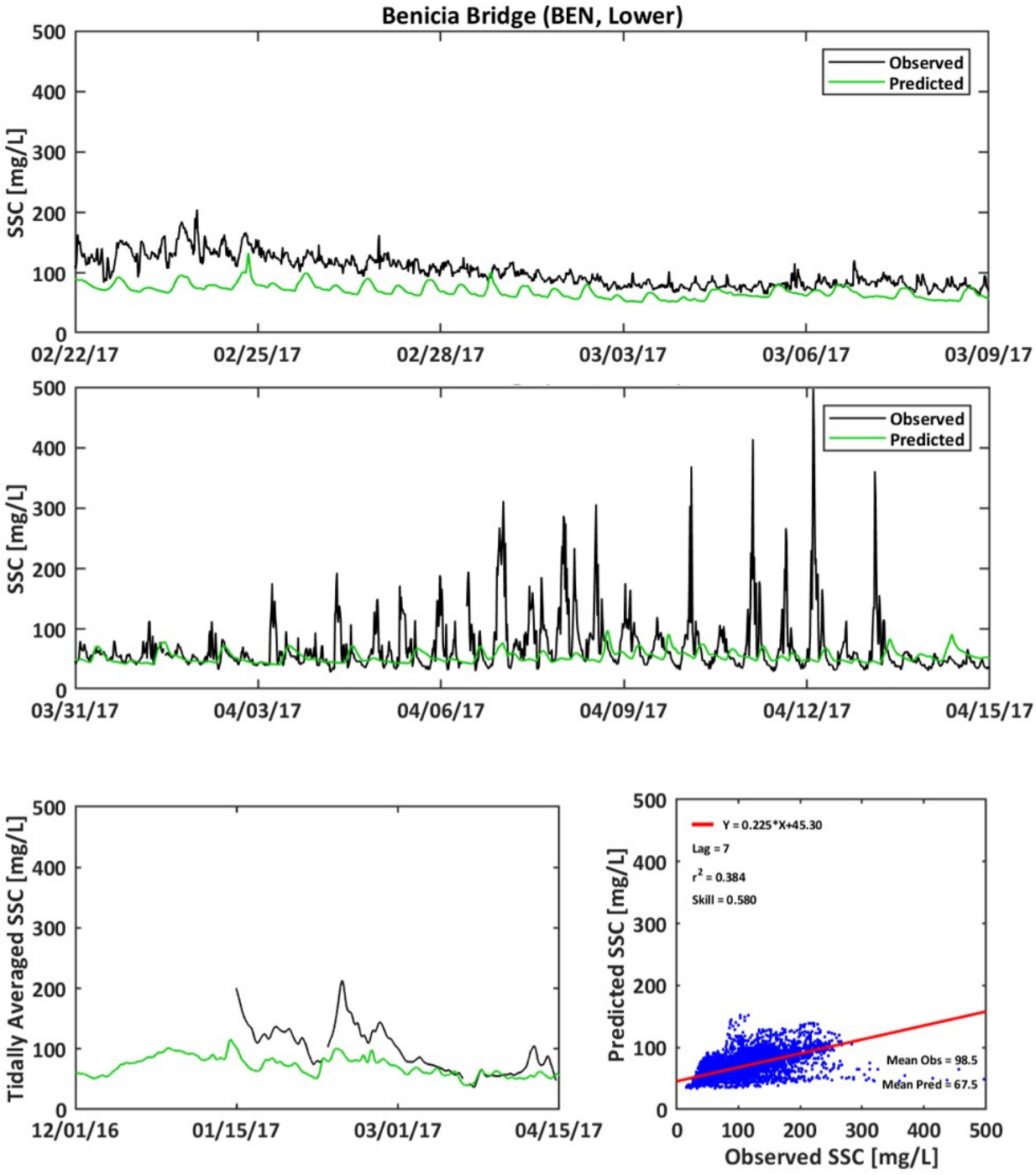

Figure A-9
Observed and Predicted SSC at USGS Dumbarton Bridge (upper)

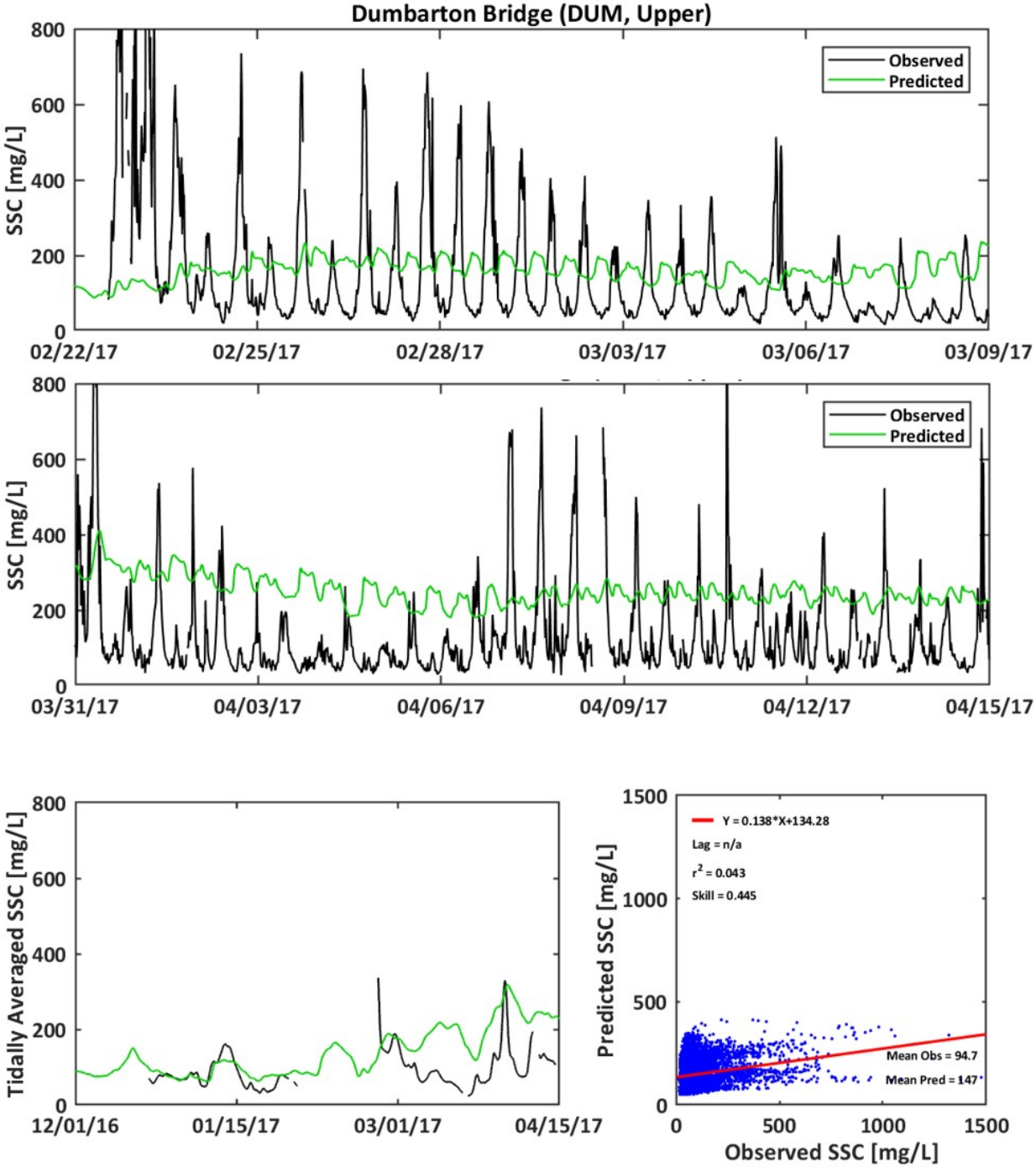

Figure A-10
Observed and Predicted SSC at USGS Dumbarton Bridge (lower)

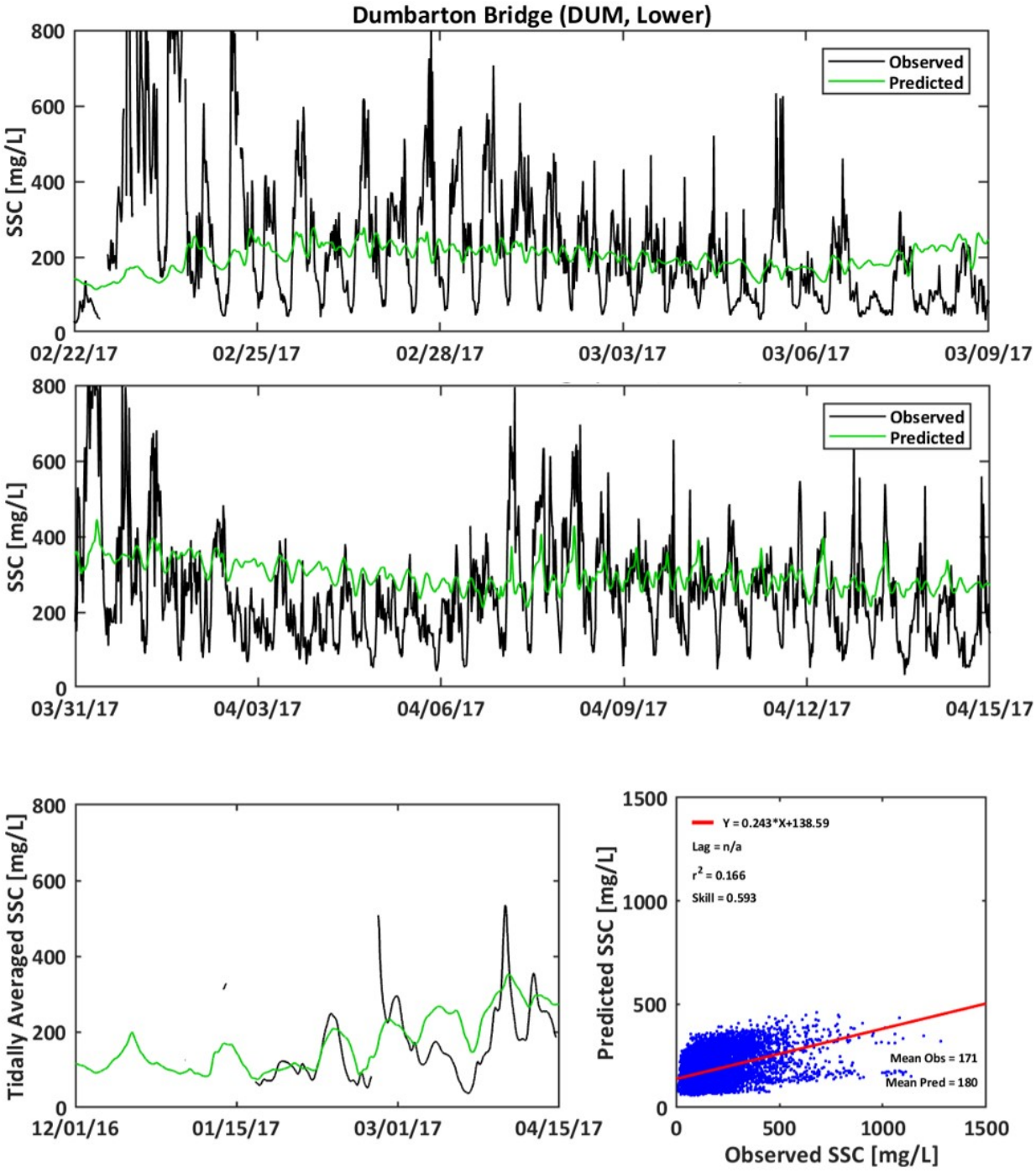

Figure A-11
Transects of Observed and Predicted SSC Profiles, Interpolated from the far South Bay to Rio Vista on December 13, 2016

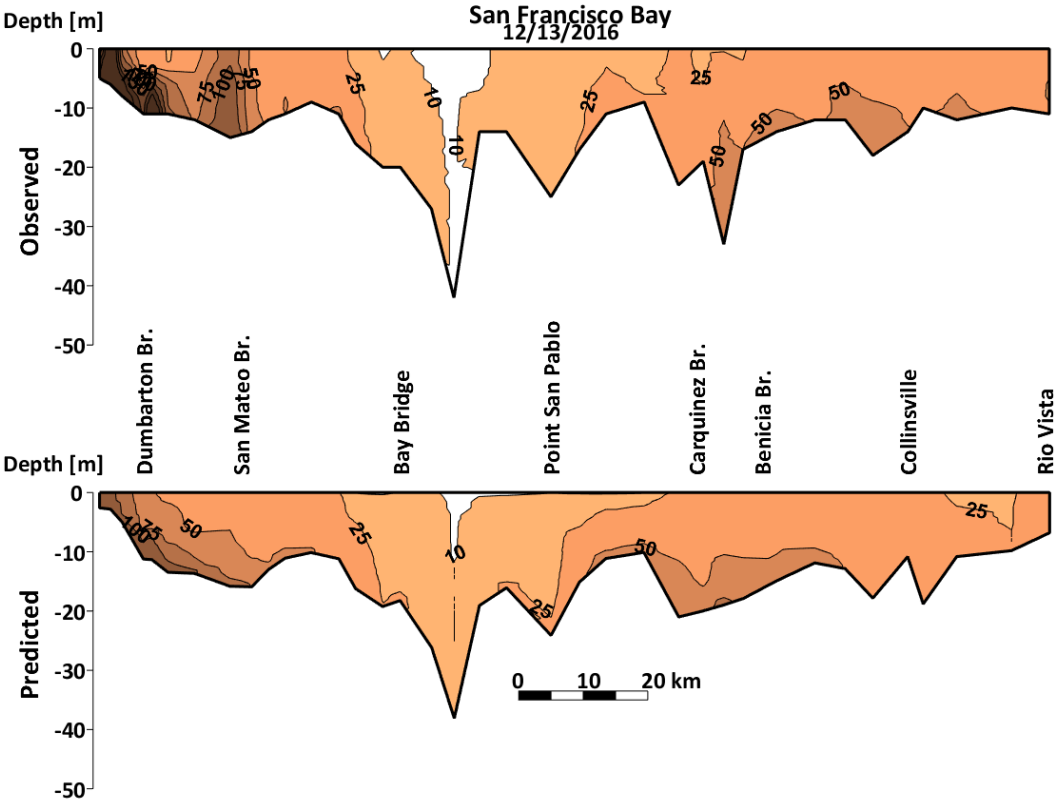

Figure A-12
Transects of Observed and Predicted SSC Profiles, Interpolated from the Far South Bay to Rio Vista on January 11, 2017

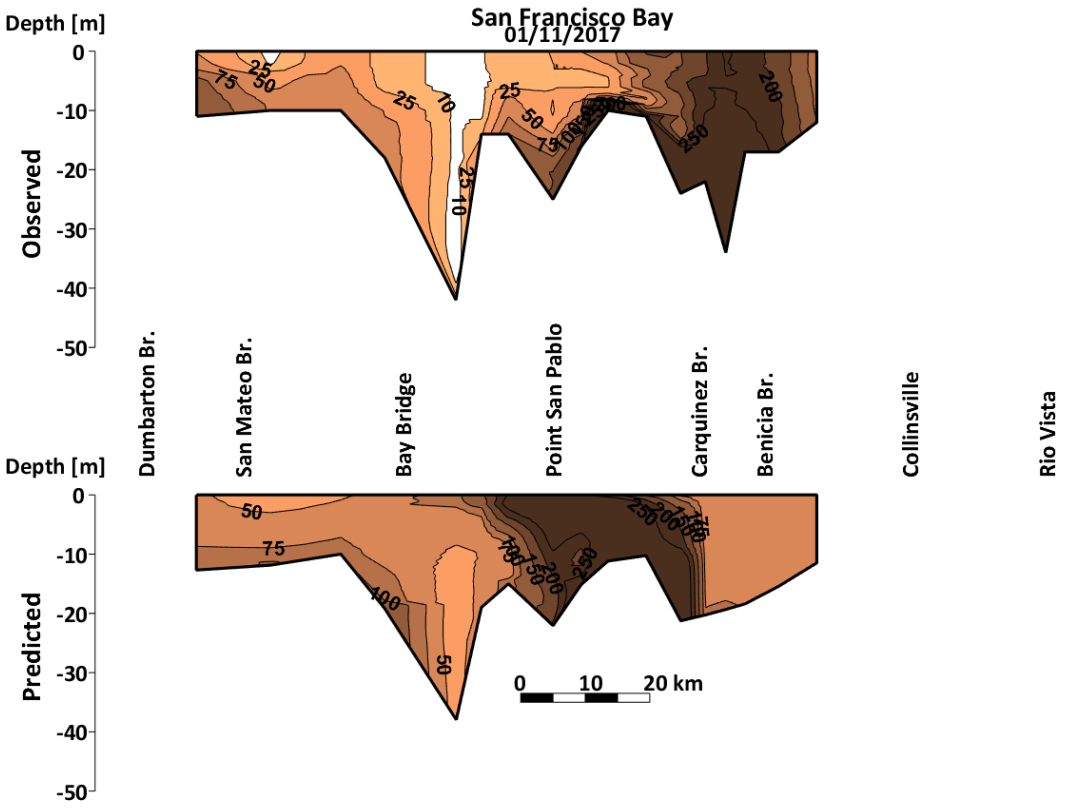

Figure A-13
Transects of Observed and Predicted SSC Profiles, Interpolated from the Far South Bay to Rio Vista on January 23, 2017

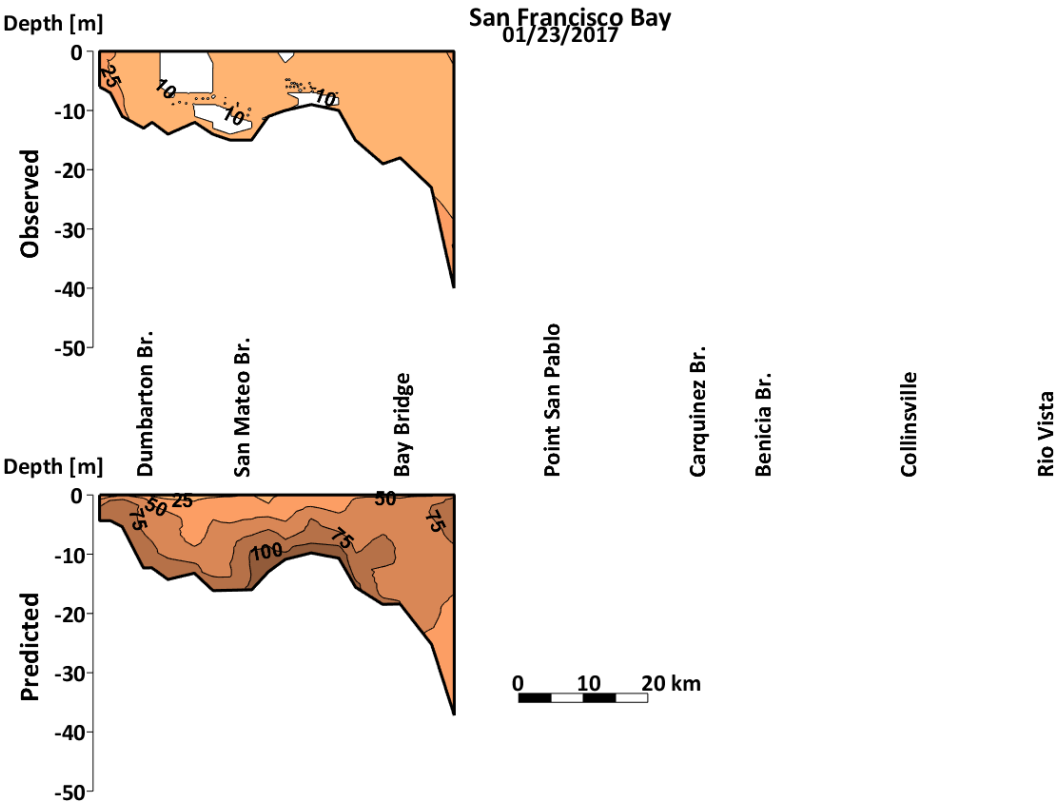

Figure A-14
Transects of Observed and Predicted SSC Profiles, Interpolated from the Far South Bay to Rio Vista on February 8, 2017

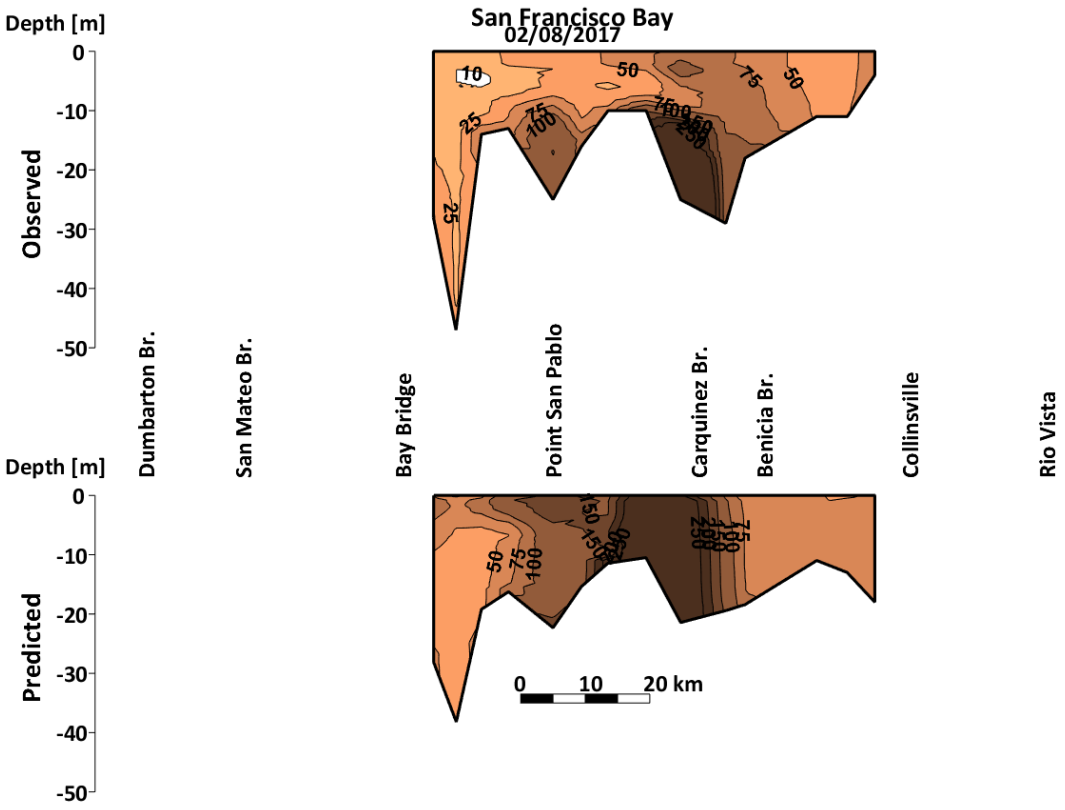

Figure A-15
Transects of Observed and Predicted SSC Profiles, Interpolated from the Far South Bay to Rio Vista on March 21, 2017

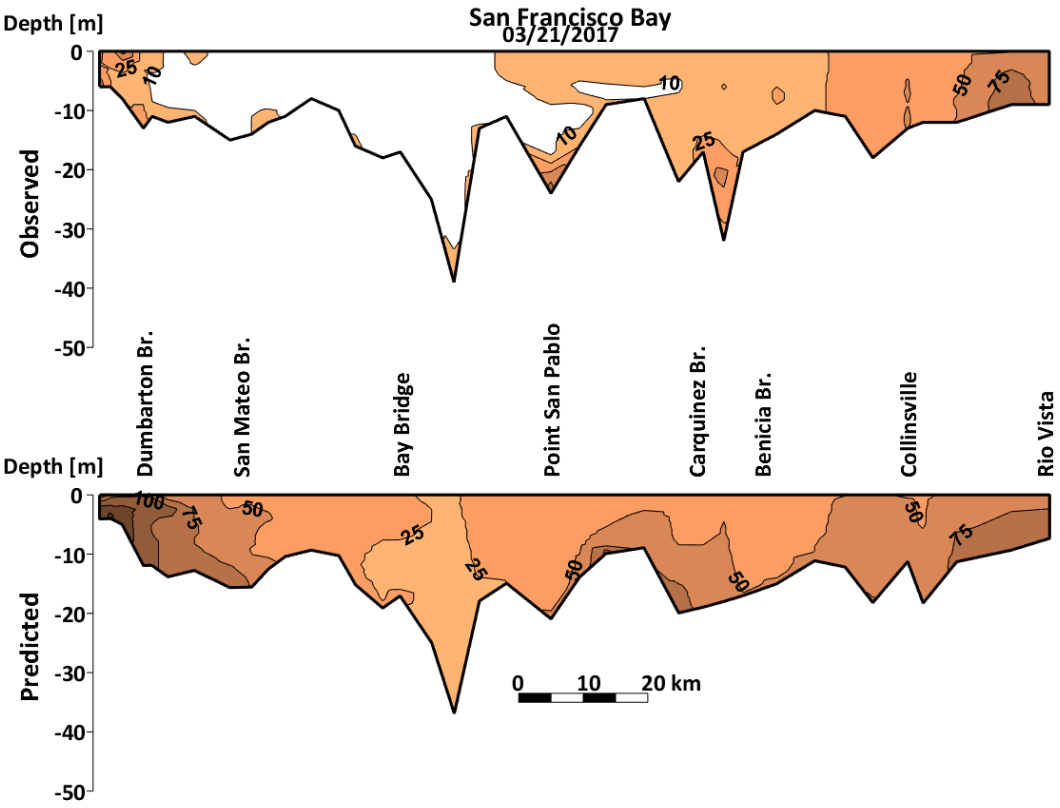

Appendix B
Assumptions and Limitations of the Coupled Modeling System

B. Assumptions and Limitations of the Coupled Modeling System

B.1 Data Sources Used Within the UnTRIM Bay-Delta Model

Detailed descriptions of the boundary conditions and the data used to develop the boundary conditions for the UnTRIM Bay-Delta model, the SWAN wave model, and the SediMorph seabed and sediment transport model are presented in MacWilliams et al. (2015), Bever and MacWilliams (2013), and Bever et al. (2018). This appendix presents a summary of the model boundary conditions and data sources that can be used as a quick reference (Figure B-1; Table B-1), while the previously mentioned references should be consulted for detailed descriptions.

The UnTRIM Bay-Delta model grid was developed with varying grid resolution along the axis of the estuary as necessary to resolve the bathymetric variability, with smaller grid cells used in narrower channels and in regions of complex bathymetry. The bathymetry was incorporated into the model using the highest-resolution data that were available at any location (MacWilliams et al. 2015). The observed water level at the NOAA San Francisco tide station (9414290) was used to force the tidal water level at the open boundary. The open boundary salinity was set using daily salinity observations from the Farallon Islands, approximately 20 kilometers west of the open boundary. The initial salinity field in the Bay was specified based on vertical salinity profiles collected by the USGS at 38 stations along the axis of the estuary and in the Delta by interpolating from continuous monitoring stations. At the bottom boundary the roughness coefficient z_0 was specified according to the elevation of each grid cell edge following the approach used by Cheng et al. (1993), Gross et al. (2010), and MacWilliams and Gross (2013), with higher roughness coefficients in shallower and higher elevation areas.

River inflows to the model included tributaries to the Bay and Delta and discharges from water pollution control plants (Figure B-1). Daily water exports were also specified at six locations. Hourly wind data was specified for six subregions of the Bay-Delta based on observations from the Bay Area Air Quality Management District (BAAQMD). Evaporation and precipitation in the Bay was set based on hourly data from the California Irrigation Management Information System (CIMIS), while evaporation and precipitation in the Delta was included in the Delta Island Consumptive Use (DICU). Monthly estimates of DICU (CDWR 1995) were used to specify the seepage, agricultural diversions, return flows, and return flow salinity within the Delta. Nine control gates and temporary barriers in the Delta were incorporated into the model to represent the effects of these gates and barriers on flow and transport in the Delta (Figure B-1). For each control structure, the seasonal timing of the installation, removal, and associated culvert and gate operations were specified (MacWilliams et al. 2009; MacWilliams and Gross 2013).

Sediment transport calculations included five sediment classes, each with different particle size, settling velocity, critical shear stress, density, and erosion rate parameter (Table 2-1). The five sediment classes were chosen to represent the dominant constituents in the real Bay grain size distribution and were fine clay/silt, single particle silt, flocculated silts and clays called "flocs," sand, and gravel, with characteristics based on data from the Bay (Kineke and Sternberg 1989; Sea Engineering 2008; Smith and Friedrichs 2011). Observed surface grain size distributions were used to generate a realistic initial sediment bed for the entire Bay-Delta system. Grain size distribution data were compiled from a USACE long-term management strategy report (Pratt et al. 1994), the dbSEABED West Coast surface grain size distribution database (Jenkins 2010), the USGS sand provenance study (Barnard et al. 2013), and the Delta sediment grain size study (Wright 2012). Suspended sediment was supplied through river input to the Delta, the North Bay, and the South Bay. Sediment was supplied to the Delta by five tributaries representing nearly 100% of the sediment inflow to the delta (Wright and Schoellhamer 2005). SSCs were set based on time series concentrations from USGS, daily concentrations from USGS, or rating curves, depending on data availability.

The SWAN wave calculations used the same model grid and bathymetry as the UnTRIM hydrodynamic model, except that the quadrilaterals in the UnTRIM grid were converted to triangles, as explained in Bever and MacWilliams (2013). The wind was the same as that used in the hydrodynamic model and the bottom roughness was the Nikuradse roughness based on the roughness from the hydrodynamic model.

Table B-1
Summary of Data Sources Used for Model Boundary Conditions

Boundary Condition Type	Boundary Condition/Forcing	Description/Sources
UnTRIM Initial Conditions	Bathymetry	High-resolution bathymetric data from several sources
	Navigation channel alignments in the grid	Provided by USACE
	Salinity	Based on USGS water quality sampling in the Bay and interpolated using continuous monitoring stations in the Delta
Hydrodynamic Forcing	Tidal forcing	6-minute data from NOAA San Francisco tide station (9414290)
	Open boundary salinity	Daily salinity at Farallon Islands
	Inflows	Daily using DAYFLOW for Delta tributaries and USGS data for Bay tributaries
	Exports	Daily from DAYFLOW and the California Data Exchange Center
	DICU	Monthly based on the Delta Island Consumptive Use Model
	Flow control structures	Seasonally nine Delta control structures (MacWilliams et al. 2009)
	Evaporation/precipitation	Hourly data from California Irrigation Management Information System (CIMIS)
	Wind	Hourly data from Bay Area Air Quality Management District (BAAQMD)
	Seabed roughness	Elevation dependent Z_0 ranging from 0.001 mm to 1.0 cm
Sediment	Sediment settling velocity, critical shear stress, diameter and erosion rate	Based on data in San Francisco Bay from Kineke and Sternberg (1989), Sea Engineering (2008), and Smith and Friedrichs (2011)
	Seabed grain size distribution	Based on surface grain size distributions from USGS (Barnard et al. 2013; Wright 2012), USACE (Pratt et al. 1994), and dbSEABED database (Jenkins 2010)
	Inflow SSC	Daily based on USGS time series observations, USGS daily measurements, or rating curves, based on data availability
Waves	Bathymetry	Same as the hydrodynamic model
	Wind	Same as the hydrodynamic model
	Bottom roughness	Nikuradse roughness based on the roughness used in the hydrodynamic model

Figure B-1
Golden Gate High-Resolution UnTRIM Bay-Delta Model Domain, Bathymetry, and Locations of Model Boundary Conditions that Include Inflows, Export Facilities, Contra Costa Water District (CCWD) Intakes, Wind Stations from the Bay Area Air Quality Management District (BAAQMD), Evaporation and Precipitation from California Irrigation Management Information System (CIMIS) Weather Stations, Delta Island Consumptive Use (DICU), and Flow Control Structures

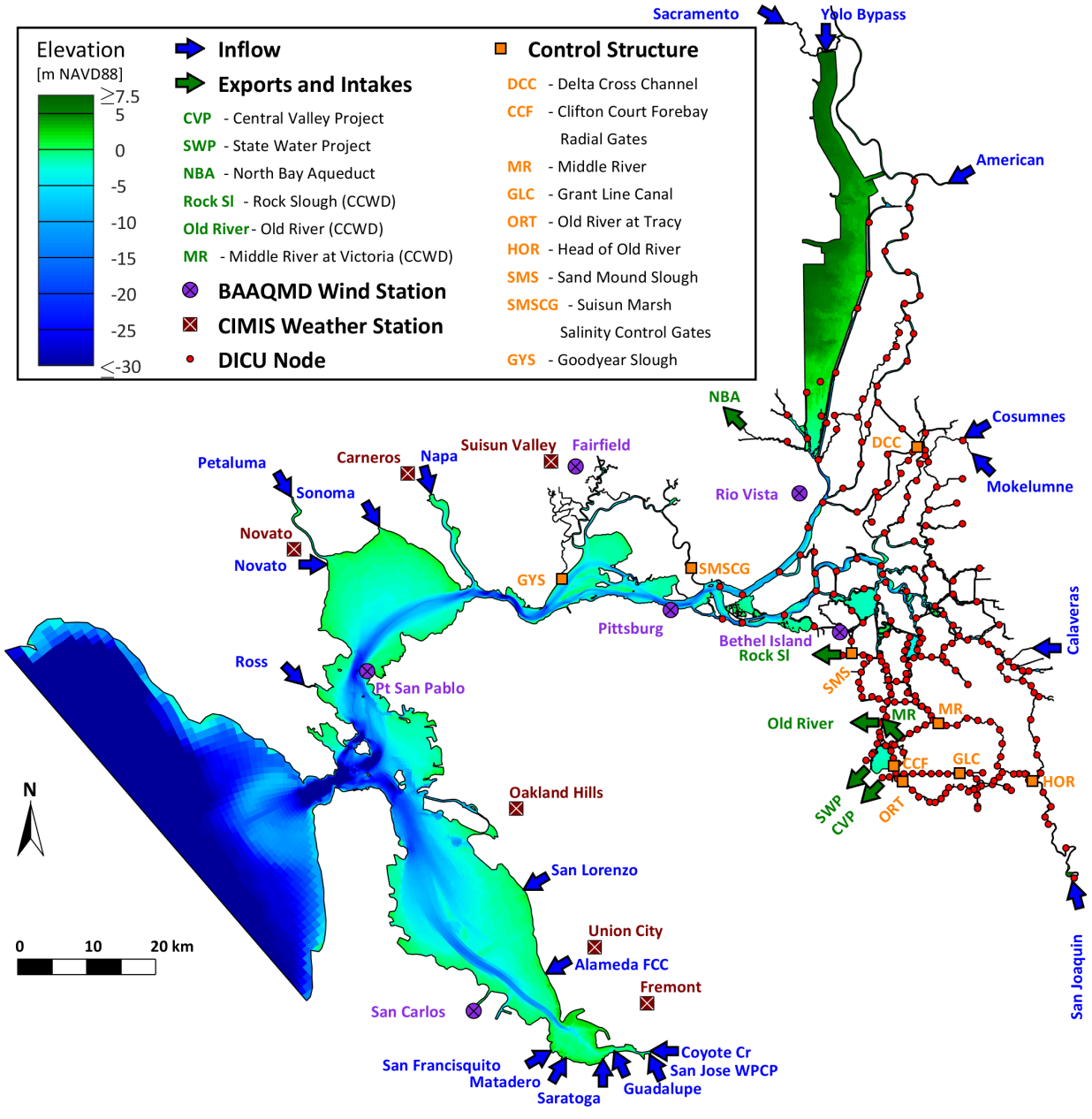

B.2 UnTRIM Numerical Model Uncertainty

As discussed in Section 2, UnTRIM model has been widely used in the Bay, and numerous detailed model calibrations have been performed. The equations governing fluid motion and salt transport, representing conservation of water volume, momentum, and salt mass, are well established but cannot be solved analytically for complex geometry and boundary conditions. Therefore numerical models are used to give approximate solutions to these governing equations. Many decisions are made in constructing and applying numerical models. The governing equations are first chosen to represent the appropriate physical processes in one, two or three dimensions and at the appropriate timescale. Then these governing equations that describe fluid motion and salt transport in a continuum are discretized, giving rise to a set of algebraic equations. The resulting discretized algebraic equations must be solved, often requiring the use of an iterative matrix solver. The discretization and matrix solution must be developed carefully to yield a numerical scheme that is consistent with the governing equations, stable, and efficient. To apply the models, the bathymetric grid, boundary conditions, initial conditions, and several model parameters must be chosen. The accuracy of the model application depends on the appropriate choice of these inputs, including site-specific parameters, the numerical scheme for solving the governing equations, and the associated choice of time step and grid size.

The 3D model applied in this project provides a more detailed description of fluid motion in the Bay than depth-averaged or 1D models. The UnTRIM model, like almost all large-scale hydrodynamic models, averages over the turbulent time scale to describe tidal timescale motions. The resulting 3D hydrodynamic models represent the effect of turbulent motions as small-scale mixing of momentum and salt, parameterized by eddy viscosity and eddy diffusivity coefficients, respectively. These turbulent mixing coefficients are estimated from the tidal flow properties (velocity and density) by turbulence closure models embedded within the 3D models. 3D models estimate the variability in velocity and salinity in all dimensions and through the tidal cycle and therefore provide a detailed description of hydrodynamics and salinity. However, several sources of uncertainty are inherent in the application of these 3D models, detailed as follows:

- **Spatial resolution/computational speed.** The spatial resolution of the bathymetry of the model domain, and velocity and salinity distributions, is limited by the large computational expense associated with high-resolution models. The description of the Bay-Delta bathymetry is improved by the use of a flexible unstructured grid, with coarser grid resolution used in the open bay portions of the grid and higher grid resolution within the project study area to optimize computational efficiency. The computational speed of the Bay-Delta model roughly scales with the number of grid cells. For example, halving of the horizontal resolution of the model would lead to four times as many 3D grid cells and an implementation that takes roughly four times the computation time, making general system-wide reductions in grid

resolution infeasible and showcasing the benefit of using grid refinement approaching study regions.

- **Bathymetric data.** Limited spatial coverage and accuracy of bathymetric data can be a substantial source of uncertainty. Converting all data to a uniform vertical datum and horizontal datum can lead to some error. In particular, Light Detection and Ranging (LiDAR) data may have substantial errors in vertical datum, and removing vegetation from the dataset can be difficult. In the present application, bathymetric data from multiple sources were merged to develop the model bathymetry.
- **Bottom roughness.** The UnTRIM model requires bottom friction coefficients to parameterize the resistance to flow at solid boundaries. These parameters are specified and adjusted in model calibration. The roughness values used in the present application have been applied in several recent applications (e.g., MacWilliams et al. 2007, 2008, 2009, 2015).
- **Turbulence closure.** The effect of turbulent motions on the tidal timescale motions is parameterized by a turbulence closure, as is done in other 3D hydrodynamic numerical models of similar spatial and temporal scale as the UnTRIM Bay-Delta model (e.g., Warner et al. 2005b; Wang et al. 2011). While many turbulence closures are available (e.g., Warner et al. 2005), this is an ongoing area of research and, particularly in stratified settings, the effect of turbulence on tidal flows and salinity is not easy to estimate accurately. Different turbulence closures may give significantly different results in stratified settings (e.g., Stacey 1996).
- **Numerical errors.** A numerical method approximates the governing equations to some level of accuracy. The mathematical properties of the numerical method of the UnTRIM model is well understood due to detailed mathematical analysis presented in several peer-reviewed publications. While the stability and conservation properties of the method are ideal, a remaining source of error in the numerical method is some limited numerical diffusion of momentum, which may cause some damping of tidal propagation.
- **Boundary conditions and initial conditions.** The salinity in the Bay varies laterally (e.g., Huzzey et al. 1990), but this lateral variability cannot be described by existing observations. In addition, only limited observations are available to describe the vertical distribution of salinity. Therefore, lateral and vertical salinity distributions must be achieved by interpolation and extrapolation from the limited observations to obtain initial salinity fields. Inflows to the estuary are also quite uncertain in several regions due to ungauged portions of watersheds and uncertainty in estimates of outflows and diversions in the Delta.

Though additional potential sources of uncertainty can be identified, the largest sources of uncertainty for hydrodynamic predictions are the accuracy and resolution of available bathymetry and the grid resolution used to represent this bathymetry in the model. This study makes use of the best available high-resolution bathymetric data, especially in Central Bay and South Bay, and the highest computationally practical grid resolution throughout the domain. However, many of the

available bathymetric data sets in other portions of the Bay are fairly outdated, and they required vertical and/or horizontal coordinate transformations for the grid used in this project. Additionally, the most recent bathymetry for the Delta does not include many in-channel islands and other subtidal areas that are subject to flooding at high water, particularly during spring tide.

The uncertainty in Delta outflows can also be a substantial source of uncertainty in predicting salinity intrusion during summer conditions, particularly when consumptive use within the Delta (which is only known approximately) is typically the same order of magnitude as Delta tributary flows. The current application makes use of monthly DICU estimates from DWR. However, because these estimates of diversions and return flows and salinities are approximate, they may not be representative of actual consumptive use in a particular year. This uncertainty would impact the accuracy of net Delta outflows predicted at the flow monitoring stations in the western Delta, when compared to observed flows, and would thereby influence salinity intrusion into the Western Delta during summer conditions. This uncertainty in Delta outflow may also influence the accuracy of sediment transport calculations.

B.3 SWAN Numerical Model Uncertainty

SWAN is a state-of-the-art and full-featured spectral wave model. However, several simplifications and limitations are associated with this model. Wave-induced currents are not computed by SWAN. Because a phase-decoupled approach is used, SWAN "does not properly handle diffraction in harbors or in front of reflecting obstacles" (SWAN Team 2009b). Some additional uncertainty is introduced by interpolation of UnTRIM parameters and variables from side and cell center locations to node locations for use by SWAN. However, in practical SWAN applications, the uncertainty is likely to be driven primarily by the limited accuracy of input parameters such as wind velocity and bottom friction.

B.4 SediMorph Numerical Model Uncertainty

Significant uncertainty exists in the prediction of sediment transport. This uncertainty results from the complexity of representing sediment physics, the limited data available to characterize heterogeneous bed sediment and inflow sediment properties in a dynamic environment, and the difficulty in the specification of representative sediment parameters, such as settling velocity, critical shear stress, and erosion rate. Erosion and deposition processes are also highly sensitive both to the specified sediment parameters and to the calculated bed shear stress, which in turn is sensitive to the selection or calculation of appropriate bed roughness parameters. Effective bed roughness is influenced by the grain size distribution of the bed material, as well as bed forms such as ripples and dunes, and can also vary significantly in both space and time.

B.5 Sediment Transport Modeling Assumptions and Limitations

The interaction of tides, winds, waves, and sediments results in complex physical processes that need to be simplified and parameterized in order to be represented in a numerical model. As a result, the numerical simulation of sediment transport processes requires some simplifying assumptions that can influence the accuracy of the model predictions. The interpretation of the model results must therefore take into account how these assumptions influence both the model predictions and any conclusions drawn from the model predictions. This section outlines the major assumptions and simplifications that were made in the development of the UnTRIM-SWAN-SediMorph coupled modeling system used in this study, and it discusses how these simplifying assumptions may affect the interpretation of the model results.

The major simplifications made in this application were the partitioning of the full range of sediment sizes in the Bay to a discrete set of sediment classes with constant sediment parameters, assuming a single sediment class to represent flocculated particles rather than modeling the aggregation and disaggregation of sediment particles, and the treatment of sediment material in the seabed. Each of these simplifying assumptions is discussed below.

SediMorph allows for multiple sediment classes, each with different settling velocity, critical shear stress, erosion rate parameter, diameter, and density. In the simulations presented in this report, the mud fraction was partitioned between the fine silt, silt, and floc sediment classes. The sediment properties for the five modeled sediment classes were selected to represent fine silts, single particles of silt (silt), aggregated clay and silt particles that behave as flocculated particles (flocs), coarser material (sand), and gravel bedload (gravel). The characteristics of the "flocs" sediment class were set based on field observations of flocs within San Pablo Bay by Kineke and Sternberg (1989), from observations of the size and settling velocity of flocs in the plume from a suction hopper dredge in the Bay by Smith and Friedrichs (2011), from data on sediment mass eroded from the top of cores collected in San Pablo Bay by Sea Engineering (2008), and through comparison of modeled and observed time-series SSCs within the Bay. However, in reality, flocs continuously undergo aggregation and disaggregation due to physical and biological changes in the water (Mikkelsen et al. 2006), such as changes to turbulence and the Kolmogrov microscale, varying SSCs, compaction of the seabed and subsequent resuspension, sediment interaction with biofilms, and incorporation into fecal pellets (some examples in Eisma 1986; Fugate and Friedrichs 2003; Hill and McCave 2001). These processes are extremely complex and are not easily incorporated into a numerical model. Previous sediment modeling studies in the Bay (e.g., Bever and MacWilliams 2013, 2014; Bever et al. 2018; van der Wegen et al. 2011; Schoellhamer et al. 2008; Ganju and Schoellhamer 2009) have also made a similar simplifying assumption by specifying a sediment class with characteristics representing flocculated material but assuming that mass is not aggregated or disaggregated between sediment classes. This simplification potentially leads to decreased peak SSCs during

energetic periods and faster settling of the sediment from the water column because large flocs are not broken into smaller flocs or constituent particles. The simplification may also lead to an underestimation of the amount of sediment transported out of a channel onto the mudflats, because flocs may be disaggregated during high tidal flows into smaller particles that are more easily transported out of the channel.

Because bed consolidation is not currently represented in the model, the model may overpredict the transport distance of the sediment. With bed consolidation, some sediment would consolidate during neap tide periods and be harder to erode the following spring tide. Neglecting bed consolidation may lead to increased SSCs at the start of spring tides in the model predictions, because the sediment deposited in the model during neap tides does not consolidate and is easily erodible as the currents start to increase approaching spring tides. Without seabed consolidation, the model also does not dewater or compact the seabed, which would reduce the depositional thicknesses and volumes over time. On a spring-neap time scale, compaction likely only negligibly affects model predictions of depositional thicknesses because of the relatively small depositional and erosional thicknesses undergoing compaction. However, on longer timescales with thicker deposition, compaction could affect model predictions of depositional thickness and the feedbacks on the hydrodynamics. This lack of compaction and dewatering is mostly counteracted by tuning the seabed porosity based on the estimates of sediment depositional volume and thickness from hydrographic survey data so the modeled thicknesses and volumes agree with the hydrographic survey estimates. However, additional data are needed to more fully validate predictions of sediment fluxes and morphologic change outside of the ship channels.

The complexity inherent in sediment transport modeling detailed previously results in the accuracy of sediment transport predictions based on numeric skill metrics such as those used by MacWilliams et al. (2015) being lower for comparisons of SSCs than is typical for modeling of salinity or water level. This is especially true when considering simulations such as those in this report that span a wide range in environmental conditions and simulate the transport of sediment over large distances from upstream portions of freshwater rivers through the entire San Francisco Estuary and into the Pacific Ocean. However, when the comparisons between observed and predicted SSCs indicate that the model is predicting a similar magnitude of concentration as the observations, captures the seasonal and spatial trends, and captures the observed tidal timescale variations and along-estuary spatial structure, this suggests that the model is capturing the primary physical processes responsible for sediment transport in the system.